Electronic Supplementary Information

Implementing the Design Cues of Dissociation Dynamics and Transmetalation into Gallium(III) Complexes to Promote Anti-Proliferative Activity of Ligands Targeting Intracellular Iron(II) Trafficking

Mahendiran Dharmasivam,[†Ψ*#] Sadia Faiz,[†§#] Busra Kaya,[Ψ#] Tharushi P. Wijesinghe,[Ψ] Mediha Suleymanoglu,[Ψφ] Mahan Gholam Azad,[†Ψ] Vera Richardson,[†Ψ] Ameer Fawad Zahoor,[§] Danuta Kalinowski,[†] William Lewis,[‡] Paul V. Bernhardt,[¶] Rukhsana Anjum,[†] and Des R. Richardson[†Ψ*]

#Co-first authors contributed equally to this manuscript.

[†]*Molecular Pharmacology and Pathology Program, Department of Pathology and Bosch Institute, The University of Sydney, Sydney, New South Wales, 2006, Australia.*

[Ψ]*Centre for Cancer Cell Biology and Drug Discovery, Institute for Biomedicine and Glycomics, Griffith University, Southport, 4215, Queensland, Australia.*

[φ]*Department of Medical Biology, Istanbul Faculty of Medicine, Istanbul University, 34093 Fatih-Istanbul, Turkiye*

[§]*Department of Chemistry, Government College University, Faisalabad, Faisalabad 38000, Pakistan.*

[‡]*School of Chemistry, The University of Sydney, Sydney, New South Wales 2006, Australia.*

[¶]*School of Chemistry and Molecular Biosciences, University of Queensland, Brisbane 4072, Australia*

[*]**Corresponding Authors: Dr. Des R. Richardson** and **Dr. Mahendiran Dharmasivam,** Centre for Cancer Cell Biology and Drug Discovery, Institute for Biomedicine and Glycomics, Griffith University, Southport, 4215, Queensland, Australia. Email: d.richardson@griffith.edu.au and m.dharmasivam@griffith.edu.au

Table of Contents

Supplementary Procedures

Supporting Results and Discussion

Supplementary Tables

Supplementary Figures

EXPERIMENTAL SECTION

Materials and methods

All reagents and solvents were of the highest quality, available from commercial sources and were used without further purification. The reagents, 2-acetyl-3-aminobenzofuran, 2-acetylnaphthofuran, 4,4-dimethyl-3-thiosemicarbazide, 4-phenyl-3-thiosemicarbazide, isoniazid, 2-thiophene carboxylic hydrazide, benzohydrazide, dichloromethane (DCM), methanol (MeOH), ethanol (EtOH), *n*-octanol, toluene, concentrated H_2SO_4, K_2CO_3, DMF, CH_3COOH, $Cu(OAc)_2.H_2O$, $Zn(OAc)_2.2H_2O$, $ZnCl_2.2H_2O$, desferrioxamine (DFO), and 3-(4,5-dimethylthiazol-2-yl)-2,5-diphenyltetrazolium bromide (MTT) were obtained from Sigma-Aldrich (St. Louis, MO). Full IUPAC names of the novel ligands, L1–L13, as referenced in the main text, **L1** ((E)-2-(1-(3-aminobenzofuran-2-yl)ethylidene)-N,N-dimethylhydrazinecarbothioamide), **L2** ((E)-2-(1-(3-aminobenzofuran-2-yl)ethylidene)-N-phenylhydrazinecarbothioamide), **L3** ((E)-N′-(1-(3-aminobenzofuran-2-yl)ethylidene)isonicotinohydrazide), **L4** ((E)- N′-(1-(3-aminobenzofuran-2-yl)ethylidene)thiophene-3-carbohydrazide), **L5** ((E)-N'-(1-(naphtho[2,1-b]furan-2-yl)ethylidene)benzohydrazide)), **L6** ((E)-N′-(1-(naphtho[2,1-b]furan-2-yl)ethylidene)isonicotinohydrazide), **L7** ((E)-N′-(1-(naphtho[2,1-b]furan-2-yl)ethylidene)thiophene-2-carbohydrazide), **L8** ((E)-N'-(1-(naphtho[2,1-b]furan-2-yl)ethylidene)furan-2-carbohydrazide), **L9** ((E)-2-(1-naphtho[2,1-b]furan-2-yl)ethylidene)-N-phenylhydrazinecarbothioamide), **L10** ((E)-N'-(1-(pyridin-2-yl)ethylidene)naphtho[2,1-b]furan-2-carbohydrazide), **L11** ((E)-N'-(phenyl(pyridin-2-yl)methylene)naphtho[2,1-b]furan-2-carbohydrazide), **L12** (N'-(di(pyridin-2-yl)methylene)naphtho[2,1-b]furan-2-carbohydrazide), and **L13** ((E)-N'-(1-(pyrazin-2-yl)ethylidene)naphtho[2,1-b]furan-2-carbohydrazide).

Physical methods

^{1}H and ^{13}C spectra were recorded on a 500 MHz Bruker Avance III 500 NMR spectrometer (Billerica, MA) using either DMSO-d_6 or $CDCl_3$. The NMR peaks were referenced using TMS or the solvent peak as an internal standard. The ESI-MS (electrospray ionization mass spectrometry) data were collected by using a Bruker amaZon SL mass spectrometer. Elemental analysis was carried out using a Thermo Scientific Flash 2000 C, H, N, S/O analyzer (Waltham, MA).

X-ray Crystallography

All the ligand crystals (L1, L5, L7, L10, L11, L12, and L13) were obtained by slow evaporation of a solution containing EtOH (2 mL) and DCM (0.5 mL). A suitable ligand crystal was selected and mounted on a loop using Paratone® protective oil. Diffraction data were collected using mirror-monochromated Cu Kα radiation (1.54184 Å) on either a SuperNova Rigaku Oxford Diffraction System equipped with an Atlas CCD area detector or a Bruker D8 Venture diffractometer. For $[Zn(L11)Cl_2]$, single crystals were obtained by slow evaporation of a solution containing EtOH (2 mL) and DCM (0.5 mL). Data were collected at 150 K using a Cu Kα radiation source on a Bruker D8 Venture diffractometer. The structures were solved using SHELXS[1] and refined with SHELXL.[2] Thermal ellipsoid plots were created using Mercury (Cambridge Crystallographic Data Centre; CCDC).[3] All crystallographic data have been deposited with the CCDC in CIF format (see **Tables S1, S2**).

Electrochemistry

Cyclic voltammograms were recorded for the Cu(II) complexes of the four tridentate ligands (L10–L13) and were also used to investigate the transmetalation of $[Ga(L12)_2]^+$. The Cu(II) and Ga(III) complexes (100 μM) were dissolved in MeCN:H_2O (70:30 *v/v*). Freshly prepared aqueous solutions of 100 μM

$Cu(OAc)_2$, Fe(III) citrate (molar ratio 1:100), and Fe(II) ascorbate (molar ratio 1:100) were sequentially added to $[Ga(L12)_2]^+$, followed by a 5-min incubation. Before measurements, all solutions were purged with N_2. Electrochemistry was performed using a Gamry Interface 1010B Potentiostat (Gamry Instruments, Philadelphia, PA) in a three-electrode system consisting of a glassy carbon working electrode, a platinum wire auxiliary electrode, and an aqueous Ag/AgCl reference electrode (0.1 M Bu_4NClO_4). Redox potentials were referenced to the normal hydrogen electrode (NHE).[4] The *in situ* complex [Cu(L13)OAc] was prepared and investigated to compare its electrochemical behavior with three other synthesized Cu(II) complexes containing acetate, allowing for a comparison of how acetate influences electrochemistry.

Synthesis of Bidentate Ligands

Synthesis of the ketones, 1-naphtho[2,1-*b*]furan-2-yl-1-ethanone and 1-(3-amino-1-benzofuran-2-yl)ethanone

The synthesis of 1-naphtho[2,1-*b*]furan-2-yl-1-ethanone and 1-(3-amino-1-benzofuran-2-yl)ethenone was conducted by using a reported literature procedure with slight modification.[5] Briefly, to a stirred solution of 2-hydroxy-1-naphthaldehyde or 2-hydroxybenzonitrile (1 equivalent) in DMF (7 mL), K_2CO_3 (2 equivalents) and chloroacetone (1.2 equivalents) were added at room temperature. The reaction mixture was heated at 94-96 ^oC until complete consumption of the starting materials, as shown by TLC. After completion, the reaction mixture was poured into ice-cold water, and the precipitate was then filtered off, washed with water, and air-dried to yield the required ketones, 1-naphtho[2,1-*b*]furan-2-yl-1-ethanone, and 1-(3-amino-1-benzofuran-2-yl)ethanone.

Synthesis of the novel bidentate hydrazones and thiosemicarbazones (L1-L9)

A hot ethanolic solution of either 1-naphtho[2,1-*b*]furan-2-yl-1-ethanone or 1-(3-amino-1-benzofuran-2-yl)ethanone (1 equivalent) was mixed with a hot ethanolic solution of the desired hydrazide or thiosemicarbazide (1 equivalent) in the presence of 3-4 drops of HCl. The reaction mixture was allowed to reflux at 80 ^{o}C for 4-5 h, and the precipitate filtered off and air-dried. The product was recrystallized from methanol to give the desired hydrazones or thiosemicarbazones (L1-L9; **Fig. 1A**).

L1: Brown powder (Yield: 23.5%). ESI-MS in MeOH: found mass: 276.98 (15%), 298.99 (35%), 575.07 (100%), Calc. mass for: $C_{13}H_{17}N_4OS$ 277.11 $[M+H]^+$, $C_{13}H_{16}N_4NaOS$ 299.09 $[M+Na]^+$, $C_{26}H_{32}N_8NaO_2S_2$ 575.20 $[2M+Na]^+$. ^{1}H NMR δ ppm (DMSO-d_6): 9.60 (s, 1H, NH), 7.77 (d, 1H, J = 7.7 Hz, ArH), 7.44 (d, 1H, J = 8.2 Hz, ArH), 7.34-7.30 (td, 1H, J = 1.1, 7.5, 7.7 Hz, ArH), 7.22 (t, 1H, J = 7.4, 7.5 Hz, ArH), 6.58 (s, 2H, NH_2), 3.32 (s, 6H, 2 x CH_3), 2.34 (s, 3H, CH_3).^{13}C NMR δ ppm (DMSO-d_6): 180.8, 152.9, 148.0, 133.0, 130.4, 126.1, 123.7, 122.3, 120.4, 111.7, 41.3, 13.1. Anal. Calc. for $C_{13}H_{16}N_4OS\cdot0.25H_2O$ (%): C, 55.59; H, 5.92; N, 19.95; S, 11.41. Found (%): C, 55.94; H, 5.90; N, 19.91; S, 11.75.

L2: Dark brown powder (Yield: 49.7%). ESI-MS in MeOH: found mass: 347.12 (100%), 671.06 (45%), Calc. mass for $C_{17}H_{16}N_4NaOS$: 347.09 $[M+Na]^+$, $C_{34}H_{32}N_8NaO_2S_2$: 671.20 $[2M+Na]^+$. ^{1}H NMR δ ppm (DMSO-d_6): 10.40 (s, 1H, NH), 9.82 (s, 1H, NH), 7.87 (d, 1H, J = 7.6 Hz, ArH), 7.61 (d, 2H, J = 7.0 Hz, 2 x ArH), 7.46 (d, 1H, J = 8.3 Hz, ArH), 7.39-7.35 (m, 3H, 3 x ArH), 7.24 (td, 1H, J = 0.6, 7.3, 7.6 Hz, ArH), 7.17 (t, 1H, J = 7.3 Hz, ArH), 6.15 (bs, 2H, NH_2), 2.41 (s, 3H, CH_3). ^{13}C NMR δ ppm (DMSO-d_6): 176.4, 153.2, 140.1, 132.7, 131.4, 129.4, 128.8, 127.0, 126.2, 125.5, 124.0, 122.7, 122.5, 121.0, 114.5,

111.8, 14.3. Anal. Calc. for $C_{17}H_{16}N_4OS \cdot 0.25H_2O$ (%): C, 62.08; H, 5.06; N, 17.03; S, 9.75. Found (%): C, 62.41; H, 4.96; N, 17.13; S, 9.94.

L3: Light orange powder (Yield: 17.2%). ESI-MS in MeOH: found mass: 317.08 (100%), 611.15 (95%), Calc. mass for $C_{16}H_{14}N_4NaO_2$: 317.10 $[M+Na]^+$, $C_{32}H_{28}N_8NaO_4$: 611.21 $[2M+Na]^+$. ^{1}H NMR δ ppm (DMSO-d_6): 11.07 (s, 1H, NH), 8.77 (d, 2H, J = 5.9 Hz, 2 x PyrH), 7.84-7.82 (m, 3H, 2 x PyrH, 1 x ArH), 7.47 (d, 1H, J = 8.3 Hz, ArH), 7.36 (td, 1H, J = 1.3, 7.2, 7.7 Hz, ArH), 7.24 (t, 1H, J = 7.5, Hz, ArH), 6.50 (s, 2H, NH_2), 2.41 (s, 3H, CH_3). ^{13}C NMR δ ppm (DMSO-d_6): 162.4, 153.2, 152.9, 150.6, 141.6, 132.6, 132.0, 126.8, 123.4, 122.4, 122.3, 120.9, 111.9, 13.9. Anal. Calc. for $C_{16}H_{14}N_4O_2$ (%): C, 65.30; H, 4.79; N, 19.04. Found (%): C, 65.19; H, 4.72; N, 18.66.

L4: Light orange powder (Yield: 15.2%). ESI-MS in DCM/MeOH: found mass: 322.03 (100%), Calc. mass for $C_{15}H_{13}N_3NaO_2S$: 322.06 $[M+Na]^+$. ^{1}H NMR δ ppm (DMSO-d_6): 10.80 (s, 1H, NH), 7.98 (d, 1H, J = 2.2 Hz, Thiophene-H), 7.86-7.81 (d, 1H, J = 16.1 Hz, Thiophene-H), 7.81 (d, 1H, J = 7.7 Hz, ArH), 7.46 (d, 1H, J = 8.2 Hz, ArH), 7.36 (td, 1H, J = 1.0, 7.7 Hz, ArH), 7.26-7.22 (m, 2H, 1 x ArH, 1 x Thiophene-H), 6.43 (s, 2H, NH_2), 2.41 (s, 3H, CH_3).^{13}C NMR δ ppm (DMSO-d_6): 158.5, 153.1, 152.0, 138.8, 132.8, 131.8, 131.6, 129.5, 128.4, 126.7, 123.5, 122.4, 120.8, 111.8, 13.8. Anal. Calc. for $C_{15}H_{13}N_3O_2S \cdot 0.25H_2O$ (%): C, 59.29; H, 4.48; N, 13.83; S, 10.55. Found (%): C, 59.42; H, 4.31; N, 13.70; S, 10.92.

L5: Light brown powder (Yield: 31.1%). ESI-MS in DCM/MeOH: found mass: 351.07 (100%), Calc. mass for $C_{21}H_{16}N_2NaO_2$: 351.11 $[M+Na]^+$. ^{1}H NMR δ ppm (DMSO-d_6): 10.87 (s, 1H, NH), 8.37 (d, 1H, J = 8.1 Hz, ArH), 8.13 (s, 1H, ArH), 8.07 (d, 1H, J = 8.1 Hz, ArH), 7.95-7.93 (m, 3H, 3 x ArH), 7.86 (d,

1H, *J* = 8.8 Hz, ArH), 7.68 (td, 1H, *J* = 1.0, 7.5, 7.5 Hz, ArH), 7.62 (t, 1H, *J* = 7.3, Hz, ArH), 7.59-7.54 (m, 3H, ArH), 2.51 (s, 3H, CH_3). ^{13}C NMR δ ppm (DMSO-d_6): 164.6, 153.7, 152.9, 134.4, 132.1, 130.5, 129.3, 128.8, 128.6, 128.6, 128.5, 128.3, 127.7, 127.4, 127.3, 125.5, 124.1, 123.9, 112.9, 107.8, 14.5. Anal. Calc. for $C_{21}H_{16}N_2O_2 \cdot 0.25EtOH$ (%): C, 75.98; H, 5.19; N, 8.24. Found (%): C, 76.32; H, 4.88; N, 8.46.

L6: Dark grey powder (Yield: 27.2%). ESI-MS in DCM/MeOH: found mass: 352.08 (100%), Calc. mass for $C_{20}H_{15}N_3NaO_2$: 352.11 $[M+Na]^+$. ^{1}H NMR δ ppm (DMSO-d_6): 11.11 (s, 1H, NH), 8.79 (s, 2H, ArH), 8.36 (d, 1H, *J* = 7.5 Hz, ArH), 8.18 (s, 1H, ArH), 8.06 (d, 1H, *J* = 7.8 Hz, ArH), 7.95-7.84 (m, 4H, 4 x ArH), 7.68 (t, 1H, *J* = 7.2 Hz, ArH), 7.56 (t, 1H, *J* = 7.3, 7.3 Hz, ArH), 2.50 (s, 3H, CH_3). ^{13}C NMR δ ppm (DMSO-d_6): 163.1, 153.3, 153.0, 148.0, 141.5, 130.5, 129.3, 127.7, 127.6, 127.4, 125.6, 124.1, 123.8, 122.5, 112.9, 108.5, 14.7. Anal. Calc. for $C_{20}H_{15}N_3O_2 \cdot 0.25H_2O$ (%): C, 71.95; H, 4.68; N, 12.59. Found (%): C, 72.19; H, 4.52; N, 12.25.

L7: Brown powder (Yield: 20.3%). ESI-MS in DCM/MeOH: found mass: 357.04 (78%), 691.11 (100%), Calc. mass for $C_{19}H_{14}N_2NaO_2S$: 357.07 $[M+Na]^+$, $C_{38}H_{28}N_4NaO_4S_2$: 691.14 $[2M+Na]^+$. ^{1}H NMR δ ppm (DMSO-d_6): 11.17 (s, 1H, NH), 8.38 (d, 1H, *J* = 8.1 Hz, ArH), 8.18 (s, 1H, ArH), 8.11 (s, 1H, ArH), 8.06 (d, 1H, *J* = 8.1 Hz, ArH), 7.98 (s, 1H, ArH), 7.92 (d, 1H, *J* = 9.0 Hz, ArH), 7.85 (d, 1H, *J* = 8.9 Hz, ArH), 7.68 (t, 1H, *J* = 7.4 Hz, ArH), 7.57 (t, 1H, *J* = 7.4 Hz, ArH), 7.27 (t, 1H, *J* = 4.4 Hz, ArH), 2.47 (s, 3H, CH_3). ^{13}C NMR δ ppm (DMSO-d_6): 162.6, 153.7, 152.9, 135.6, 130.5, 129.3, 127.7, 127.3, 127.3, 125.6, 124.1, 123.9, 112.9, 107.2, 13.9. Anal. Calc. for $C_{19}H_{14}N_2O_2S$ (%): C, 68.25; H, 4.22; N, 8.38; S, 9.59. Found (%): C, 68.08; H, 4.16; N, 8.34; S, 9.69.

L8: Dark brown powder (Yield: 21.4%). ESI-MS in MeOH: found mass: 341.07 (72%), 659.17 (100%), Calc. mass for: $C_{19}H_{14}N_2NaO_3$, 341.09 $[M+Na]^+$, $C_{38}H_{28}N_4NaO_6$, 659.19 $[2M+Na]^+$. ^1H NMR δ ppm (DMSO-d_6): 10.72 (s, 1H, NH), 8.36 (d, 1H, J = 8.1 Hz, ArH), 8.13 (s, 1H, ArH), 8.06 (d, 1H, J = 8.1 Hz, ArH), 7.99 (s, 1H, ArH), 7.92 (d, 1H, J = 8.9 Hz, ArH), 7.85 (d, 1H, J = 8.9 Hz, ArH), 7.67 (td, 1H, J = 1.1, 7.0, 8.1 Hz, ArH), 7.57 (td, 1H, J = 8.1, 7.0, 1.2 Hz, ArH), 6.77 (s, 1H, ArH), 2.47 (s, 3H, CH_3). ^{13}C NMR δ ppm (DMSO-d_6): 153.6, 152.9, 146.6, 146.6, 130.5, 129.3, 129.2, 127.7, 127.4, 127.4, 127.3, 125.5, 124.1, 123.9, 112.8, 112.6, 107.9, 14.1. Anal. Calc. for $C_{19}H_{14}N_2O_3$ (%): C, 71.69; H, 4.43; N, 8.80; Found (%): C, 71.52; H, 4.45; N, 8.65.

L9: Light brown powder (Yield: 44.8%). ESI-MS in CH_3CN: found mass: 382.14 (100%), 741.06 (77%), Calc. mass for: $C_{21}H_{17}N_3NaOS$, 382.10 $[M+Na]^+$, $C_{42}H_{34}N_6NaO_2S_2$, 741.20 $[M+Na]^+$. ^1H NMR δ ppm (DMSO-d_6): 10.92 (s, 1H, NH), 10.08 (s, 1H, NH), 8.31 (t, 2H, J = 4.1 Hz, 2 x ArH), 8.06 (d, 1H, J = 8.1 Hz, ArH), 7.91 (d, 1H, J = 9.0 Hz, ArH), 7.84 (d, 1H, J = 9.1 Hz, ArH), 7.69-7.66 (m, 3H, 3 x ArH), 7.56 (td, 1H, J = 1.2, 7.2, 7.6 Hz, ArH), 7.42 (t, 2H, J = 7.9, 7.9 Hz, 2 x ArH), 7.25 (t, 1H, J = 7.3, 7.6 Hz, ArH), 2.51 (s, 3H, CH_3). ^{13}C NMR δ ppm (DMSO-d_6): 177.2, 153.5, 152.8, 141.0, 139.4, 130.5, 129.3, 128.7, 127.7, 127.3, 127.2, 126.0, 125.9, 125.6, 124.1, 124.0, 112.9, 107.1, 14.3. Anal. Calc. for $C_{21}H_{17}N_3OS{\cdot}0.25H_2O$ (%): C, 69.30; H, 4.85; N, 11.55; S, 8.81. Found (%): C, 69.65; H, 4.74; N, 11.60; S, 8.91.

Synthesis of Novel Tridentate Ligands

Synthesis of ethyl naphtho[2,1-*b*]furan-2-carboxylate. This ligand was prepared using the procedure reported by Kowalewska *et al.*[5] with slight alterations. Briefly, a mixture of 2-hydroxy-1-naphthaldehyde (1 equivalent), ethyl chloroacetate (1 equivalent), anhydrous K_2CO_3 (1.5 equivalents), and dry DMF (30

mL) was heated for 4 h/94-96 °C. The progress of the reaction was checked using TLC. After completion, distilled H_2O (50 mL) was added, and the reaction mixture was extracted with ethyl acetate (3 x 50 mL). The combined organic layers were dried over anhydrous Na_2SO_4 and evaporated to yield the crude product. The product was purified with flash column chromatography [petroleum ether/ethyl acetate; 97:3].

Synthesis of naphtho[2,1-*b*]furan-2-carbohydrazide. Synthesis was achieved using a reported procedure with slight modification.[6] In this case, ethyl naphtho[2,1-*b*]furan-2-carboxylate (1 equivalent) was dissolved in MeOH (15 mL), and the reaction mixture cooled in an ice bath. Hydrazine monohydrate (5 equivalent) was added, and the reaction mixture was stirred at room temperature for 16 h. The white precipitate formed was filtered, washed with water, and air-dried to afford naphtho[2,1-*b*]furan-2-carbohydrazide.

Synthesis of the tridentate hydrazones (L10-13)

Naphtho[2,1-*b*]furan-2-carbohydrazide (1 equivalent) and the desired *N*-aromatic heterocyclic ketone (1 equivalent) were dissolved in a hot ethanolic solution and 4-5 drops of an acid catalyst was added (*i.e.*, AcOH in the case of L10 and L12, while HCl was used to for L11 and L13). The reaction mixture was heated at reflux at 90 °C for 4-6 h. After completion, the reaction mixture was allowed to return to RT. The formed precipitate was filtered off, air dried and recrystallized from MeOH.

L10: Off-white powder (Yield: 31.0%). ESI-MS in $CHCl_3$: found mass: 352.14 (100%), Calc. mass for $C_{20}H_{15}N_3NaO_2$: 352.11 $[M+Na]^+$. ^1H NMR δ ppm (DMSO-d_6): 11.03 (s, 1H, NH), 8.66 (dd, 1H, J = 4.1 Hz, ArH), 8.51 (s, 1H, ArH), 8.41 (d, 1H, J = 8.1 Hz, ArH), 8.16 (d, 1H, J = 8.0 Hz, ArH), 8.11 (d, 1H,

J = 8.1 Hz, ArH), 8.05 (d, 1H, *J* = 9.0 Hz, ArH), 7.93-7.89 (m, 2H, 2 x ArH), 7.72 (td, 1H, *J* = 1.0, 7.1, 7.6 Hz, ArH), 7.61 (td, 1H, *J* = 1.0, 7.0, 7.6 Hz, ArH), 7.47 (ddd, 1H, *J* = 7.4, 4.8, 1.0 Hz, ArH), 2.55 (s, 3H, CH_3). ^{13}C NMR δ ppm (DMSO-d_6): 155.4, 153.0, 149.2, 148.4, 139.3, 137.2, 130.6, 129.4, 129.1, 128.1, 127.9, 125.9, 125.5, 125.3, 124.8, 124.1, 123.1, 121.0, 113.1, 13.1. Anal. Calc. for $C_{20}H_{15}N_3O_2$ (%): C, 72.94; H, 4.59; N, 12.76. Found (%): C, 72.60; H, 4.55; N, 12.58.

L11: Off-white powder (Yield: 34.4%). ESI-MS in MeOH: found mass: 414.16 (100%), 805.24 (82%), Calc. mass for: $C_{25}H_{17}N_3NaO_2$, 414.12 $[M+Na]^+$, $C_{50}H_{34}N_6NaO_4$, 805.25 $[2M+Na]^+$. ^1H NMR δ ppm ($CDCl_3$): 15.29 (s, 1H, NH), 8.99 (s, 1H, ArH), 8.18-8.15 (m, 2H, 2 x ArH), 7.96 (d, 1H, *J* = 8.1 Hz, ArH), 7.89-7.84 (m, 2H, 2 x ArH), 7.70-7.66 (m, 4H, 4 x ArH), 7.55-7.41 (m, 6H, 6 x ArH). ^{13}C NMR δ ppm ($CDCl_3$): 155.9, 153.0, 148.7, 148.1, 148.0, 137.6, 137.5, 130.5, 129.5, 129.3, 128.9, 128.6, 128.6, 128.4, 128.0, 127.3, 126.7, 125.4, 124.4, 123.5, 123.3, 112.3, 110.9. Anal. Calc. for $C_{25}H_{17}N_3O_2$ (%): C, 76.71; H, 4.38; N, 10.74. Found (%): C, 76.41; H, 4.33; N, 10.77.

L12: Off-white powder (Yield: 44.0%). ESI-MS in DCM: found mass: 393.25 (94%), 807.22 (100%), Calc. mass for: $C_{24}H_{17}N_4O_2$, 393.14 $[M+H]^+$, $C_{48}H_{32}N_8NaO_4$, 807.24 $[2M+Na]^+$. ^1H NMR (DMSO-d_6) δ: 10.07 (s, 1H, NH), 8.66 – 8.47 (m, 1H, ArH), 8.33 (d, *J* = 8.1 Hz, 1H, ArH), 8.15 (s, 1H, ArH), 8.12 – 8.09 (m, 1H, ArH), 8.08 – 8.04 (m, 2H, 2 x ArH), 8.04 – 8.01 (m, 1H, ArH), 7.97 (d, *J* = 9.1 Hz, 1H, ArH), 7.81 (dd, *J* = 9.0, 0.6 Hz, 1H, ArH), 7.70 (dtd, *J* = 9.3, 8.1, 1.1 Hz, 3H, 3 x ArH), 7.63 – 7.59 (m, 1H, ArH), 7.58 – 7.54 (m, 2H, 2 x ArH). ^{13}C NMR δ ppm (DMSO-d_6): 155.9, 153.1, 151.8, 149.0, 148.7, 138.5, 137.9, 130.7, 129.5, 129.4, 128.0, 127.9, 127.8, 126.1, 125.6, 124.6, 124.5, 123.3, 113.3. Anal. Calc. for $C_{24}H_{16}N_4O_2 \cdot 0.75MeOH$ (%): C, 71.38; H, 4.60; N, 13.45. Found (%): C, 71.06; H, 4.26; N, 13.13.

L13: Off-white powder (Yield: 62.5%). ESI-MS in MeOH: found mass: 353.07 (100%), 683.07 (54%), Calc. mass for: $C_{19}H_{14}N_4NaO_2$, 353.10 $[M+Na]^+$, $C_{38}H_{28}N_8NaO_4$, 683.21 $[2M+Na]^+$. ^1H NMR δ ppm (DMSO-d_6): 11.23 (s, 1H, NH), 9.32 (d, 1H, J = 1.4 Hz, ArH), 8.72 (dd, 1H, J = 1.5, 2.5 Hz, ArH), 8.70 (d, 1H, J = 2.6 Hz, ArH), 8.54 (s, 1H, ArH), 8.41 (d, 1H, J = 8.5 Hz, ArH), 8.12 (d, 1H, J = 8.1 Hz, ArH), 8.05 (d, 1H, J = 9.0 Hz, ArH), 7.92 (d, 1H, J = 9.2 Hz, ArH), 7.72 (td, 1H, J = 1.6, 7.1, 8.0 Hz, ArH), 7.61 (td, 1H, J = 1.1, 7.0, 8.1 Hz, ArH), 2.54 (s, 3H, CH_3). ^{13}C NMR δ ppm (DMSO-d_6): 153.1, 144.9, 144.0, 142.9, 130.6, 129.4, 129.3, 129.2, 128.5, 128.0, 127.9, 126.0, 125.9, 124.1, 123.0, 122.9, 113.1, 113.0, 12.9. Anal. Calc. for $C_{19}H_{14}N_4O_2$ (%): C, 69.08; H, 4.27; N, 16.96. Found (%): C, 69.24; H, 4.15; N, 16.73.

Synthesis of Cu(II), Zn(II), and Ga(III) complexes using tridentate ligands

General synthetic procedure for the synthesis of Cu(II) complexes of the tridentate ligands, L10-L13

The tridentate hydrazones, L10-L13 (1 equivalent), were mixed with 1 equivalent of $Cu(OAc)_2.H_2O$ (in the case of L10-L12) or $CuCl_2$ (in the case of L13) in a hot solvent mixture, MeOH:CH_2Cl_2 (1:1), with constant stirring. The reaction mixture was then refluxed for 4-5 h. The reaction mixture was allowed to cool to RT and the resulting precipitate was collected, washed with diethyl ether (10 mL), and dried *in vacuo*. The use of $[Cu(OAc)_2]$ facilitated ligand deprotonation due to the basic nature of the acetate anion, while $CuCl_2$ did not promote deprotonation, consistent with the weaker basicity of chloride. This difference directly influenced the observed protonation states of the coordinated ligands.

[Cu(L10)(OAc)]: Dark Green powder (Yield: 42.3%). ESI-MS in DMF/MeOH: found mass: 472.97 (100%), Calc. mass for $C_{22}H_{17}CuN_3NaO_4$: 473.04 $[M+Na]^+$. Anal. Calc. for $C_{22}H_{17}CuN_3O_4$ (%): C, 58.60; H, 3.80; N, 9.32. Found (%): C, 58.97; H, 3.77; N, 9.40.

[Cu(L11)(OAc)]: Dark green powder (Yield: 95.9%). ESI-MS in CH_3CN: found mass: 965.24 (100%), Calc. mass for $C_{52}H_{35}Cu_2N_6O_6$: 965.12 $[2M-OAc]^+$. Anal. Calc. for $C_{27}H_{19}CuN_3O_4 \cdot 0.5MeOH$ (%): C, 62.44; H, 4.00; N, 7.94. Found (%): C, 62.16; H, 4.10; N, 7.64.

[Cu(L12)(OAc)]: Dark green powder (Yield: 44.4%). ESI-MS in CH_3CN: found mass: 536.11 (100%), Calc. mass for $C_{26}H_{18}CuN_4NaO_4$: 536.05 $[M+Na]^+$. Anal. Calc. for $C_{26}H_{18}CuN_4O_4 \cdot 3H_2O$ (%): C, 54.98; H, 4.26; N, 9.86. Found (%): C, 54.70; H, 3.95; N, 9.53.

[Cu(L13)Cl_2]: Reddish brown powder (Yield: 78.1%). ESI-MS in DMF/MeOH: found mass: 465.09 (100%), Calc. mass for $C_{19}H_{15}Cl_2CuN_4O_2$: 465.8 $[M+H]^+$. Anal. Calc. for $C_{19}H_{14}Cl_2CuN_4O_2$ (%): C, 49.10; H, 3.04; N, 12.05. Found (%): C, 49.20; H, 2.81; N, 11.91.

General synthetic procedure for the synthesis of Zn(II) complexes of the tridentate ligands, L10-L13

Equimolar quantities of the tridentate hydrazones L10-L13 and $ZnCl_2$ were dissolved in a 1:1 mixture of MeOH:CH_2Cl_2 (1:1 toluene: MeOH in the case of L11) with constant stirring. The reaction mixture was then refluxed for 4-5 h and then allowed to cool to RT. The precipitates were collected, washed with diethyl ether (10 mL), and dried *in vacuo*.

[Zn(L10)Cl_2]: Light yellow powder (Yield: 42.9%). ESI-MS in MeOH: found mass: 464.01 (100%), Calc. mass for $C_{20}H_{14}Cl_2N_3O_2Zn$: 463.97 $[M-H]^-$. ^1H NMR (DMSO-d_6) δ 11.55. 11.17 (s, 1H), 8.65 (s, 1H), 8.54 (s, 1H), 8.46 – 8.39 (m, 1H), 8.20 – 8.03 (m, 4H), 7.92 (d, J = 9.1 Hz, 1H), 7.76 – 7.58 (m, 3H), 2.64 (s, 3H). ^{13}C NMR δ ppm (DMSO-d_6): 153.25, 152.86, 149.66, 149.00, 148.39, 139.30, 137.99, 130.61, 129.40, 128.02, 127.90, 126.00, 124.16, 123.12, 121.63, 113.11, 13.48. Anal. Calc. for $C_{20}H_{15}Cl_2N_3O_2Zn$ (%): C, 51.59; H, 3.25; N, 9.02. Found (%): C, 51.49; H, 3.22; N, 8.80.

[Zn(L11)Cl_2]: Bright yellow powder (Yield: 29.9%). ESI-MS in MeOH: found mass: 526.01 (100%), Calc. mass for $C_{25}H_{16}Cl_2N_3O_2Zn$: 525.99 $[M-H]^-$. ^1H NMR δ ppm (DMSO-d_6): 9.18 (s, 1H), 8.66 (d, J = 4.4 Hz, 1H), 8.50 (d, J = 8.3 Hz, 2H), 8.14 – 7.98 (m, 7H), 7.72 – 7.53 (m, 6H). ^{13}C NMR δ ppm (DMSO-d_6): 155.42, 152.61, 151.26, 148.66, 148.47, 148.27, 138.07, 137.95, 137.49, 130.20, 128.94, 128.79, 127.51, 127.23, 125.67, 125.16, 125.04, 124.10, 123.91, 122.81, 112.85. Anal. Calc. for $C_{25}H_{17}Cl_2N_3O_2Zn \cdot 1.5H_2O$ (%): C, 54.13; H, 3.63; N, 7.57. Found (%): C, 53.97; H, 3.80; N, 7.37.

[Zn(L12)Cl_2]: Bright yellow powder (Yield: 78.4%). ESI-MS in MeOH: found mass: 527.11 (100%), Calc. mass for $C_{24}H_{15}Cl_2N_4O_2Zn$: 526.98 $[M-H]^-$. ^1H NMR (DMSO-d_6): δ 9.13 (s, 1H), 8.66 (s, 1H), 8.49 – 8.45 (m, 2H), 8.05 (ddd, J = 27.1, 16.2, 8.2 Hz, 6H), 7.95 (s, 1H), 7.71 (t, J = 6.7 Hz, 2H), 7.65 – 7.55 (m, 3H). ^{13}C NMR δ ppm (DMSO-d_6): δ 153.09, 151.51, 149.00, 148.87, 146.88, 138.35, 130.64, 129.33, 127.96, 127.83, 127.77, 126.04, 125.53, 124.85, 124.61, 124.41, 123.29, 113.20, 111.79. Anal. Calc. for $C_{24}H_{16}Cl_2N_4O_2Zn$ (%): C, 54.52; H, 3.05; N, 10.60. Found (%): C, 54.36; H, 3.01; N, 10.45.

[Zn(L13)Cl_2]: Bright yellow powder (Yield: 49.3%). ESI-MS in MeOH: found mass: 464.95 (100%), Calc. mass for $C_{19}H_{13}Cl_2N_4O_2Zn$: 464.97 $[M-H]^-$. ^1H NMR (DMSO-d_6): δ 9.32 (s, 1H), 8.70 (s, 1H), 8.51

(dd, J = 87.1, 52.2 Hz, 2H), 8.07 (dd, *J* = 36.5, 8.4 Hz, 3H), 7.92 (d, *J* = 9.0 Hz, 1H), 7.67 (dt, *J* = 55.3, 7.4 Hz, 3H), 3.18 (s, 3H). ^{13}C NMR δ ppm (DMSO-d_6): 153.09, 130.60, 129.38, 128.05, 127.88, 127.81, 125.92, 124.16, 113.13, 12.88. Anal. Calc. for $C_{19}H_{14}Cl_2N_4O_2Zn$ (%): C, 48.91; H, 3.02; N, 12.01. Found (%): C, 48.59; H, 3.03; N, 11.70.

General synthetic procedure for the synthesis of Ga(III) complexes of the tridentate ligands, L10-L13

A hot alcoholic solution (15 mL) of tridentate hydrazones L10-L13 (1 mmol) was added slowly, with constant stirring, to a hot methanolic solution (15 mL) of $Ga(NO_3)_3 \cdot H_2O$ (0.5 mmol), and the resulting solution was refluxed for 4 h. After cooling the reaction mixture to room temperature, the resulting solid product was collected by filtration, washed with diethyl ether, dried under vacuum, and recrystallized from methanol.

[Ga(L10)$_2$](NO$_3$): Orange powder (Yield: 75%). ESI-MS (positive mode) in MeOH, found mass: 725.21 (100%). Calc. mass for $C_{40}H_{28}N_6O_4Ga$, 725.14 $[M - NO_3]^+$. ^{1}H NMR (DMSO-d_6) δ 8.56 (d, *J* = 7.9 Hz, 1H), 8.51 (s, 1H), 8.47 (t, *J* = 7.7 Hz, 1H), 8.43 (d, *J* = 8.2 Hz, 1H), 8.38 (d, *J* = 4.9 Hz, 1H), 8.08 (d, *J* = 8.0 Hz, 1H), 8.02 (d, *J* = 9.2 Hz, 1H), 7.88 (d, *J* = 9.1 Hz, 1H), 7.84 (t, *J* = 6.2 Hz, 1H), 7.67 (t, *J* = 7.5 Hz, 1H), 7.58 (t, *J* = 7.4 Hz, 1H), 3.13 (s, 3H). ^{13}C NMR δ ppm (DMSO-d_6): 166.77, 155.65, 154.09, 148.04, 147.18, 146.01, 144.64, 130.73, 129.59, 129.45, 128.03, 126.44, 126.17, 124.52, 123.55, 113.35, 113.17, 14.56. Anal. Calc. (%) for $C_{40}H_{28}N_6O_4Ga \cdot NO_3$: C 60.94, H 3.58, N 12.44. Found: C 60.61, H 3.23, N 12.08.

[Ga(L11)$_2$](NO$_3$): Orange powder (Yield: 49%). ESI-MS (positive mode) in MeOH, found mass: 849.17 (100%). Calc. mass for $C_{50}H_{32}N_6O_4Ga$, 849.15 $[M - NO_3]^+$. ^{1}H NMR (DMSO-d_6) δ 8.55 (d, *J* = 5.1 Hz,

1H), 8.48 (d, *J* = 5.8 Hz, 1H), 8.45 – 8.38 (m, 2H), 8.18 (dd, *J* = 6.4, 2.7 Hz, 2H), 8.06 – 7.98 (m, 3H), 7.93 – 7.88 (m, 4H), 7.84 (d, *J* = 9.1 Hz, 1H), 7.64 (t, *J* = 7.5 Hz, 1H), 7.56 (t, *J* = 7.8 Hz, 1H). ^{13}C NMR δ ppm (DMSO-d_6): 167.87, 154.13, 152.31, 147.72, 147.64, 145.64, 144.68, 132.34, 131.23, 130.57, 129.75, 129.37, 129.29, 128.29, 128.07, 127.87, 126.07, 124.46, 123.41, 114.03, 113.01. Anal. Calc. (%) for $C_{50}H_{32}N_6O_4Ga{\cdot}NO_3$: C 65.81, H 3.53, N 10.74. Found: C 65.78, H 3.38, N 10.87.

[Ga(L12)$_2$](NO$_3$): Orange powder (Yield: 73%). ESI-MS (positive mode) in MeOH, found mass: 851.21 (100%). Calc. mass for $C_{48}H_{30}N_8O_4Ga$, 851.16 $[M - NO_3]^+$. ^{1}H NMR (DMSO-d_6) δ 9.06 (d, *J* = 4.8 Hz, 1H), 8.74 (d, *J* = 7.8 Hz, 1H), 8.61 (d, *J* = 5.2 Hz, 1H), 8.57 (s, 1H), 8.45 – 8.39 (m, 3H), 8.34 (d, *J* = 8.0 Hz, 1H), 8.05 (d, *J* = 8.0 Hz, 1H), 8.00 (d, *J* = 4.9 Hz, 1H), 7.92 – 7.88 (m, 2H), 7.83 (d, *J* = 9.2 Hz, 1H), 7.65 (t, *J* = 7.7 Hz, 1H), 7.55 – 7.54 (t, *J* = 7.9 Hz 1H). ^{13}C NMR δ ppm (DMSO-d_6): 168.39, 154.46, 150.41, 149.01, 147.63, 147.60, 147.57, 145.39, 144.52, 138.07, 130.82, 130.73, 130.13, 129.87, 129.73, 129.66, 129.47, 129.02, 128.06, 128.02, 127.11, 126.27, 125.71, 124.62, 123.60, 114.72, 113.18. Anal. Calc. (%) for $C_{48}H_{30}N_8O_4Ga{\cdot}NO_3$: C 63.04, H 3.31, N 13.78. Found: C 62.88, H 3.19, N 13.62.

[Ga(L13)$_2$](NO$_3$)

Orange powder (Yield: 65%). ESI-MS (positive mode) in MeOH, found mass: 727.11 (100%). Calc. mass for $C_{38}H_{26}N_8O_4Ga$, 727.13 $[M - NO_3]^+$. ^{1}H NMR δ ppm (DMSO-d_6): 9.84 (s, 1H), 9.31, 9.14 (d, J = 2.7 Hz, 2H), 8.71 (dd, J = 11.1, 2.0 Hz, 2H), 8.54 (s, 2H), 8.41 (dd, J = 16.1, 8.6 Hz, 3H), 8.13 – 8.04 (m, 4H), 7.90 (dd, J = 20.7, 9.1 Hz, 2H), 7.70 – 7.62 (m, 4H), 3.18 , 2.87 (s, 6H). ^{13}C NMR δ ppm (DMSO-d_6):166.73, 154.74, 154.10, 153.08, 151.38, 150.84, 147.51, 147.41, 144.92, 143.93, 142.92, 140.58, 139.49, 130.62, 130.59, 129.71, 129.42, 129.33, 129.24, 128.08, 127.94, 127.89, 126.09, 125.98, 124.36,

124.08, 123.52, 123.40, 123.03, 113.73, 113.11, 112.99, 14.55. Anal. Calc. (%) for $C_{38}H_{26}N_8O_4Ga{\cdot}NO_3$: C 57.74, H 3.32, N 15.95. Found: C 57.38, H 3.10, N 15.58.

Calculation of log P_{calc}

For the ligands and Ga(III) complexes, log P_{calc} was calculated using Molinspiration cheminformatics (SK-900 26, Slovensky Grob, Slovak Republic).

***n*-Octanol/Water Partition Coefficient (log *P*) Determination**

The *n*-octanol/water partition coefficient (log *P*) was determined using the shake-flask method. *n*-Octanol and water were mutually pre-saturated by mixing (1:1 *v/v*) overnight at 25 °C. Calibration curves were prepared for each compound (5–25 μM) in both *n*-octanol and water to confirm Beer–Lambert linearity at the selected analytical wavelength. Equal volumes (5 mL each) of pre-saturated *n*-octanol and water phases were combined, and the compound was added to achieve a final concentration of 50–100 μM. The mixture was shaken for 30 min/25 °C, centrifuged (3000 rpm, 3 min), and allowed to separate completely. Aliquots from both phases were analyzed by UV–Vis spectrophotometry, and concentrations were determined from the respective calibration plots. The partition coefficient was calculated using; partition coefficient (P) = C_{oct}/C_{aq}, and log P = $\log_{10}$ (P). where C_{oct} and C_{aq} are the equilibrium concentrations in the *n*-octanol and aqueous phases, respectively. Each measurement was performed in triplicate, and values are reported as mean ± SD.

Transmetalation Studies of the L12-Ga(III), Zn(II), and Cu(II) Complexes

Titration Studies Using UV-Vis Spectrophotometry

The Ga(III) and Zn(II) complexes of L12 (50 μM) were titrated with increasing concentrations (5–50 μM) of [$Cu(OAc)_2$], while the Ga(III), Zn(II), and Cu(II) complexes of L12 were titrated with either

Fe(III) citrate (1:100 metal-to-citrate molar ratio), or Fe(II) Asc (1:100 metal-to-ascorbate molar ratio) in DMSO/H_2O (7:3 *v/v*) to ensure solubility. The Fe(III) citrate was freshly prepared immediately before an experiment by mixing $FeCl_3$ and sodium citrate in a 1:100 molar ratio to ensure Fe(III) remained soluble, leading to a pale-yellow solution. The Fe(II) Asc was also immediately prepared before each study by mixing $(NH_4)_2Fe(SO_4)_2$ with sodium Asc (1:100 metal-to-ascorbate molar ratio) to ensure an aqueous solution of Fe(II) that was pale green. As controls, titrations were also performed with increasing concentrations (5–70 μM) of sodium citrate and sodium Asc alone, using the Ga(III) and Zn(II) complexes (50 μM).

Ligand binding studies of L12 were performed with increasing concentrations of Fe(III) citrate and Fe(II) Asc (5–70 μM) in DMSO/H_2O (7:3 *v/v*), 100% DMSO, or NaCl (0.14 M)/HEPES buffer (pH 7.4). After each titer was added and vigorously mixed, it was incubated for 5 min/20 °C. The UV-Vis spectrum was then recorded using a Shimadzu UV-Vis spectrophotometer (UV-1800; Shimadzu, Kyoto, Japan).

Liquid Chromatography-Mass Spectroscopy (LC-MS) and Direct MS

The transmetalation of the Ga(III), Zn(II), and Cu(II) complexes of the ligand SL12 were studied by preparing equimolar solutions (1 mM) of the Ga(III) or Zn(II) complexes with either [$Cu(OAc)_2$], Fe(III) citrate (molar ratio: 1:100), or Fe(II) Asc (molar ratio: 1:100) in DMSO/H_2O (7:3 *v/v*). Similarly, the transmetalation of the Cu(II) complexes was studied under the same conditions with Fe(III) citrate, or Fe(II) Asc. Reactivity studies were also conducted using equimolar solutions (1 mM) of Asc and citrate with the Ga(III), Zn(II), and Cu(II) complexes (1 mM). The mixtures were incubated for 24 h/20 °C on an orbital mixer set at 200 rpm. Control samples containing only the Ga(III), Zn(II), and Cu(II) complexes in DMSO/H_2O (7:3 *v/v*) were also incubated under the same conditions.[7, 8] Following

incubation, all samples were diluted 1:1 with methanol to improve ionization efficiency before MS analysis. The samples were then analyzed using LC-MS with a C18 column (implementing a mobile phase consisting of 90% MeOH, 9.9% water, and 0.1% formic acid) in positive ionization mode and direct injection MS in positive ionization mode. All MS analyses were conducted on a Thermo Fisher ISQ™ EM Single Quadrupole Mass Spectrometer (Thermo Fisher, MA) with electrospray ionization (ESI), following our established protocols to detect potential transmetalation products.[7, 9]

Assessment of ROS Generation of Naphthofuran-Based Tridentate Ligands (L10-L13) and their Cu(II) and Ga(III) Complexes

Reactive oxygen species (ROS) generation was evaluated using a validated fluorescence-based method that detects the oxidation of 2′,7′-dichlorodihydrofluorescein diacetate (H_2DCF-DA) into its fluorescent product, 2′,7′-dichlorofluorescein (DCF). Stock solutions (5 mM) of $CuCl_2$, tetrathiomolybdate (TM), the naphthofuran-based tridentate ligands (L10-L13), along with their Cu(II) complexes were prepared in DMSO.

Working solutions (10 μM) were prepared in either Hank's balanced salt solution (HBSS, pH 7.4) to simulate cytosolic conditions or 150 mM acetate buffer (pH 5) to simulate lysosomal conditions. To initiate the reaction, L-cysteine (100 μM) was added as a reducing agent, followed by H_2DCF (5 μM), which was generated by alkaline hydrolysis of H_2DCF-DA (Sigma-Aldrich) implementing NaOH.[9] Hydrogen peroxide (H_2O_2; 100 μM) was then introduced to induce hydroxyl radical formation. Control samples contained buffer, L-cysteine, H_2DCF, and H_2O_2 but lacked the ligands or their metal complexes. Fluorescence intensity was recorded using a CLARIOstar Plus microplate reader (BMG LABTECH, Australia) at an excitation wavelength of 485 nm and an emission wavelength of 530 nm.[4, 7, 9, 10]

The transmetalation of Ga(III) complexes of naphthofuran-based ligands was investigated under cytosolic (pH 7.4) and lysosomal (pH 5) conditions. Ga(III) complexes (10 μM) were incubated with $CuCl_2$ (10 μM) and L-cysteine (100 μM) in either HBSS or acetate buffer. H_2DCF (5 μM) was then introduced, followed by H_2O_2 (100 μM) to initiate hydroxyl radical formation. Reactions were incubated at 20°C for 2 to 12 minutes. To examine the role of Cu in redox activity, TM was added under three conditions: alone, in combination with $CuCl_2$, or alongside $CuCl_2$ and the naphthofuran-Ga(III) complexes. Fluorescence measurements were performed as described above.[7]

BIOLOGICAL STUDIES

Cell culture

SK-N-MC neuroepithelioma cells, MCF-7, and MDA-MB-231 breast cancer cells were obtained from the American Type Culture Collection (ATCC®, Manassas, VA). The cells were maintained in an incubator (Forma Scientific, Marietta, OH) using a humidified atmosphere at 37 ºC and containing 5% CO_2. Authentication of the cells was based on viability, growth, recovery, and morphology, as well as by cytogenetic analysis, antigen expression, and isoenzymology by the provider. Cells were grown in Eagle's minimal essential medium (MEM; Invitrogen; CA), supplemented with 10% fetal calf serum (FCS; Sigma), 1% penicillin/streptomycin/glutamine (Gibco, Vic, Australia), 1% non-essential amino acids (Gibco), sodium pyruvate (Invitrogen) and Fungizone™ (0.28 ng/mL; Gibco), at 37°C in an atmosphere of 5% CO_2/21% O_2.

MTT proliferation assay

The effect of the bidentate and tridentate ligands and their Cu(II), Zn(II), and Ga(III) complexes on cellular proliferation was determined *via* the MTT (3-(4,5-dimethylthiazol-2-yl)-2,5-diphenyltetrazolium

bromide) assay using well-established procedures.[13] Briefly, SK-N-MC, MCF-7, and MDA-MB-231 cells were seeded in 96-well microtiter plates at 1.5×10^4 cells/well and allowed to adhere overnight. After 24 h/37°C, the agents (0-12.5 μM) were added and incubated in a humidified atmosphere of 5% CO_2/95% air for 72 h/37°C. After this incubation, 20 μL of MTT (5 mg/mL) was added to each well and further incubated for 2 h/37°C. After dissolving the cells in 100 μL of DMSO, the absorbance was measured at 570 nm. Viable cell counts using Trypan blue were proportional to MTT color formation.[13]

Gallium uptake determined by inductively coupled plasma–mass spectrometry (ICP-MS).

SK-N-MC cells (5×10^5) were seeded in T75 flasks and, after 24 h/37°C, treated with vehicle (untreated control), $[Ga(NO_3)_3]$, or $[Ga(L12)_2]^+$ (25 μM) for 4 h/37°C. Following incubation, cells were washed three times with 0.9% NaCl, detached using trypsin, and centrifuged (1200 rpm/3 min/4 °C). The washing–centrifugation cycle was repeated twice. The cell pellet was digested in 250 μL of analytical grade HNO_3 (Sigma; 65%), diluted to 3 mL with water (final HNO_3; 2% v/v), and analyzed by ICP–MS (Agilent 720 ICP-OES). Gallium content was quantified using calibration standards and expressed as μg of Ga/10^5 cells.

Intracellular reactive oxygen species (ROS) Measurement by DCF Assay

SK-N-MC cells (6×10^5) were seeded in black 96-well plates and allowed to adhere for 24 h/37 °C. The medium was then replaced with medium alone (control) or medium containing 5 μM of $CuCl_2$, tetrathiomolybdate (TM), $[Ga(NO_3)_3]$, or ligands L10–L13 and their respective Cu(II) and Ga(III) complexes. For transmetalation experiments, Ga(III) complexes of L10–L13 (5 μM) were co-incubated with $CuCl_2$ (5 μM). After a 4 h/37 °C incubation, 2′,7′-dichlorodihydrofluorescein diacetate (DCF-DA;

10 μM, Sigma-Aldrich) was added and the cells incubated for 30 min/37 °C in the dark. Fluorescence was measured at λ_{ex} = 485 nm and λ_{em} = 530 nm using a BMG Labtech FLUOstar Omega plate reader.

Human transferrin labeled with ^{59}Fe

The human iron-transport protein, transferrin (Tf; Sigma-Aldrich), was labeled with iron-59 (^{59}Fe; PerkinElmer Life and Analytical Sciences, Boston, MA) to generate diferric holo-Tf (*i.e.*, $^{59}Fe_2$-Tf), using well-established methods.[11, 12]

Examination of ^{59}Fe mobilization by the novel ligands from SK-N-MC cells prelabelled with ^{59}Fe

The effect of the novel ligands and control chelators on ^{59}Fe efflux from SK-N-MC cells prelabelled with ^{59}Fe was determined by cellular ^{59}Fe mobilization experiments using a well-established protocol.[11, 13, 14] Briefly, SK-N-MC cells were prelabeled with ^{59}Fe implementing $^{59}Fe_2$-transferrin (0.75 μM), using a 3 h/37°C incubation. The cells were then washed four times on ice with ice-cold PBS and then reincubated for 3 h/37°C with either control media (MEM), or this medium containing either the control chelators, namely desferrioxamine (DFO; 25 μM), 311 (25 μM), DpC (25 μM), Dp44mT (25 μM), or the novel ligands (25 μM). Three technical replicates were implemented *per* sample *per* experiment, and the experiment repeated three times.

Inhibition of $^{59}Fe_2$-Tf uptake from $^{59}Fe_2$-Tf by the novel ligands using SK-N-MC cells

To determine the efficacy of the new ligands and the positive control chelators to intercept and prevent the cellular uptake of ^{59}Fe from the iron-transport protein, $^{59}Fe_2$-Tf, standard procedures using SK-N-MC cells were utilized.[11, 14, 15] Briefly, SK-N-MC cells were incubated for 3 h/37°C with ^{59}Fe-Tf (0.75 μM) in either control media (MEM), or this medium containing either DFO; 25 μM), 311 (25 μM), DpC (25

μM), Dp44mT (25 μM), or the novel ligands (25 μM). Three technical replicates were implemented *per* sample *per* experiment and the experiment then repeated three times.

In the studies examining cellular ^{59}Fe mobilization and ^{59}Fe uptake from $^{59}Fe_2$-Tf above, there was no decrease in viability during the very short incubation (*i.e.*, 3 h/37°C) with any of the ligands, as determined by Trypan blue staining and phase contrast microscopy.

Statistical Analysis

Results for all biological experiments were generated from three independent experiments and presented as mean ± standard deviation (SD). Data were normally distributed around the mean with Student's paired *t*-test being used for statistical analysis implementing GraphPad Prism 9.2.0 software (Boston, MA). Data were considered statistically significant when $p < 0.05$.

Supporting Results and Discussion

Transmetalation of [Zn(L12)Cl$_2$] with Cu(II) Acetate, Fe(III) Citrate, or Fe(II) Asc

UV-Vis spectrophotometry was first used to assess transmetalation of [Zn(L12)Cl_2] (pale yellow solution) with Cu(II) acetate, Fe(III) citrate, or Fe(II) Asc (**Fig. S6A-C**). These studies may also aid in explaining the lower anti-proliferative activity of [Zn(L12)Cl_2] *versus* $[Ga(L12)_2]^+$ (see paper; **Table 2**).

Titration of [Zn(L12)Cl$_2$] with Cu(II) Acetate

[Zn(L12)Cl_2] exhibited two moderately intense peaks (black dotted line; **Fig. S6A**), one at 363 nm, attributed to $\pi \rightarrow \pi^*$ transitions within the L12 naphthofuran ligand, and another at 410 nm, assigned to a LMCT.[16] Titration of [Zn(L12)Cl_2] with [Cu(OAc)$_2$] (5–50 μM) resulted in the development of a more intensely yellow solution (**Fig. S6A**). A single isosbestic point was observed at 376 nm, accompanied by

a bathochromic shift from 410 nm to 419 nm and the disappearance of the 363 nm peak (**Fig. S6A**). The resulting spectrum is superimposable with that of synthesized [Cu(L12)(OAc)] (solid blue line; **Fig. S6A**), confirming complete transmetalation in 70% DMSO/30% water. Similar observations were also obtained using 100% DMSO (data not shown). This conclusion was confirmed by direct MS, where only $[Cu(L12)DMSO]^+$ was evident after mixing equimolar concentrations of $[Zn(L12)Cl_2]$ with $[Cu(OAc)_2]$ (**Fig. S7A, C**). Under dissociative conditions using LC-MS,[7, 8] L12, $[Cu(L12)DMSO]^+$ and $[Cu(L12)_2]$ were observed upon mixing $[Zn(L12)Cl_2]$ with $[Cu(OAc)_2]$ (**Fig. S7B, D**). In summary, these studies demonstrating complete transmetalation of $[Zn(L12)Cl_2]$ with $[Cu(OAc)_2]$ were similar to those showing the facile transmetalation of $[Ga(L12)_2]^+$ with $[Cu(OAc)_2]$ (see paper; **Fig. 4A**).

Titration of [Zn(L12)Cl$_2$] with Fe(III) Citrate

Upon incremental titration of $[Zn(L12)Cl_2]$ (50 μM) with Fe(III) citrate (1:100 metal-to-citrate molar ratio; 5–50 μM), a single isosbestic point at 376 nm was evident (**Fig. S6B**). This change was accompanied by a small hypsochromic shift from 410 nm to 407 nm, with the disappearance of the 363 nm peak and the solution remaining pale yellow (**Fig. S6B**). The spectrum of $[Zn(L12)Cl_2]$ after titration of Fe(III) citrate (**Fig. S6B**) was different to that obtained after titration of $[Ga(L12)_2]^+$ with Fe(III) citrate (see paper; **Fig. 4B**), where the solution turned from pale yellow to colorless, suggesting formation of different species in each case. This alteration was examined further using direct MS and LC-MS analysis after mixing equimolar $[Zn(L12)Cl_2]$ with Fe(III) citrate (500 μM), which resulted in L12 and $[Zn(L12)citrate]^+$ (**Fig. S7E, F**). In contrast, mixing equimolar $[Ga(L12)_2]^+$ with Fe(III) citrate (500 μM) led, after direct MS (**Fig. 5E**) or LC-MS (**Fig. 5F**), to both L12 and $[Ga(citrate)_2]$. It is notable from this analysis that $[Zn(L12)Cl_2]$ did not completely dissociate, with the formation of a mixed Zn(II) complex with both L12 and citrate, and again, L12 did not form an Fe(III) complex upon adding Fe(III) citrate.

Additional experiments with [Zn(L12)$_2$] titrated with increasing concentrations of $FeCl_3$ in 100% DMSO also demonstrated no dissociation and transmetalation (**Fig. S8A**), indicating the critical role of citrate.

Thus, the reaction of [Zn(L12)Cl_2] with Fe(III) citrate was in contrast to the titration of $[Ga(L12)_2]^+$ with Fe(III) citrate, which led to the complete dissociation of $[Ga(L12)_2]^+$ and the formation of Ga(III) citrate complexes and L12 (see paper; **Fig. 5E, F**). The complete dissociation of $[Ga(L12)_2]^+$ may help to partly explain the greater amplification of the anti-proliferative activity of L12 relative to the incomplete dissociation of [Zn(L12)Cl_2] (see paper; **Table 2**). In this case, the complete liberation of L12 from $[Ga(L12)_2]^+$ would be beneficial in two ways. First, L12 could effectively intercept crucial cellular Fe(II) pools needed for proliferation.[17-19] Second, the release of Ga(III) would enable the inactivation of key Fe-containing cellular enzymes such as ribonucleotide reductase. [20-25]

To further understand the coordination dynamics, [Zn(L12)Cl_2] was also titrated with citrate alone (**Fig. S8B**). This resulted in a pale yellow solution and the disappearance of the 363 nm peak, suggesting a ligand exchange reaction with the potential formation of $[Zn(L12)citrate]^+$. This hypothesis was confirmed using direct MS (**Fig. S9C**) and LC-MS (**Fig. S9D**), where L12 and $[Zn(L12)citrate]^+$ were identified upon mixing equimolar [Zn(L12)Cl_2] and citrate (500 μM). Hence, in contrast to $[Ga(L12)_2]^+$ (**Fig. S5C, D**), where upon adding citrate there was complete ligand exchange to $[Ga(citrate)_2]$, this does not occur for [Zn(L12)Cl_2], where a mixed ligand complex eventuates *i.e.*, $[Zn(L12)citrate]^+$. These observations again demonstrate the difference in dissociation between the Ga(III) and Zn(II) complexes of L12 that could be significant in interpreting their differences in anti-proliferative activity (see paper; **Table 2**).

Titration of [Zn(L12)Cl_2] with Fe(II) Asc

Similarly to [Ga(L12)$_2$]$^+$ (**Fig. 4C**), [Zn(L12)Cl_2] was also titrated with Fe(II) Asc (1:100 metal-to-Asc molar ratio; 5–50 μM) to investigate coordination chemistry (**Fig. S6C**). Titration of [Zn(L12)Cl_2] (50 μM) with increasing concentrations of Fe(II) Asc (1:100 metal-to-ascorbate molar ratio; 5–50 μM), revealed even after the initial addition of Fe(II) Asc (5 μM), the disappearance of the 356 nm band of [Zn(L12)Cl_2], with a minor hypsochromic shift from 410 nm to 407 nm and a single isosbestic point at 376 nm (**Fig. S6C**). The solution changed from pale yellow to pale green, suggesting the formation of a Fe(II) complex. However, these spectra did not completely match the Fe(II) Asc titration studies of [Ga(L12)$_2$]$^+$, where an isosbestic point occurred at 370 nm and a bathochromic shift was observed from 356 nm to 391 nm, with the development of a dark green color and a robust MLCT band at 680 nm (see paper; **Fig. 4C**).

This difference in the spectra after titration of [Zn(L12)Cl_2] or [Ga(L12)$_2$]$^+$ with Fe(II) Asc suggests potential differences in the species formed, and this was confirmed using direct MS and LC-MS (**Fig. S7G, H,** relative to **Fig. 5G, H**). In fact, titration of [Zn(L12)Cl_2] with Fe(II) Asc led after direct MS to a mixture of L12, [Zn(L12)Asc]$^+$, and [Fe(L12)$_2$] (**Fig. S7G**). Similarly, under the more dissociative conditions of LC-MS,[7, 8] titration of [Zn(L12)Cl_2] with Fe(II) Asc resulted in L12, [Zn(L12)Asc]$^+$, and [Fe(L12)Asc] (**Fig. S7H**). Relevant to these observations, when [Zn(L12)Cl_2] was titrated with Asc alone (**Fig. S8C)**, this resulted in a pale yellow solution and the disappearance of the 363 nm peak, suggesting a ligand exchange reaction with the potential formation of [Zn(L12)Asc]$^+$. In fact, both direct MS and LC-MS demonstrated the addition of Asc alone to [Zn(L12)Cl_2] resulted in dissociation of the free ligand and the formation of [Zn(L12)Asc]$^+$ (**Fig. S9E, F**). In summary, as observed for Fe(III) citrate (**Fig. S7E,**

F), in the presence of Fe(II) Asc, [Zn(L12)Cl_2] does not completely dissociate and transmetalate (**Figure S7G, H**), unlike the complete dissociation and transmetalation of $[Ga(L12)_2]^+$ (see paper; **Fig. 5G, H**).

Transmetalation of [Cu(L12)(OAc)] with Fe(III) Citrate or Fe(II) Asc

Considering the studies above with $[Ga(L12)_2]^+$ and [Zn(L12)Cl_2], UV-Vis spectrophotometry was then used to assess transmetalation of [Cu(L12)(OAc)] with Fe(III) citrate or Fe(II) Asc (**Fig. S10**). These studies may also aid in explaining the lower anti-proliferative activity of [Cu(L12)(OAc)] than $[Ga(L12)_2]^+$ (see paper; **Table 2**).

Titration of [Cu(L12)(OAc)] with Fe(III) Citrate

Upon gradual titration of [Cu(L12)(OAc)] (50 μM) with Fe(III) citrate (1:100 metal-to-citrate molar ratio; 5–50 μM), only a minor hypsochromic shift was observed, from 419 nm to 407 nm, without any noticeable color change **(Fig. S10A)**. The UV-Vis spectra of [Cu(L12)(OAc)] after titration with Fe(III) citrate **(Fig. S10A)** closely resembled that observed after titration with citrate alone **(Fig. S10B)**, suggesting a ligand exchange reaction leading to the potential formation of [Cu(L12)(citrate)]. This hypothesis was further investigated through direct MS and LC-MS analysis **(Figs. S11, S12)**, with direct MS revealing L12, [Cu(L12)(citrate)], and [Fe(citrate)] upon mixing equimolar amounts of [Cu(L12)(OAc)] (500 μM) with Fe(III) citrate (500 μM) (**Fig. S11C**).

Similar results demonstrating ligand exchange were also obtained under the more dissociative conditions of LC-MS,[7, 8] where this latter reaction led to L12 and [Cu(L12)(citrate)] (**Fig. S11D**). When equimolar [Cu(L12)(OAc)] was mixed with citrate alone (500 μM), direct MS (**Fig. S12C**) and LC-MS (**Fig. S12D**) demonstrated both L12 and [Cu(L12)(citrate)]. This analysis reveals that, analogous to [Zn(L12)Cl_2],

[Cu(L12)(OAc)] did not undergo transmetalation with Fe(III) citrate, forming a mixed Cu(II) complex with L12 and citrate.

Titration of [Cu(L12)(OAc)] with Fe(II) Asc

Analogously to the Ga(III) and Zn(II) complexes, the Cu(II) complex of L12 was titrated with Fe(II) Asc (1:100 metal-to-ascorbate molar ratio; 5–50 μM) or Asc (5–50 μM), with the solution being examined using UV-Vis (**Fig. S10C, D**), direct MS (**Fig. S11E, F**), and LC-MS (**Fig. S12E, F**). Titration of [Cu(L12)(OAc)] (50 μM) with increasing concentrations of Fe(II) Asc resulted in the appearance of a pale green color, suggesting the formation of an Fe(II) complex (**Fig. S10C**). This was accompanied by a hypsochromic shift from 419 nm to 398 nm and the emergence of an MLCT band at 680 nm, with a single isosbestic point at 409 nm (**Fig. S10C**). However, these spectra did not fully align with the L12 binding studies with Fe(II) Asc (**Fig. S3D-F**), where the maximum absorbance was observed at 391 nm (blue line in **Fig. S10C**).

To study this further, MS was performed after mixing equimolar amounts of [Cu(L12)(OAc)] with Fe(II) Asc, followed by direct MS analysis, which resulted in a mixture of L12, [Cu(L12)$(Asc)_2$], and [Fe(L12)HCOO] (**Fig. S11E**). The formate anion in the latter species arises from the formic acid in the mobile phase used for LC-MS (see *Experimental Section*). Under more dissociative LC-MS conditions,[7, 8] the analysis of mixing equimolar [Cu(L12)(OAc)] and Fe(II) Asc (500 μM) revealed the formation of L12, [Cu(L12)$(Asc)_2$], and [Fe(L12)Asc] (**Fig. S11F**). When equimolar [Cu(L12)(OAc)] was mixed with Asc alone (500 μM), the detection of L12 and [Cu(L12)$(Asc)_2$] was demonstrated by direct MS (**Fig. S12E**), while L12, [Cu(L12)$(Asc)_2$], and [Cu(L12)(Asc)] were detected after LC-MS (**Fig. S12F**).

Overall, these data indicate that similar to [Zn(L12)Cl_2], [Cu(L12)(OAc)] does not undergo complete dissociation followed by transmetalation with Fe(II) Asc, which was demonstrated with $[Ga(L12)_2]^+$ (**Fig. 5G, H**). This observation may explain the marked amplification of anti-proliferative activity observed for the Ga(III) complex of L12 relative to its Cu(II) and Zn(II) counterparts (**Table 2**), which do not completely liberate the cytotoxic L12 ligand (**Table 1**). As such, sequestration of L12 within the Cu(II) and Zn(II) complexes could prevent its effective delivery to the tumor cell and suppresses its cytotoxicity. Moreover, the complete dissociation of $[Ga(L12)_2]^+$ also results in Ga(III) release, which inhibits critical Fe-containing intracellular targets, such as ribonucleotide reductase. [20-25]

Table S1. Selected bond lengths of L1, L5, L7, L10, L11, L12 and L13.

	Distance (Å)						
Bond	**L1**	**L5**	**L7**	**L10**	**L11**	**L12**	**L13**
O1−C1	1.4001(15)	1.381(2)	1.390(3)	1.3823(18)	1.384(2)	1.409(5)	1.380(10)
O2−C2	-	-	-	1.2221(19)	1.221(2)	1.225(5)	1.245(10)
O2−C3	-	1.227(3)	1.235(3)	-	-	-	-
C1−C2	1.4396(18)	1.455(3)	1.457(3)	1.4777(18)	1.477(3)	1.466(5)	1.464(11)
C3−C4	-	1.494(3)	1.483(3)	1.4935(18)	1.492(2)	1.498(5)	1.502(11)
N1−N2	1.3702(16)	1.380(2)	1.364(3)	1.3769(16)	1.370(2)	1.367(4)	1.372(10)
N1−C2	1.2981(17)	1.297(3)	1.288(3)	1.3642(19)	1.358(2)	1.358(5)	1.368(11)
N2 –C3	1.3653(17)	1.363(3)	1.351(3)	1.2883(19)	1.299(2)	1.283(5)	1.272(11)
N3−C4	1.4591(17)	-	-	1.3385(19)	1.350(2)	1.349(5)	1.322(12)
N4−C5	1.3672(17)	-	-	-	-	-	-
S1−C3	1.6961(13)	-	-	-	-	-	-
S1−C4	-	-	1.714(3)	-	-	-	-

Table S2. Crystal and refinement data.

	L1	**L5**	**L10**	**L7**	**L11**	**L12**	**L13**	**[Zn(L11)Cl_2].CH_2Cl_2**
Empirical formula	$C_{13}H_{16}N_4OS$	$C_{21}H_{16}N_2O_2$	$C_{20}H_{15}N_3O_2$	$C_{19}H_{14}N_2O_2S$	$C_{25}H_{17}N_3O_2$	$C_{24}H_{16}N_4O_2$	$C_{19}H_{14}N_4O_2$	$C_{26}H_{19}Cl_4N_3O_2Zn$
Formula weight	276.36	328.36	329.35	334.38	391.41	392.41	330.34	612.61
Color	Brown	Light brown	Yellow	Brown	Off-white	Off-white	Off-white	Yellow
Crystal system	Monoclinic	Monoclinic	Monoclinic	Monoclinic	Monoclinic	Monoclinic	Monoclinic	Triclinic
Temperature (K)	100(2)	100(2)	100(2)	100(2)	100(2)	100(2)	100(2)	150(2)
Wavelength (Å)	1.54184	1.54184	1.54184	1.54184	1.54184	1.54184	1.54184	1.54184
Space group	$P2_1/c$	$P2_1/c$	$P2_1/c$	$P2_1/c$	$P2_1/c$	$P2_1/c$	Pn	$P\bar{1}$
a (Å)	11.9480(4)	14.606(1)	9.5986(4)	10.6903(5)	4.4595(2)	6.0168(5)	5.5860(4)	11.615(1)
b (Å)	8.2148(3)	5.3852(4)	5.3235(2)	18.2865(7)	24.1919(8)	18.990(2)	9.8008(7)	11.930(1)
c (Å)	14.0992(5)	19.669(1)	29.789(1)	8.5178(4)	17.1497(6)	16.529(1)	27.264(2)	11.894(1)
α (deg)	90	90	90	90	90	90	90	118.435(3)
β (deg)	104.638(4)	92.433(7)	92.314(4)	108.100(5)	90.031(4)	99.923(8)	93.122(6)	91.579(3)
γ (deg)	90	90	90	90	90	90	90	114.295(3)
Volume (Å^3)	1338.92(9)	1545.7(2)	1520.9(1)	1582.7(1)	1850.2(1)	1860.3(3)	1490.4(2)	1268.5(2)
Z	4	4	4	4	4	4	4	2
ρ_{calc} (g/cm^3)	1.371	1.411	1.438	1.403	1.405	1.401	1.472	1.604
R_1 (obsd data)	0.0306	0.0526	0.0382	0.0497	0.0446	0.0781	0.0888	0.0410
wR_2	0.0840	0.1459	0.1017	0.1358	0.1295	0.1872	0.2520	0.1019
GOF	1.054	1.096	1.028	1.046	1.031	1.141	1.080	1.070
CCDC	1982908	1982909	1982904	1982911	1982907	1982905	1982906	2424290

Table S3. Anti-proliferative activity (IC_{50} µM) of $[Ga(L12)_2]^+$, its free ligand (L12), $[Ga(NO_3)_3]$, and the reference compound DpC in SK-N-MC and MCF-7 cells after a 72 h/37 °C incubation. The Ga(III) complex shows a pronounced enhancement in cytotoxic potency relative to $[Ga(NO_3)_3]$, consistent with improved cellular uptake. Data represent mean ± SD (n = 3).

IC_{50} (µM) 72 h		
Compounds	**SK-N-MC**	**MCF-7**
DpC	0.007 ± 0.010	0.005 ± 0.010
$[Ga(NO_3)_3]$	88.611 ± 1.230	78.878 ± 1.960
[L12]	0.591 ± 0.070	0.699 ± 0.180
$[Ga(L12)_2]^+$	0.099 ± 0.010	0.292 ± 0.050

Table S4. Comparison between calculated and experimentally determined log *P* values for ligands (L10–L13) and their corresponding Ga(III) complexes. Calculated log *P* values were obtained from computational predictions, while experimental log *P* values represent the mean ± SD from three independent *n*-octanol–water partition experiments.

Compounds	Calculated log *P* values	Experimental log *P* values

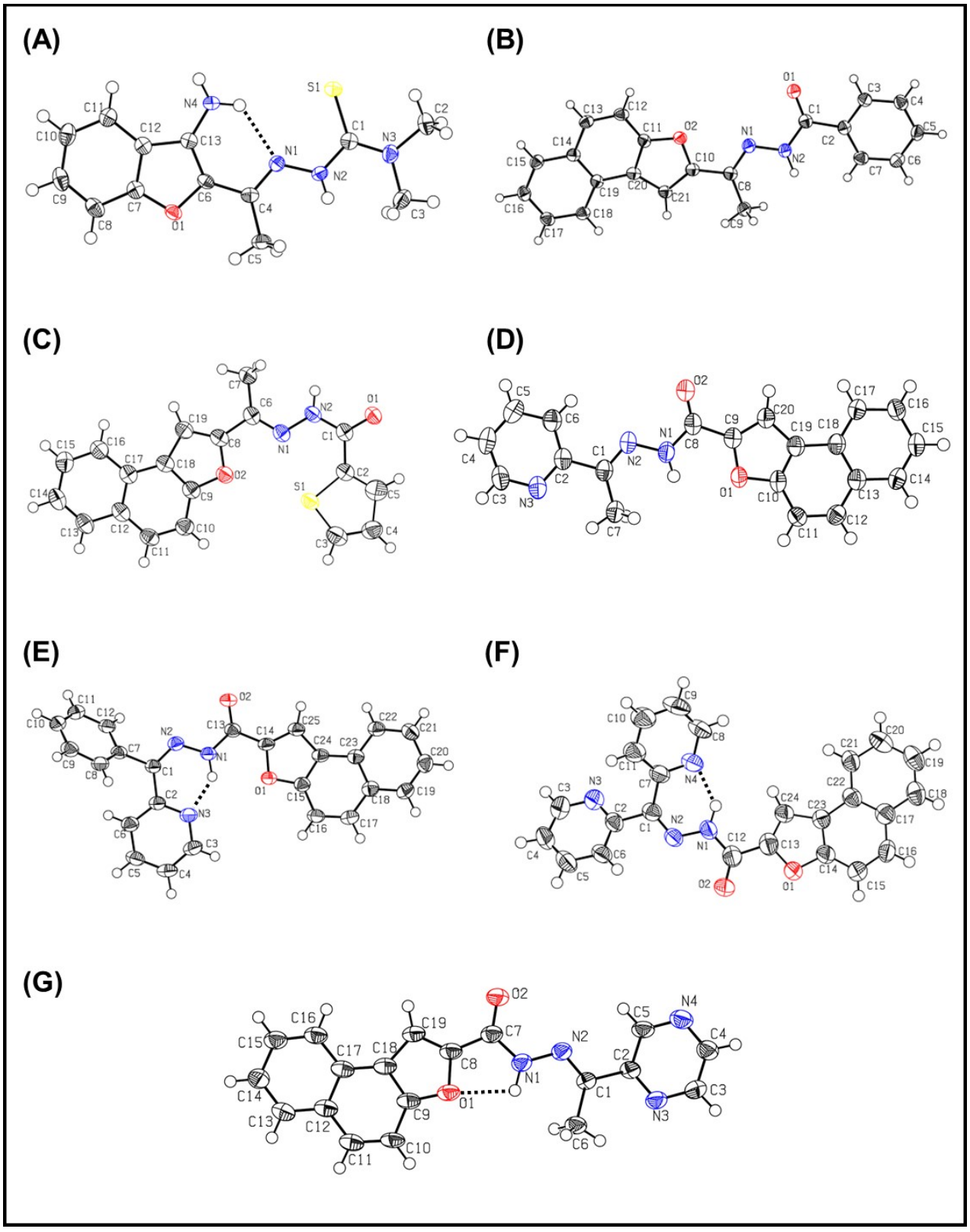

Fig. S1. ORTEP representation of: **(A)** L1, **(B)** L5, **(C)** L7, (**D**) L10, **(E)** L11, **(F)** L12, and **(G)** L13 (using 50% probability ellipsoids).

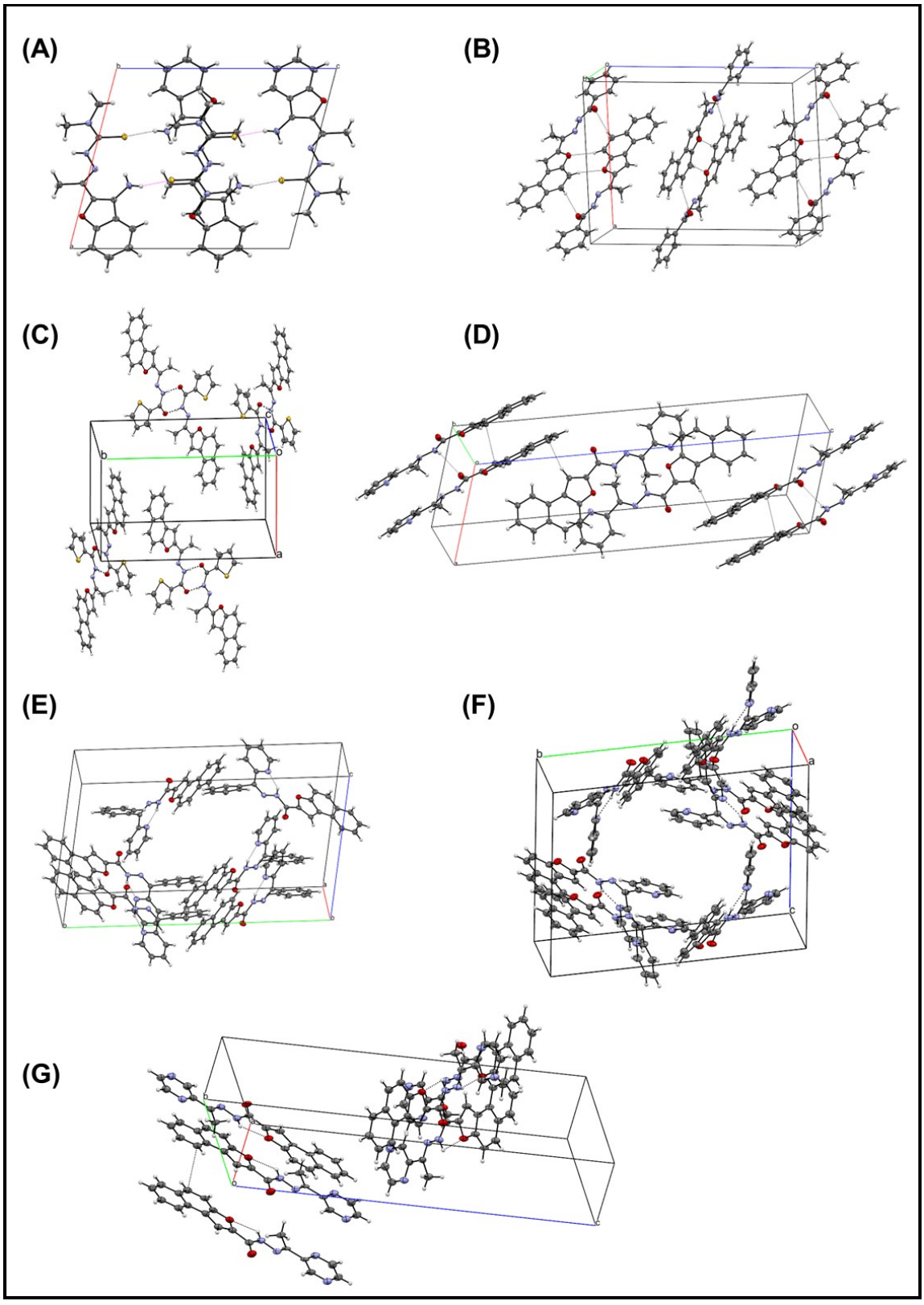

Fig. S2. Crystal packing diagrams of: **(A)** L1, **(B)** L5, **(C)** L7, (**D**) L10, **(E)** L11, **(F)** L12, and **(G)** L13.

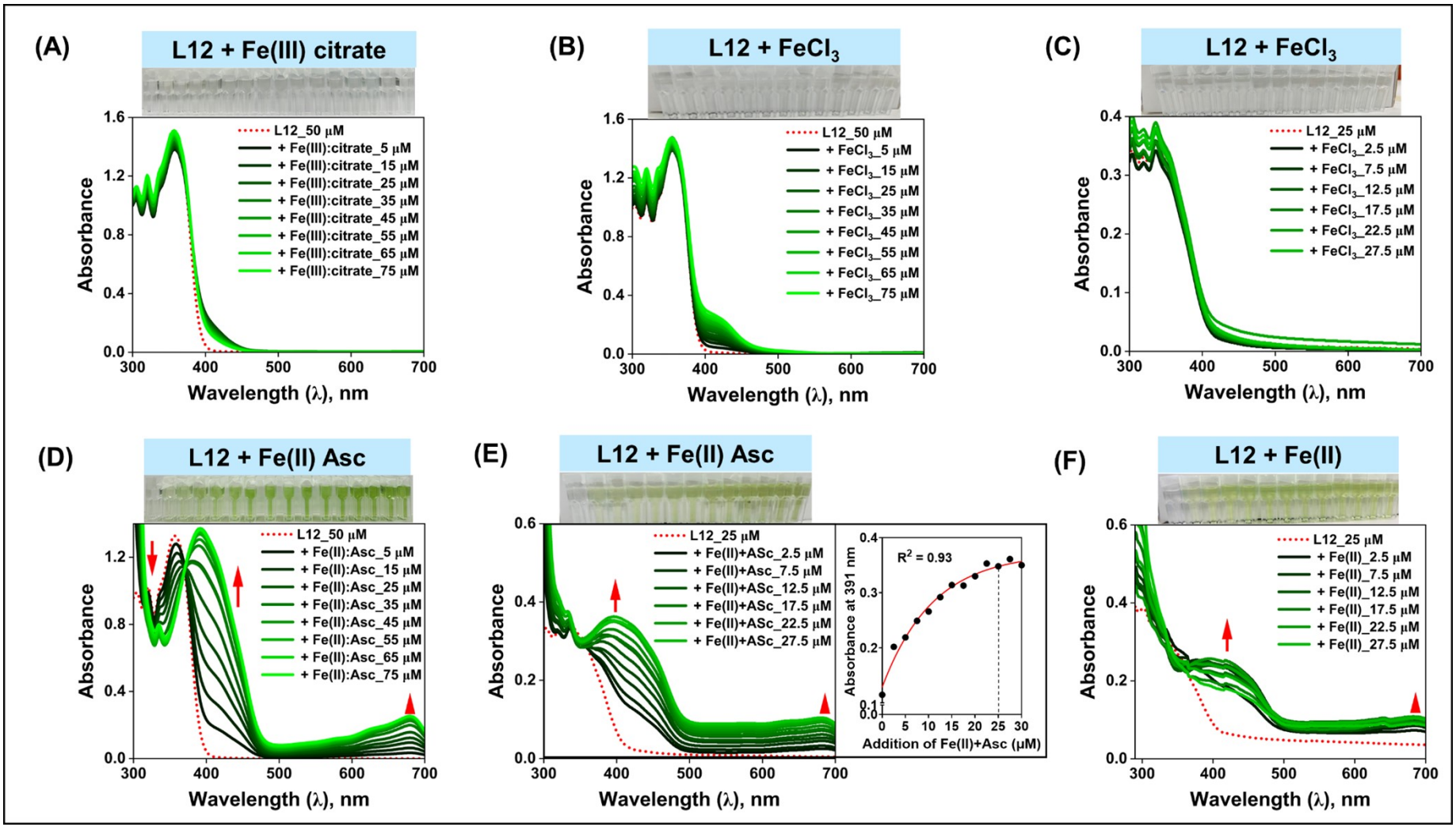

Fig. S3. (A-F) UV-Vis spectral changes of L12 (25 or 50 µM) upon titration with increasing concentrations of iron salts under various conditions: **(A)** Fe(III)-citrate (1:100 metal-to-citrate molar ratio; 5–75 µM) in DMSO/H_2O (7:3 *v/v*); **(B)** $FeCl_3$ (5–75 µM) in 100% DMSO; **(C)** $FeCl_3$ (2.5–27.5 µM) in NaCl (0.14 M)/HEPES buffer (pH 7.4); **(D)** Fe(II) Asc (1:100 metal-to-ascorbate molar ratio; 5–75 µM) in DMSO/H_2O (7:3 *v/v*); **(E)** **(E)** Fe(II) Asc (1:100 molar ratio; 2.5–27.5 µM) and L12 (25 µM) in NaCl (0.14 M)/HEPES buffer (pH 7.4); and the stoichiometric titration curve at 391 nm demonstrating saturation at 25 µM (R^2 = 0.93), consistent with 1:1 Fe(II)–L12 complex formation. The corresponding Benesi–Hildebrand[26] analysis yielded a formation constant of $K_f = (7.4 \pm 0.8) \times 10^9$ M^{-1} (log K_f = 9.87), indicative of stable ligation. **(F)** Fe(II) (added as $(NH_4)_2Fe(SO_4)_2$; in NaCl (0.14 M)/HEPES buffer (pH 7.4) 2.5–27.5 µM). Each titration step was followed by gentle mixing and a 5 min incubation at 20 °C prior to spectral acquisition.

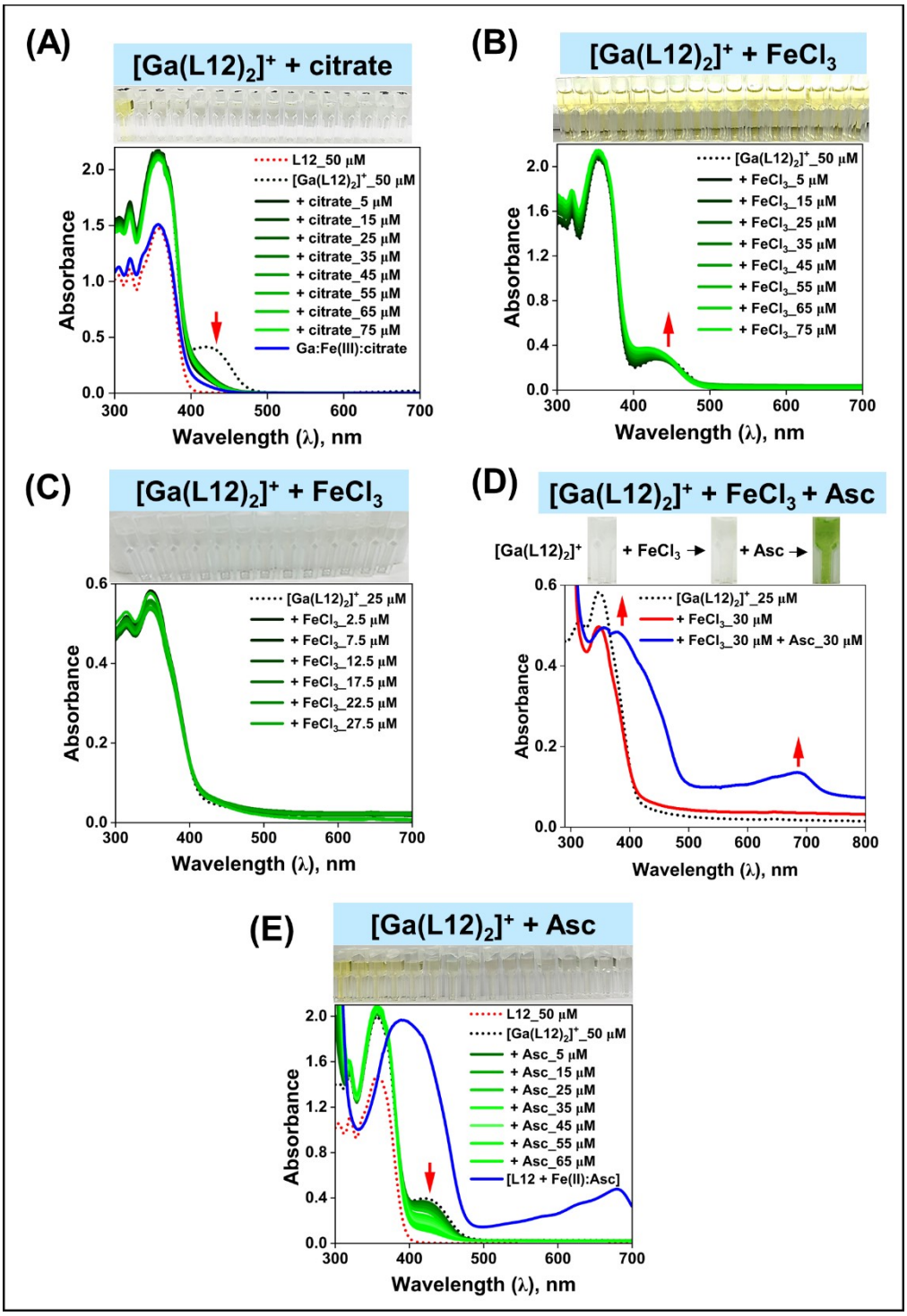

Fig. S4. (A-E) UV-Vis spectral changes of $[Ga(L12)_2]^+$ (25 or 50 µM) upon titration with increasing concentrations of: **(A)** citrate (5–75 µM) in DMSO/H_2O (7:3 *v/v*); **(B)** $FeCl_3$ (5–75 µM) in 100% DMSO; **(C)** $FeCl_3$ (2.5–27.5 µM) in NaCl (0.14 M)/HEPES buffer (pH 7.4); **(D)** $FeCl_3$ (30 µM) or $FeCl_3$ (30 µM) and Asc (30 µM) in NaCl (0.14 M)/HEPES buffer (pH 7.4); and **(E)** Asc (5–65 µM) in DMSO/H_2O (7:3 *v/v*). Each titration step was followed by gentle mixing and a 5 min incubation at 20 °C prior to spectral acquisition. Spectral shifts indicate Ga(III) coordination and ligand exchange behavior.

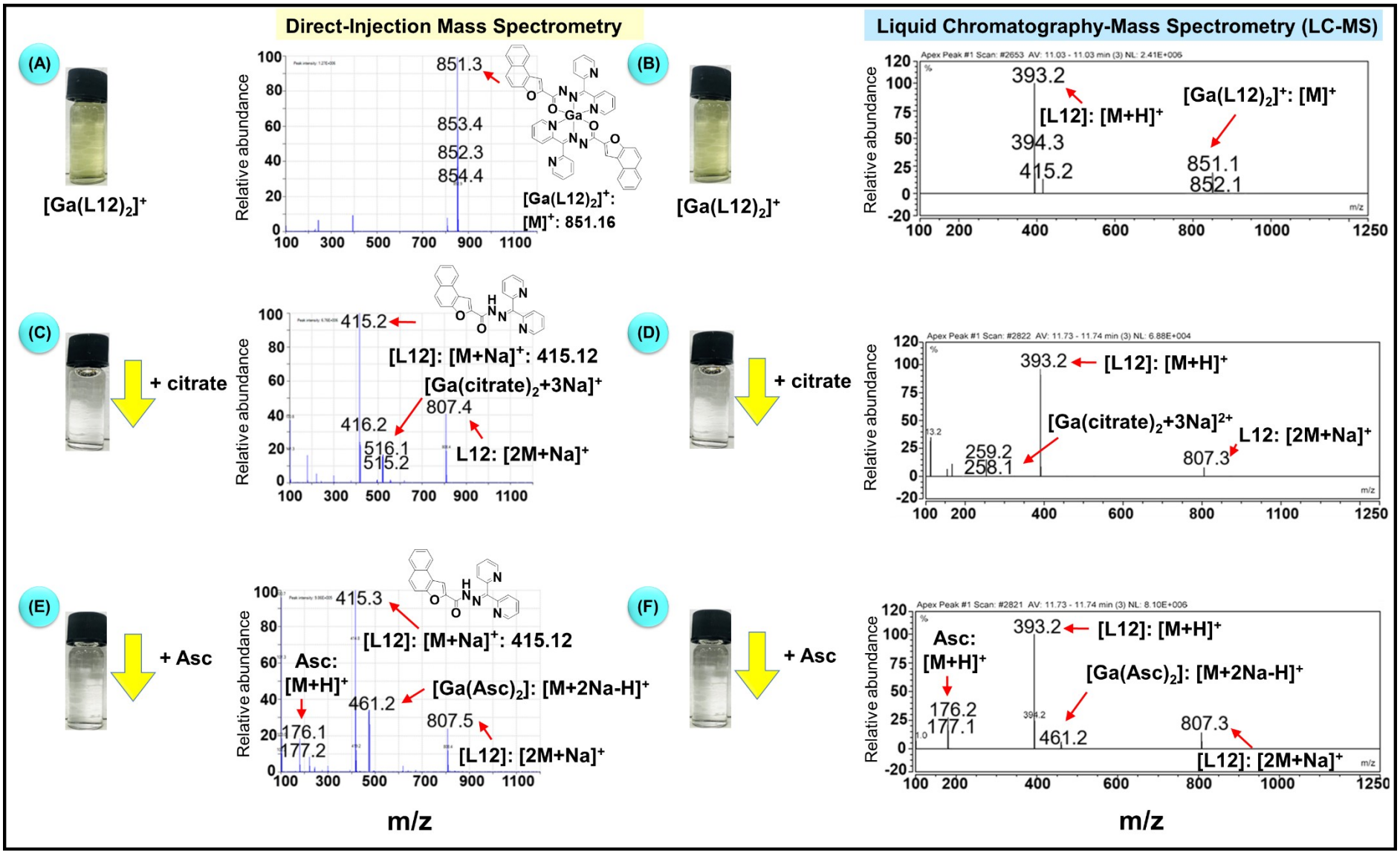

Fig. S5. **(A-F)** Direct MS and LC-MS analysis of $[Ga(L12)_2]^+$ (500 µM) reactivity with either Asc (500 µM) or citrate (500 µM) in DMSO/H_2O (7:3 *v/v*) after vigorous mixing and an incubation for 24 h/20°C. Prior to analysis, samples were diluted 1:1 with MeOH.

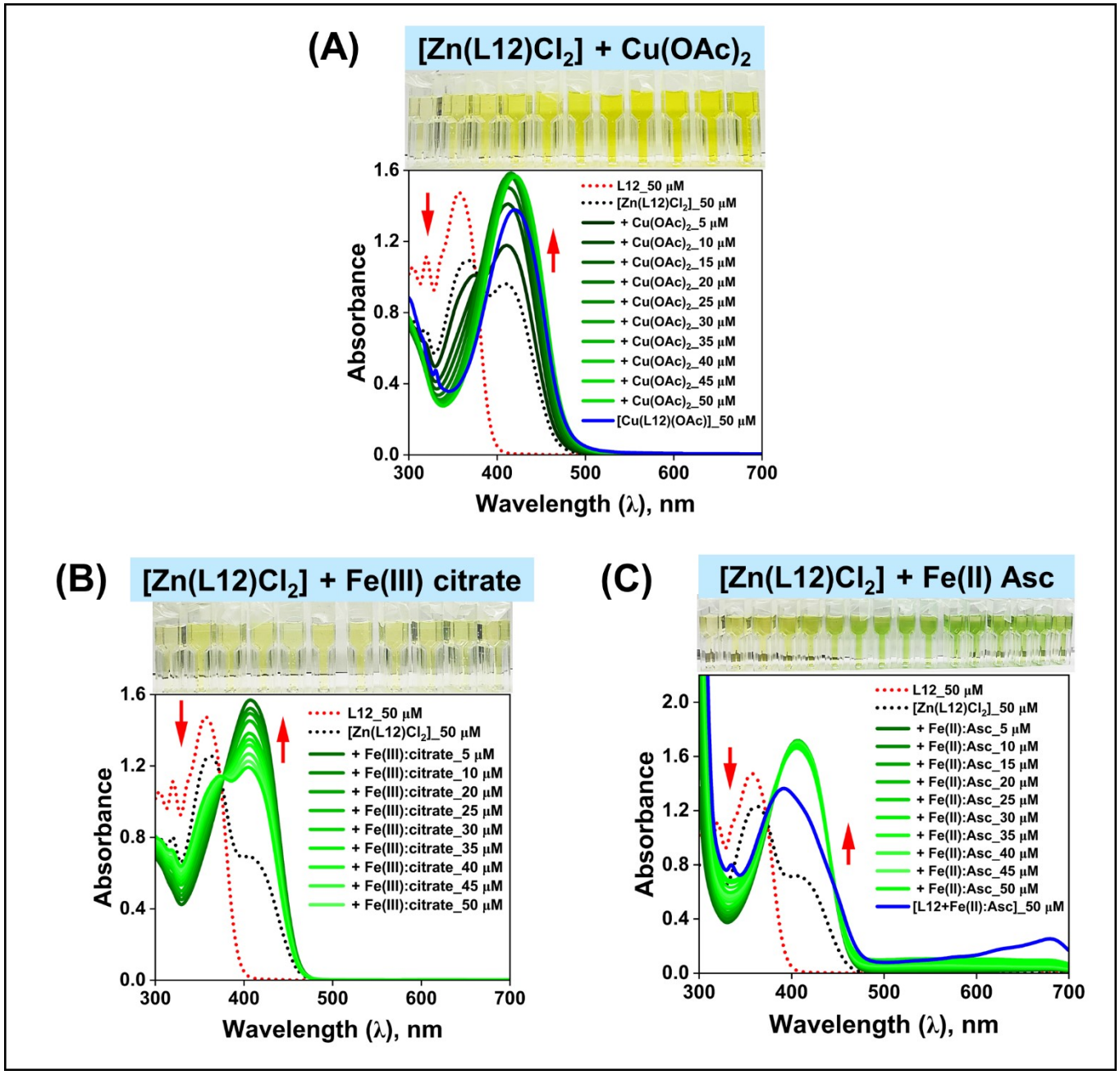

Fig. S6. (A-C) Spectral alterations of [Zn(L12)Cl_2] (50 µM) upon titration with either **(A)** [$Cu(OAc)_2$] (5–50 µM); **(B)** Fe(III) citrate (5–50 µM; 1:100 metal-to-citrate molar ratio), and **(C)** Fe(II) ascorbate (Asc; 5–50 µM; 1:100 metal-to-ascorbate molar ratio) using UV-Vis spectroscopy in DMSO: H_2O (7:3 *v/v*)/20°C. After each titer was added and vigorous mixing, solutions were incubated for 5 min/20°C before recording each spectrum. The spectral changes include color transitions, and isosbestic points.

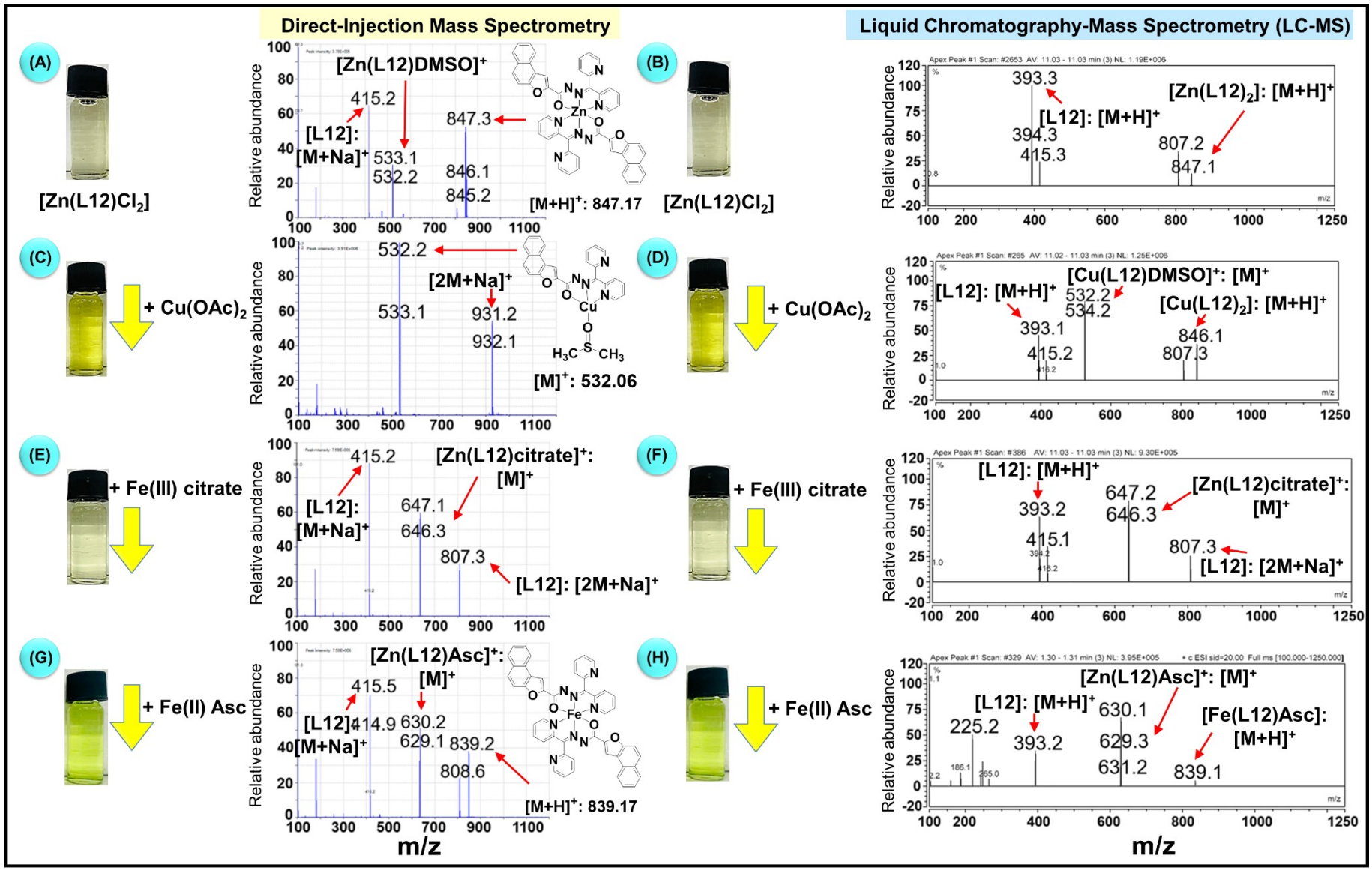

Fig. S7. **(A-H)** Direct MS and LC-MS analysis of the transmetalation of [Zn(L12)Cl_2] (500 µM) with either [$Cu(OAc)_2$] (500 µM), Fe(II) Asc (1:100 molar ratio; 500 µM), or Fe(III) citrate (1:100 molar ratio; 500 µM) in DMSO/H_2O (7:3 *v/v*) after vigorous mixing and an incubation for 24 h/20°C. Prior to analysis, samples were diluted 1:1 with MeOH.

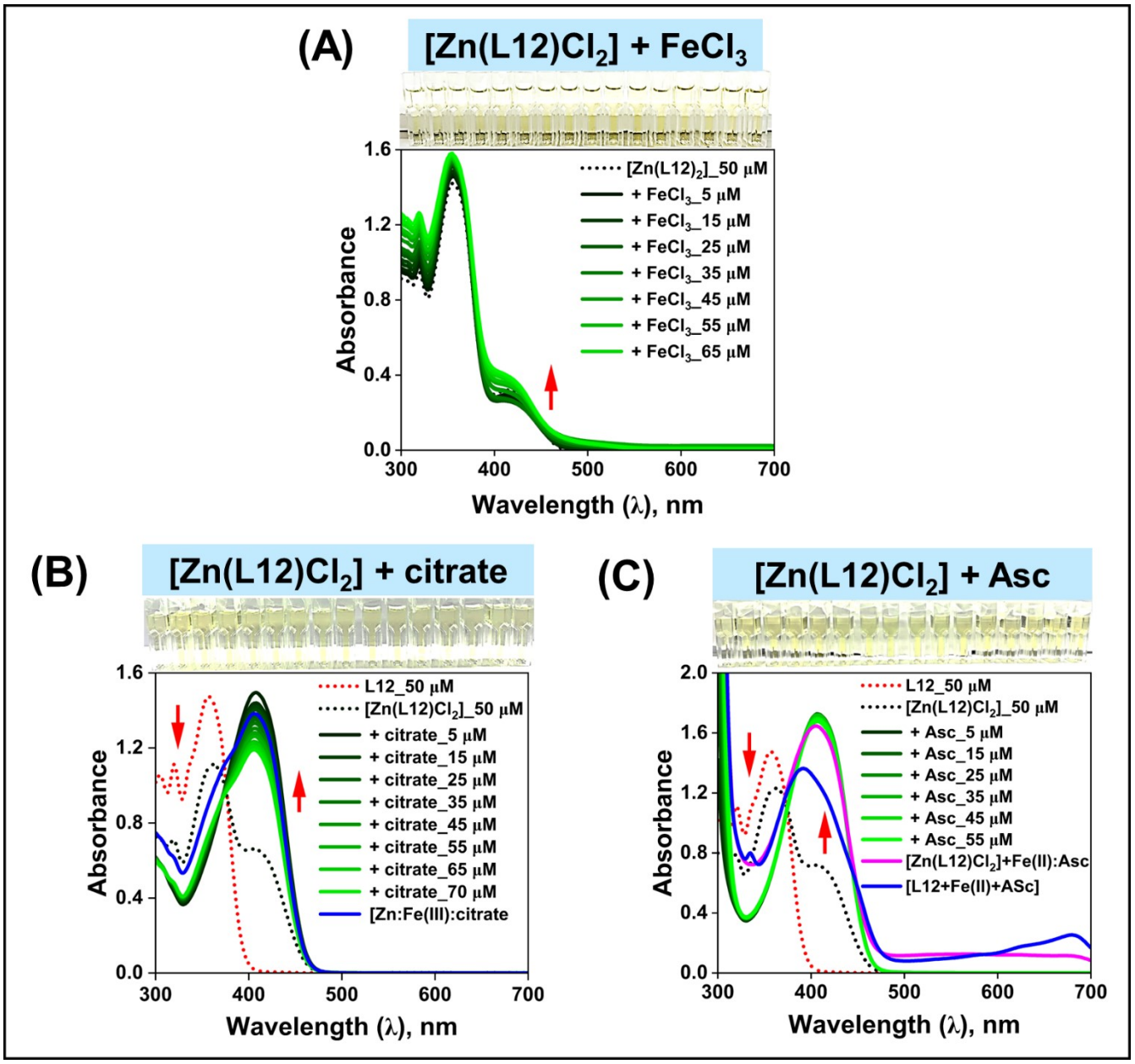

Fig. S8. (A-C) UV-Vis spectral changes of [Zn(L12)Cl_2] (50 µM) upon titration with increasing concentrations of: **(A)** $FeCl_3$ (5–65 µM) in 100% DMSO; **(B)** citrate (5–70 µM); and **(C)** Asc (5–55 µM) in DMSO/H_2O (7:3 *v/v*). Each titration step was followed by gentle mixing and a 5 min incubation at 20 °C prior to spectral acquisition. The resulting spectral shifts provide insight into the coordination behavior and ligand exchange dynamics of the Zn(II) complex.

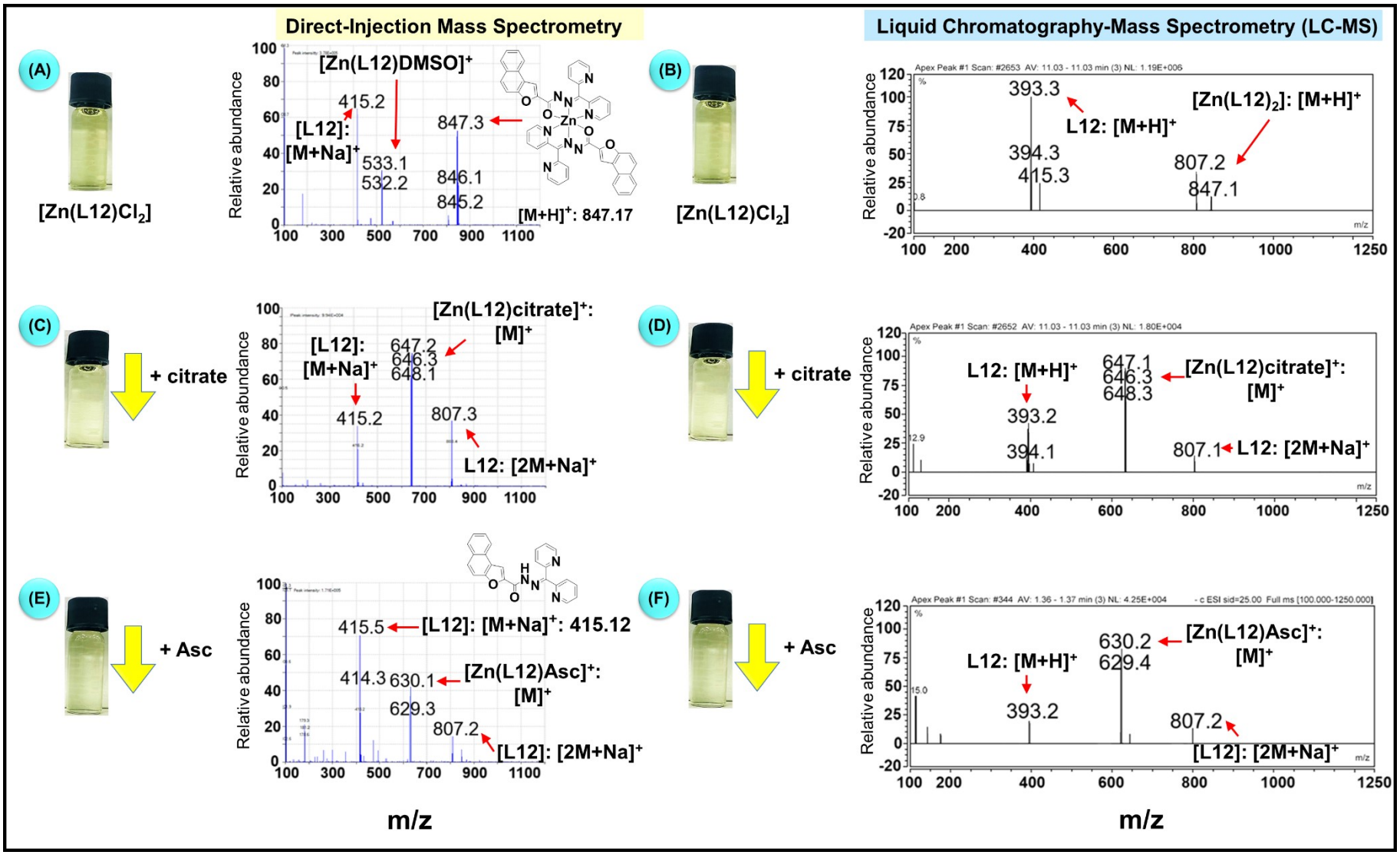

Fig. S9. **(A-F)** Direct MS and LC-MS analysis of [Zn(L12)Cl_2] (500 µM) reactivity with either Asc (500 µM) or citrate (500 µM) in DMSO/H_2O (7:3 *v/v*) after vigorous mixing and an incubation for 24 h/20°C. Prior to analysis, the samples were diluted 1:1 with MeOH.

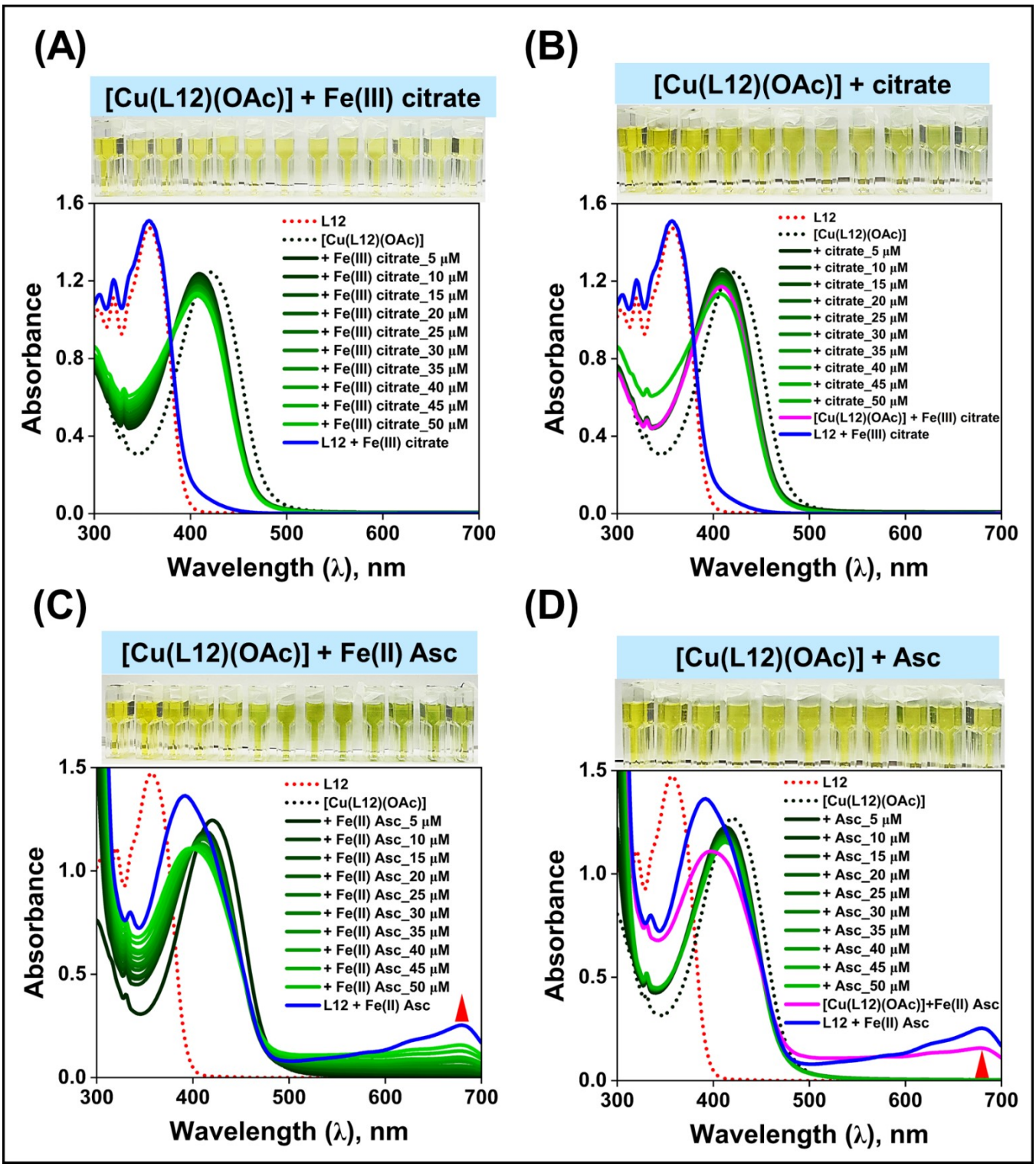

Fig. S10. Spectral alterations of [Cu(L12)(OAc)] (50 μM) upon titration with either: **(A)** Fe(III) citrate (5–50 μM; 1:100 metal-to-citrate molar ratio); **(B)** citrate (5–50 μM) **(C)**; Fe(II) ascorbate (Asc; 1:100 molar ratio; 5–50 μM); or **(D)** Asc (5–50 μM) using UV-Vis spectroscopy in DMSO: H_2O (7:3 *v/v*)/20°C. After each titer was added and vigorous mixing, solutions were incubated for 5 min/20°C before recording each spectrum. The spectral changes include color transitions and isosbestic points.

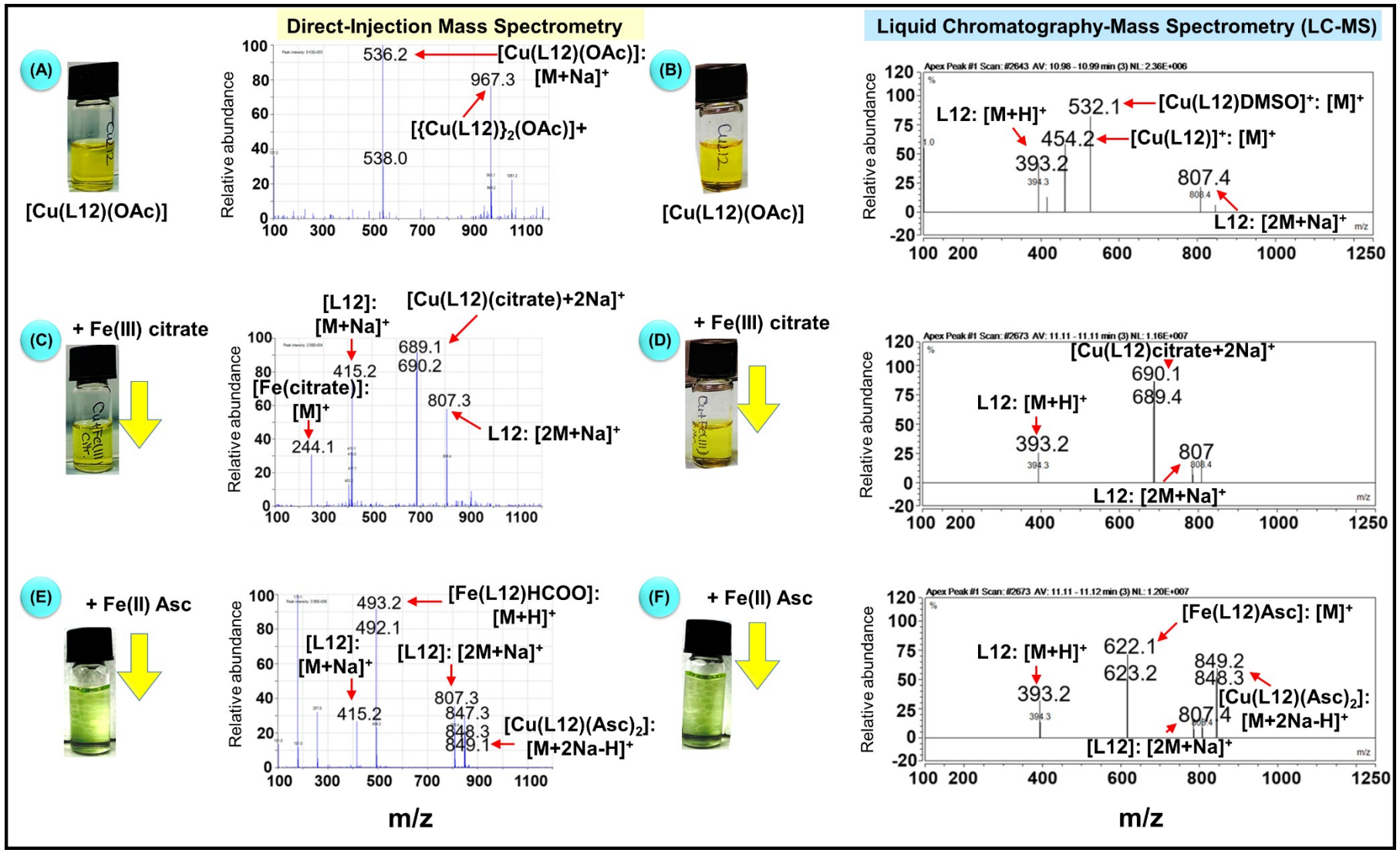

Fig. S11. (A-F) Direct MS and LC-MS analysis of the transmetalation of [Cu(L12)(OAc)] (500 µM) with either Fe(III) citrate (1:100 molar ratio; 500 µM) or Fe(II) Asc (1:100 molar ratio; 500 µM) in DMSO/H_2O (7:3 *v/v*) after vigorous mixing and an incubation for 24 h/20°C. Prior to analysis, samples were diluted 1:1 with MeOH.

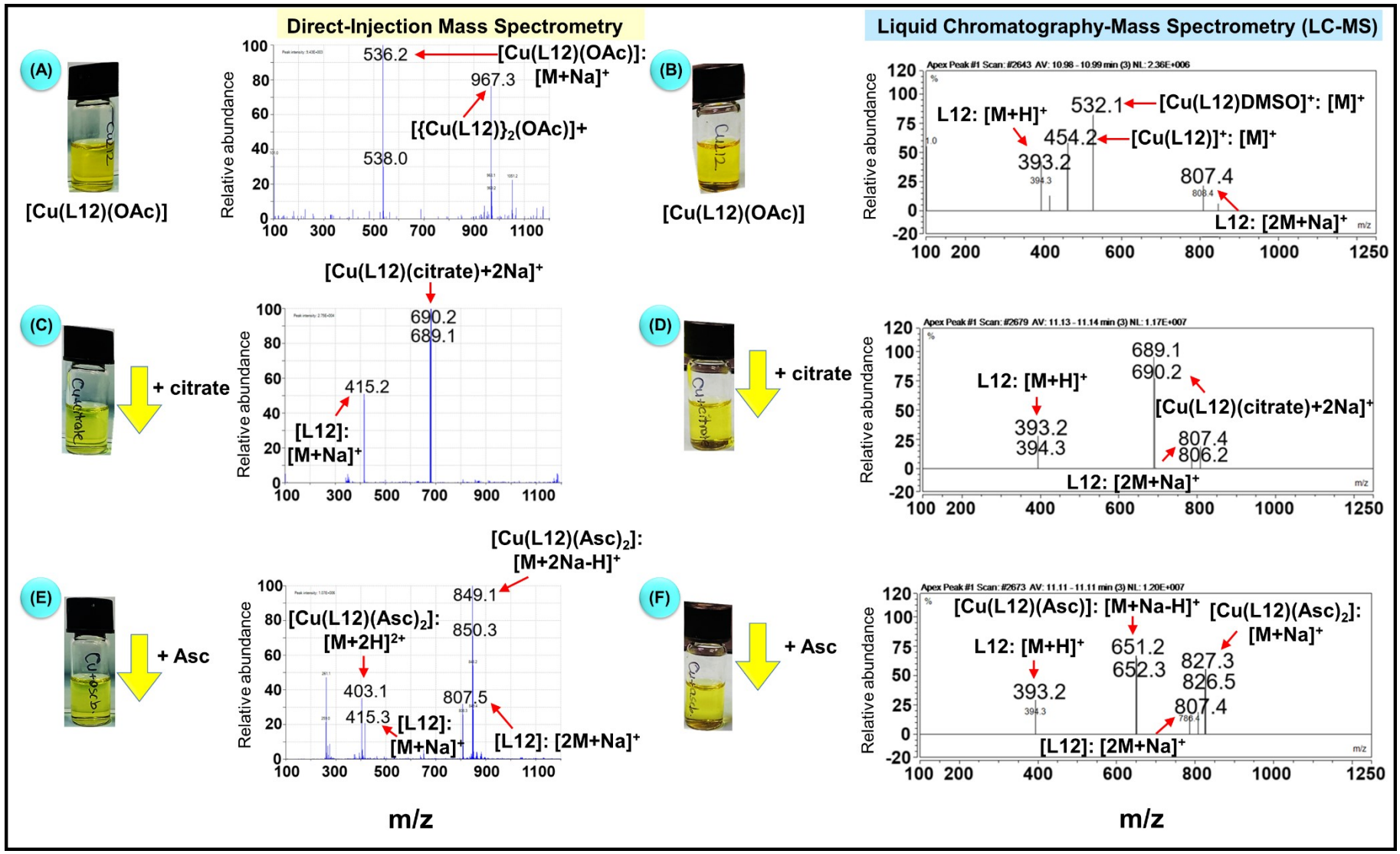

Fig. S12. (A-F) Direct MS and LC-MS analysis of [Cu(L12)(OAc)] (500 µM) reactivity with either citrate (500 µM) or Asc (500 µM) in DMSO/H_2O (7:3 *v/v*) after vigorous mixing and an incubation for 24 h/20°C. Prior to analysis, the samples were diluted 1:1 with MeOH.

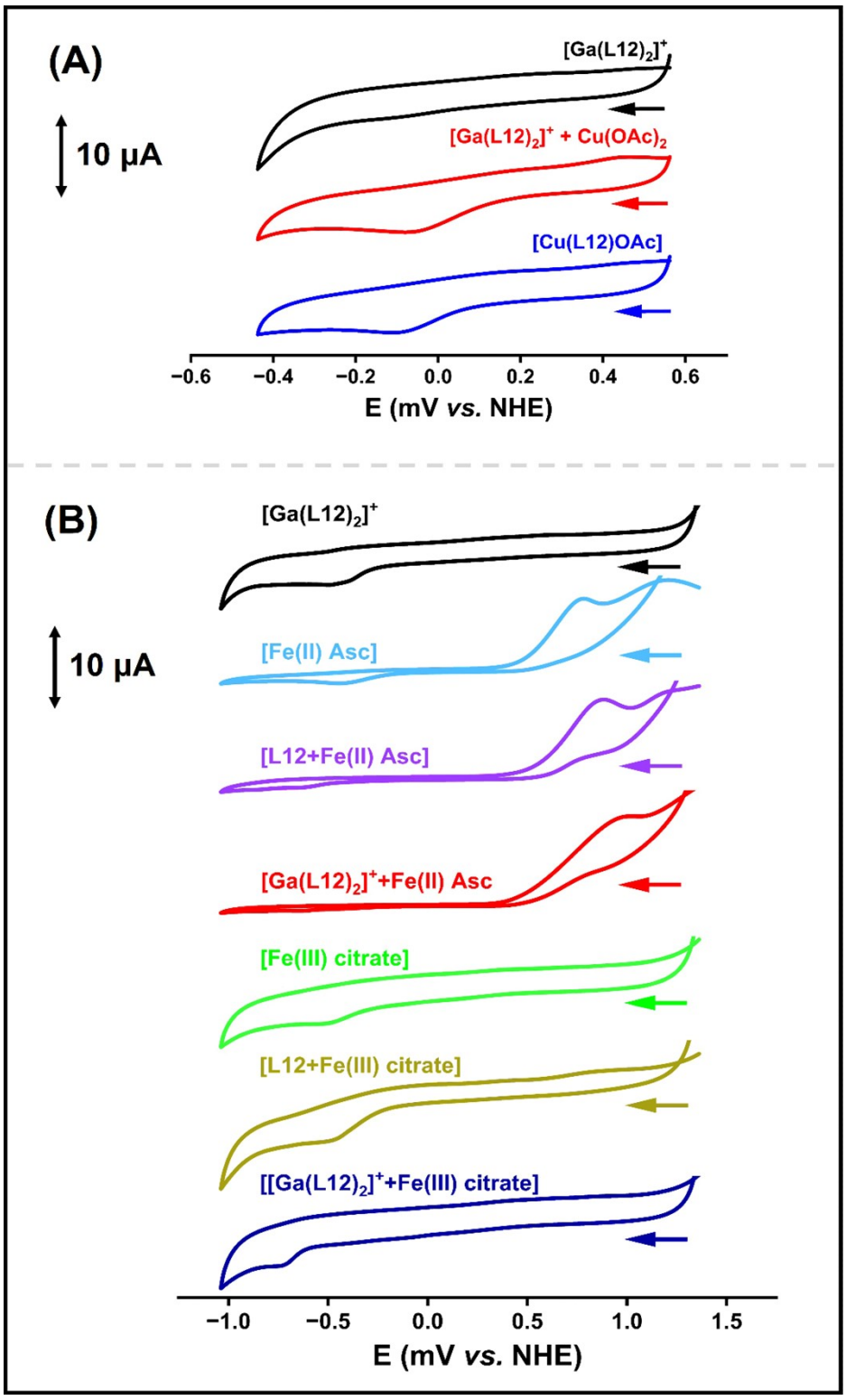

Fig. S13. Cyclic voltammograms of: **(A)** $[Ga(L12)_2]^+$; $[Ga(L12)_2]^+$ + $Cu(OAc)_2$; and [Cu(L12)OAc]; **(B)** $[Ga(L12)_2]^+$; Fe(II) Asc; L12 + Fe(II) Asc; $[Ga(L12)_2]^+$ + Fe(II) Asc; Fe(III) citrate; L12 + Fe(III) citrate and $[Ga(L12)_2]^+$ + Fe(III) citrate; all in MeCN/H_2O (7:3 *v/v*). All agents were examined at 100 µM with the molar ratio of Fe(II) to Asc or Fe(III) to citrate being 1:100. The sweep rate was 100 mV s^{-1}, and all sweeps were initiated in the direction of the arrow. The redox potentials are given relative to the NHE.

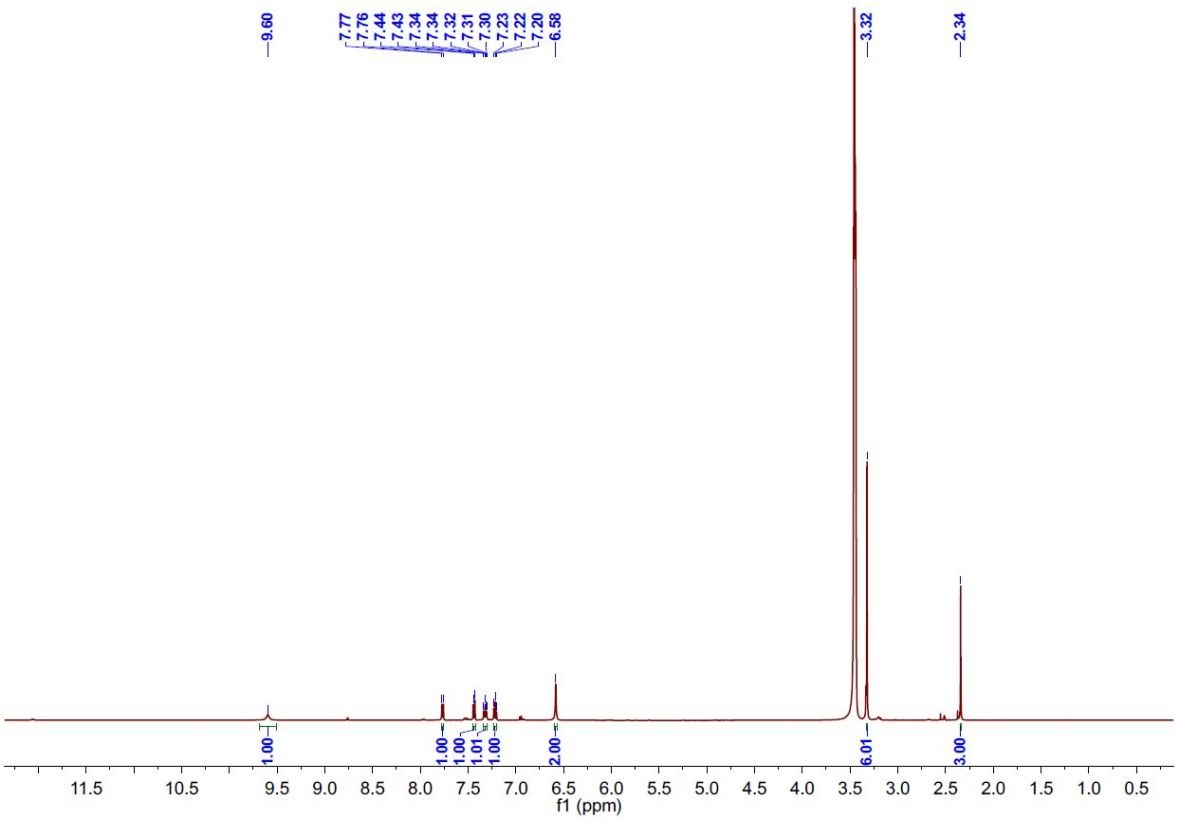

Fig. S14. [1]H NMR spectrum of L1 in d_6-DMSO.

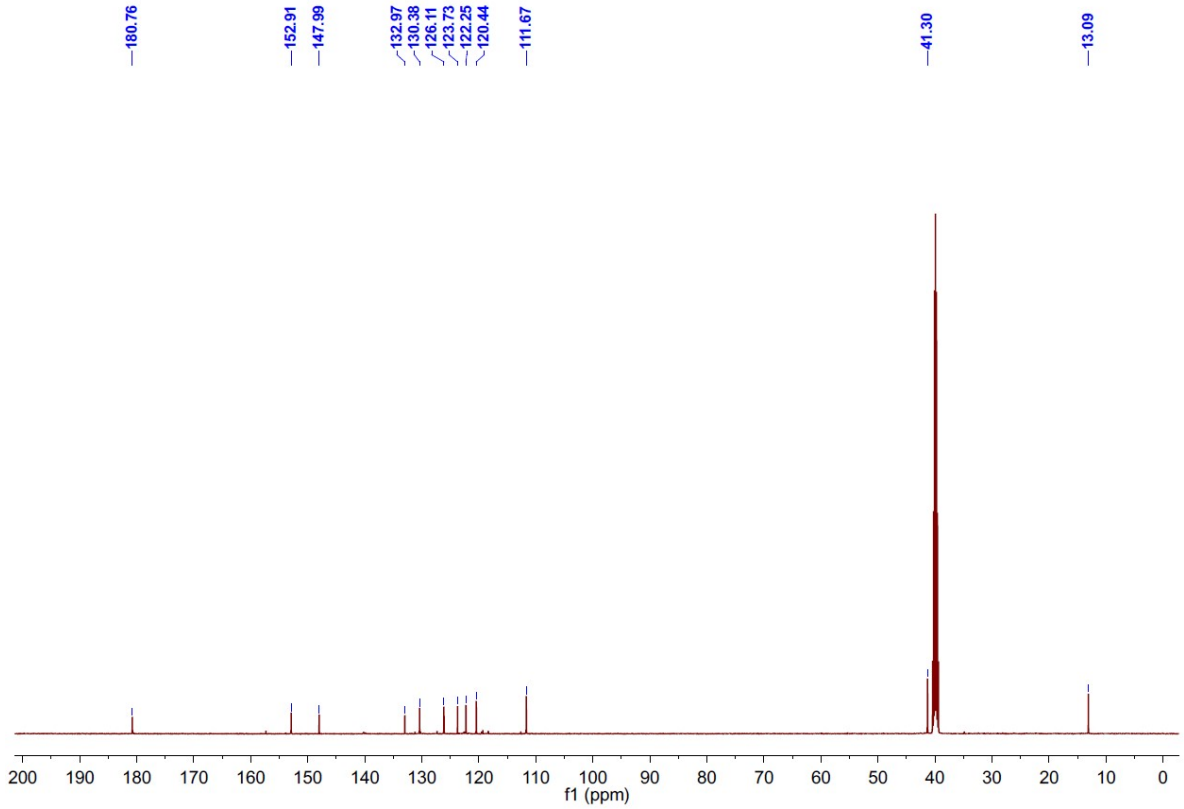

Fig. S15. [13]C NMR spectrum of L1 in d_6-DMSO.

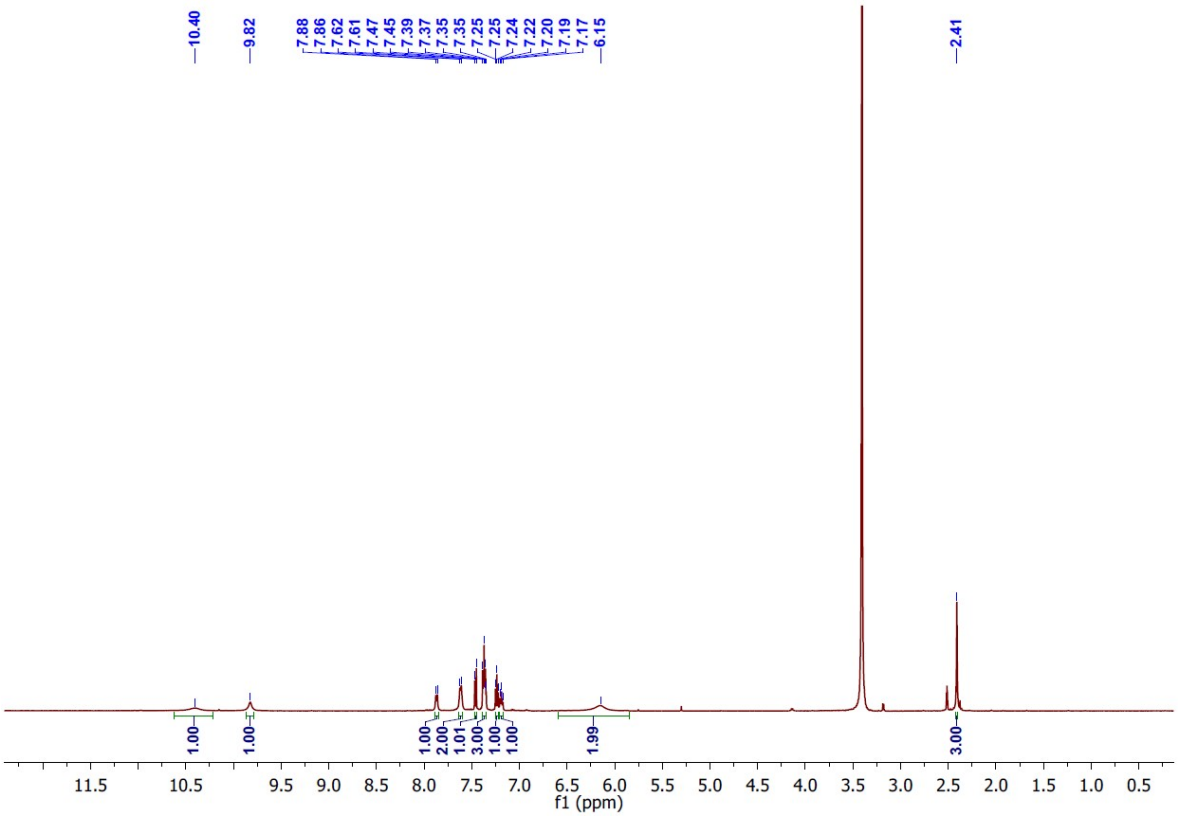

Fig. S16. ^{1}H NMR spectrum of L2 in d_6-DMSO.

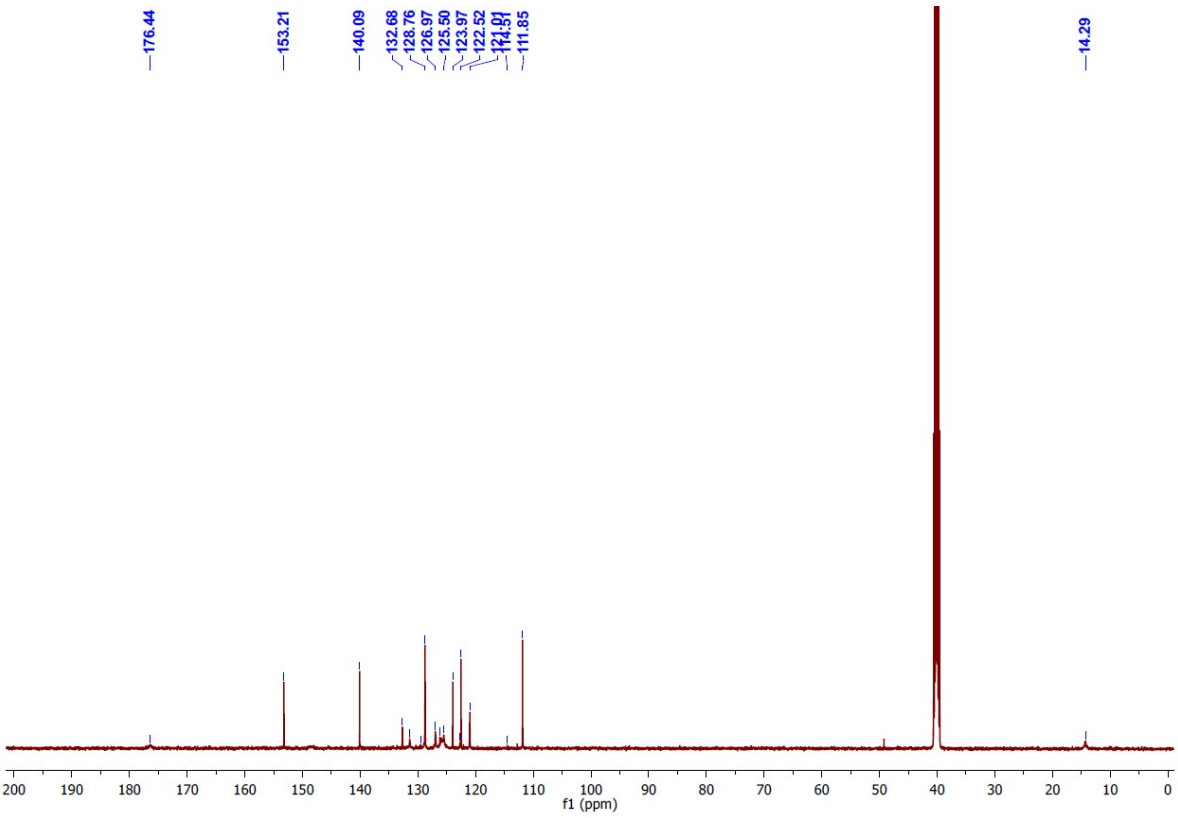

Fig. S17. ^{13}C NMR spectrum of L2 in d_6-DMSO.

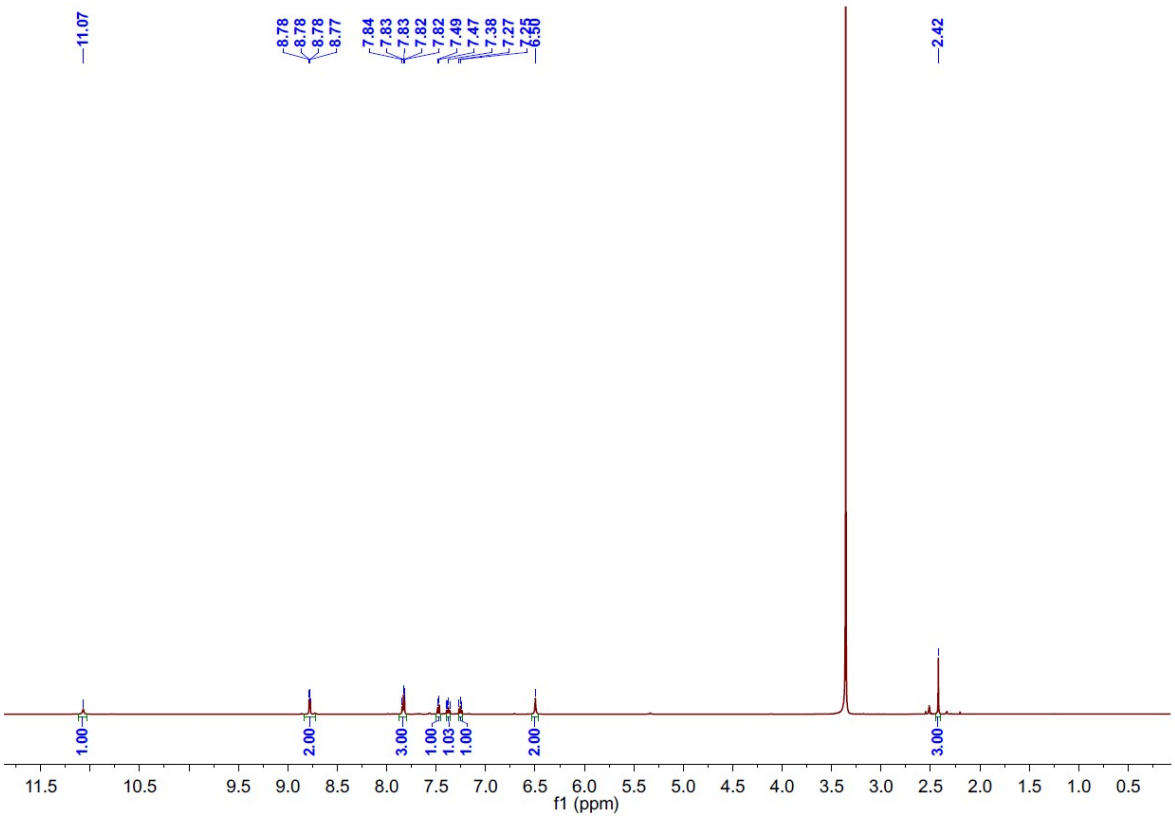

Fig. S18. ^{1}H NMR spectrum of L3 in d_6-DMSO.

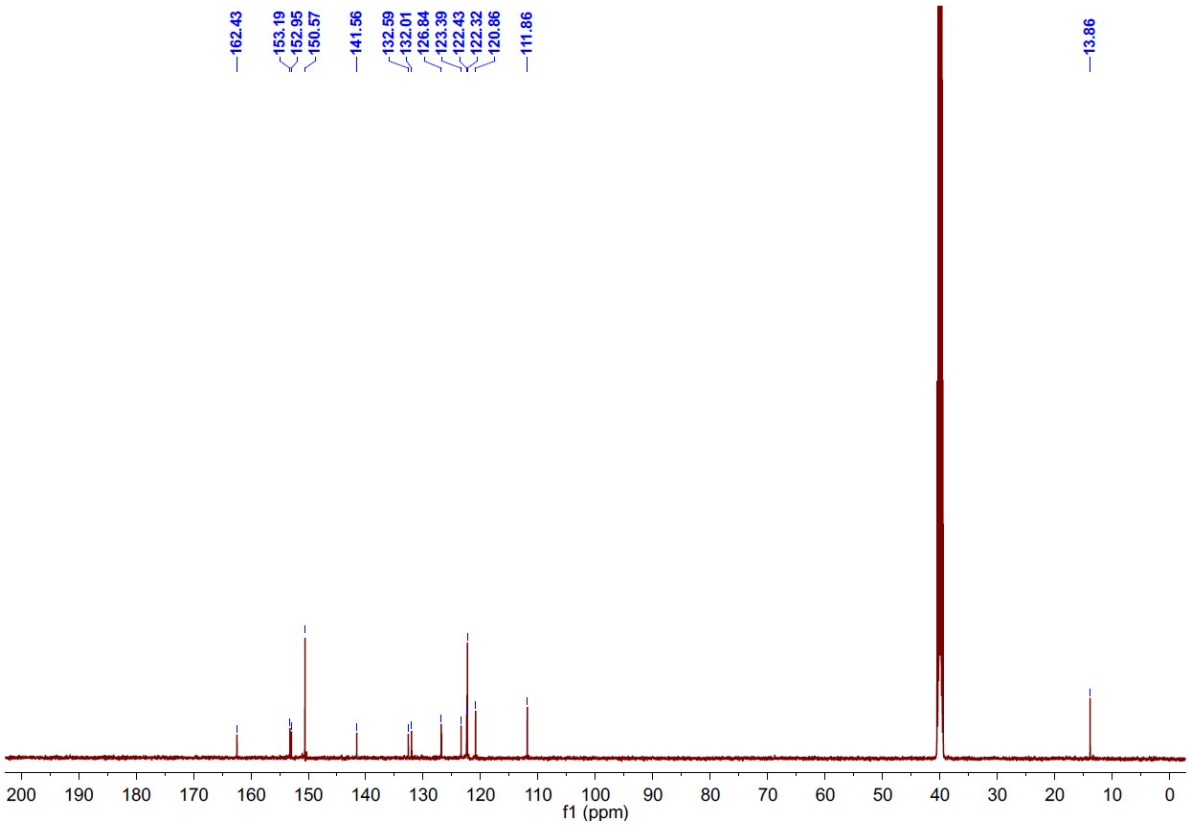

Fig. S19. ^{13}C NMR spectrum of L3 in d_6-DMSO.

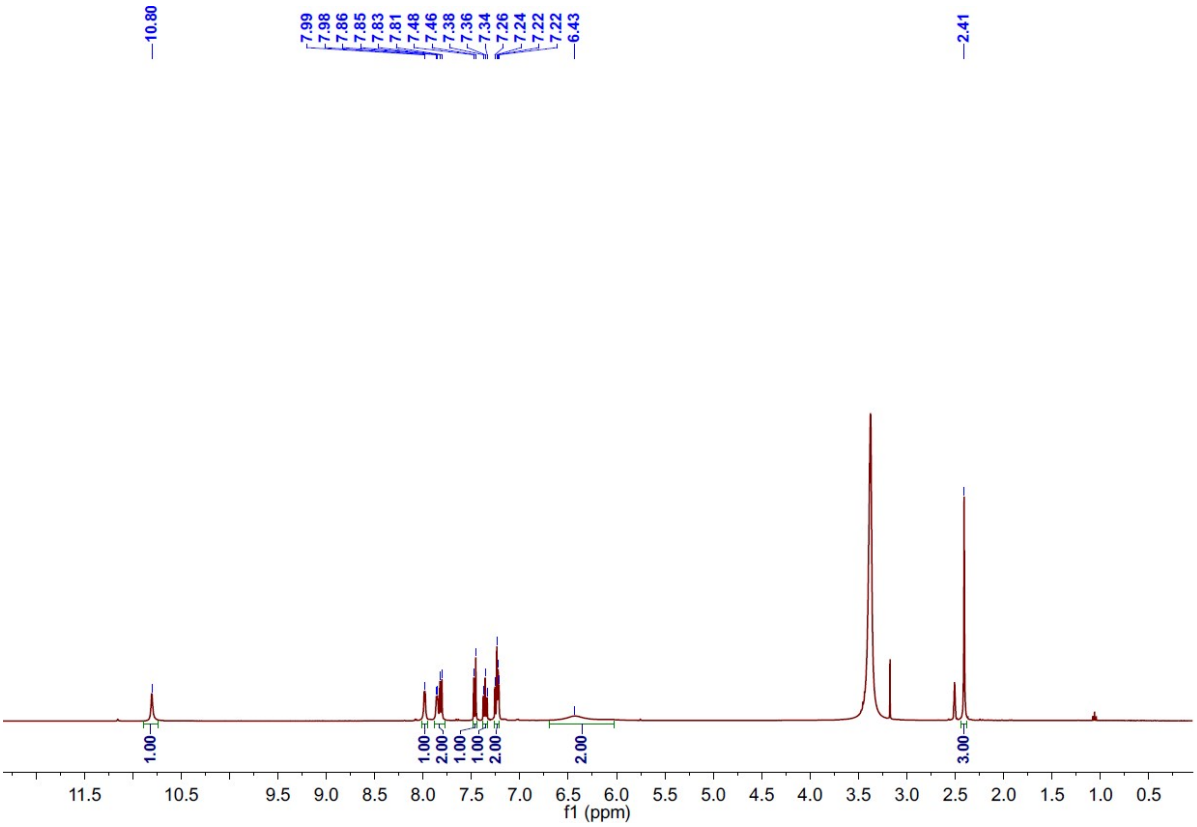

Fig. S20. ^{1}H NMR spectrum of L4 in d_6-DMSO.

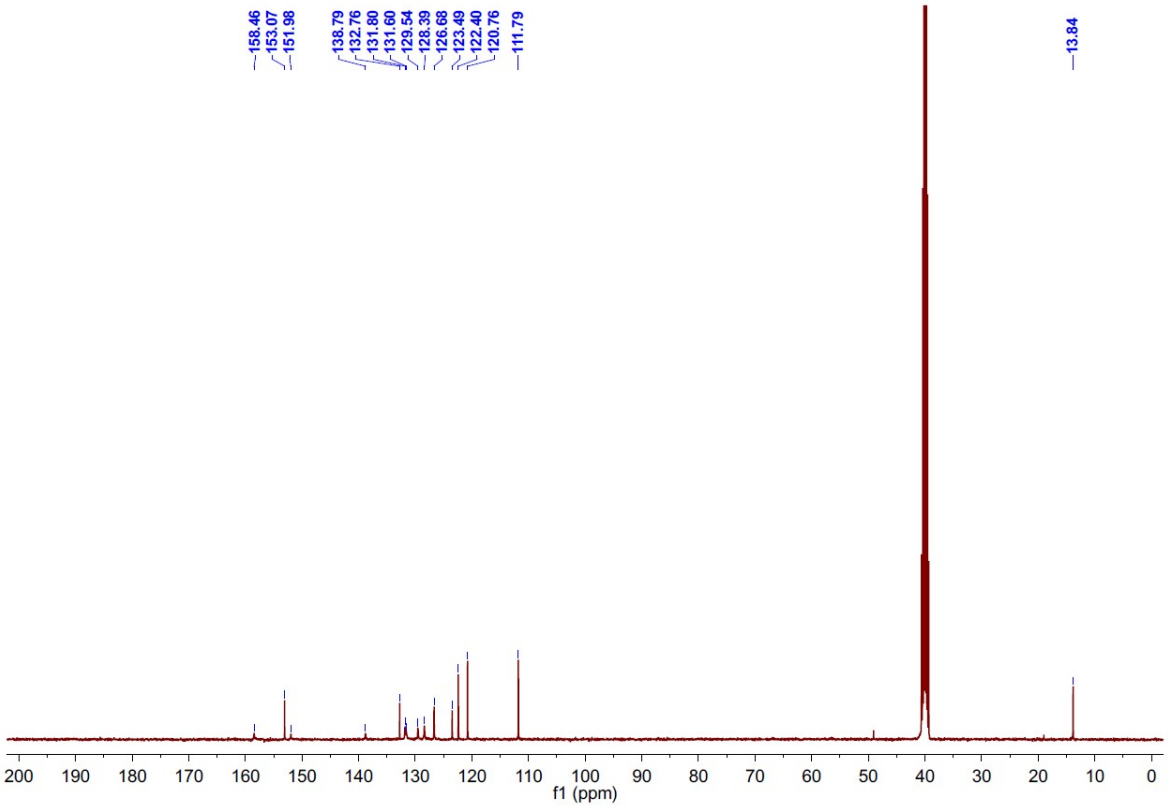

Fig. S21. ^{13}C NMR spectrum of L4 in d_6-DMSO.

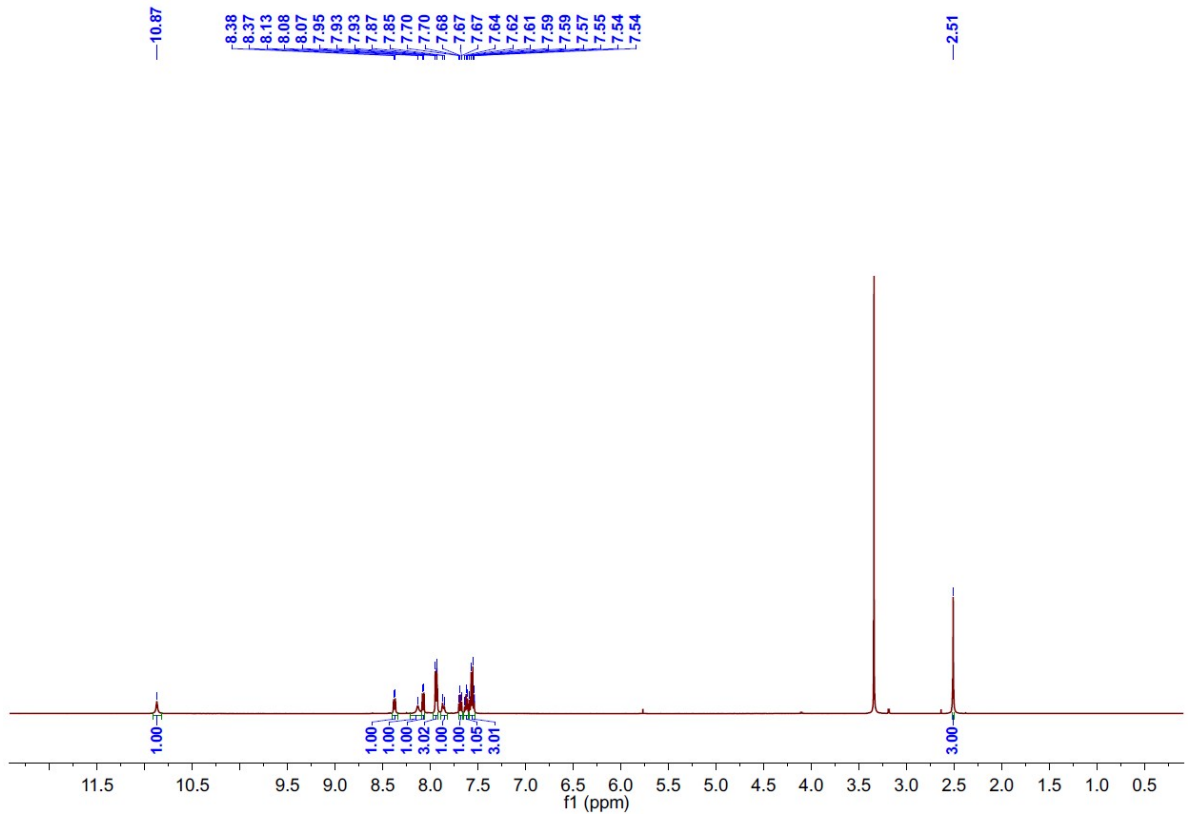

Fig. S22. ^{1}H NMR spectrum of L5 in d_6-DMSO.

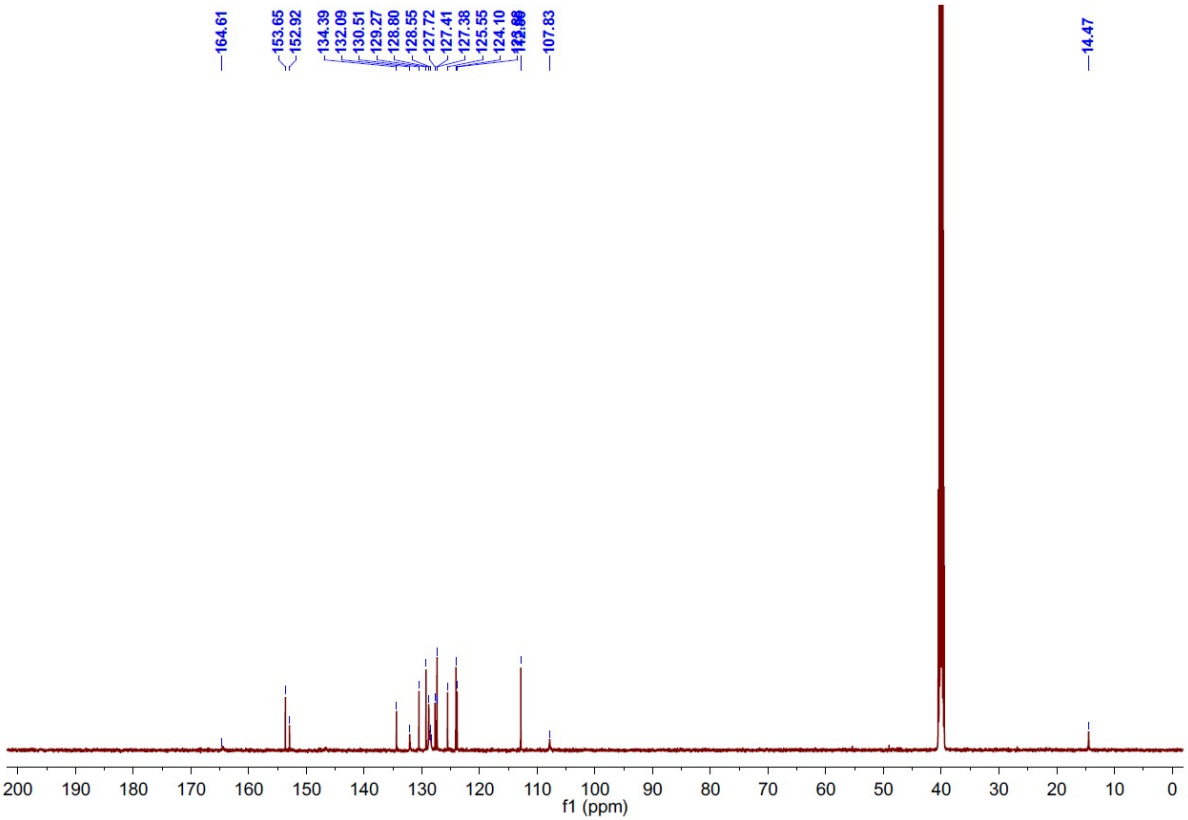

Fig. S23. ^{13}C NMR spectrum of L5 in d_6-DMSO.

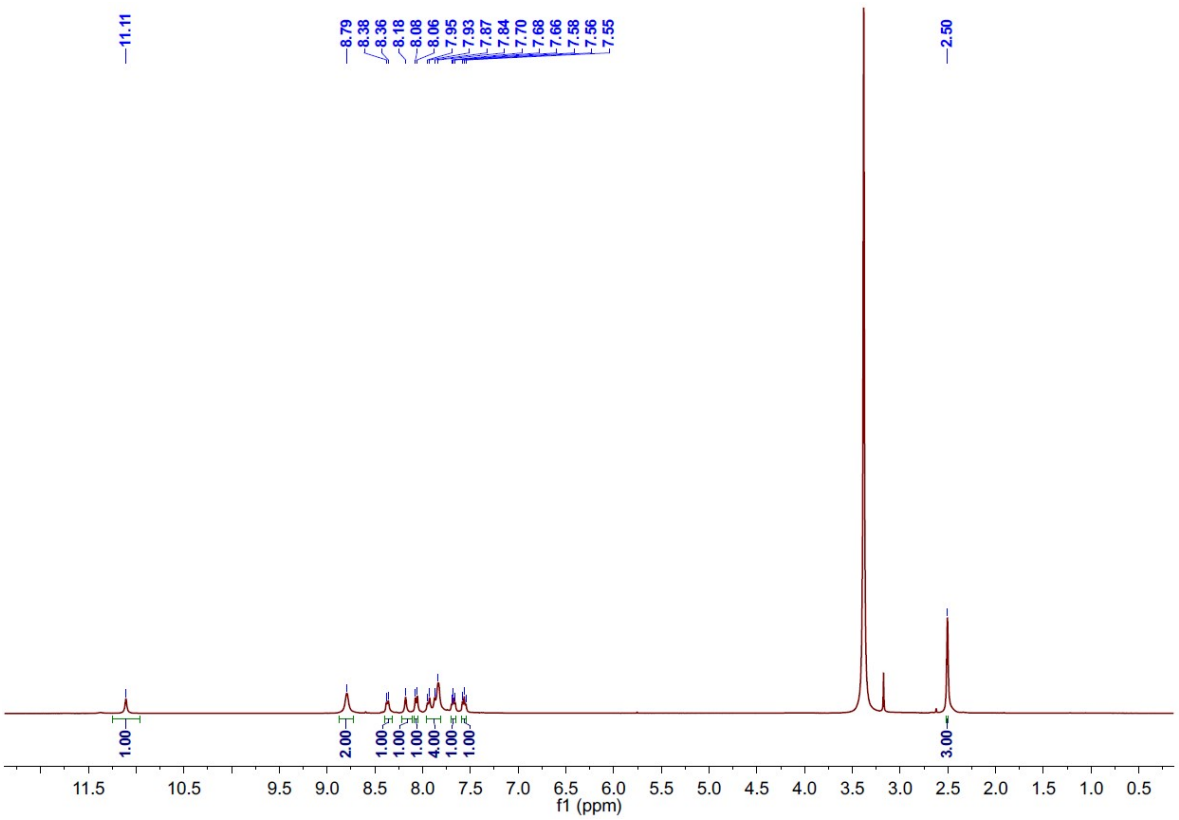

Fig. S24. ^{1}H NMR spectrum of L6 in d_6-DMSO.

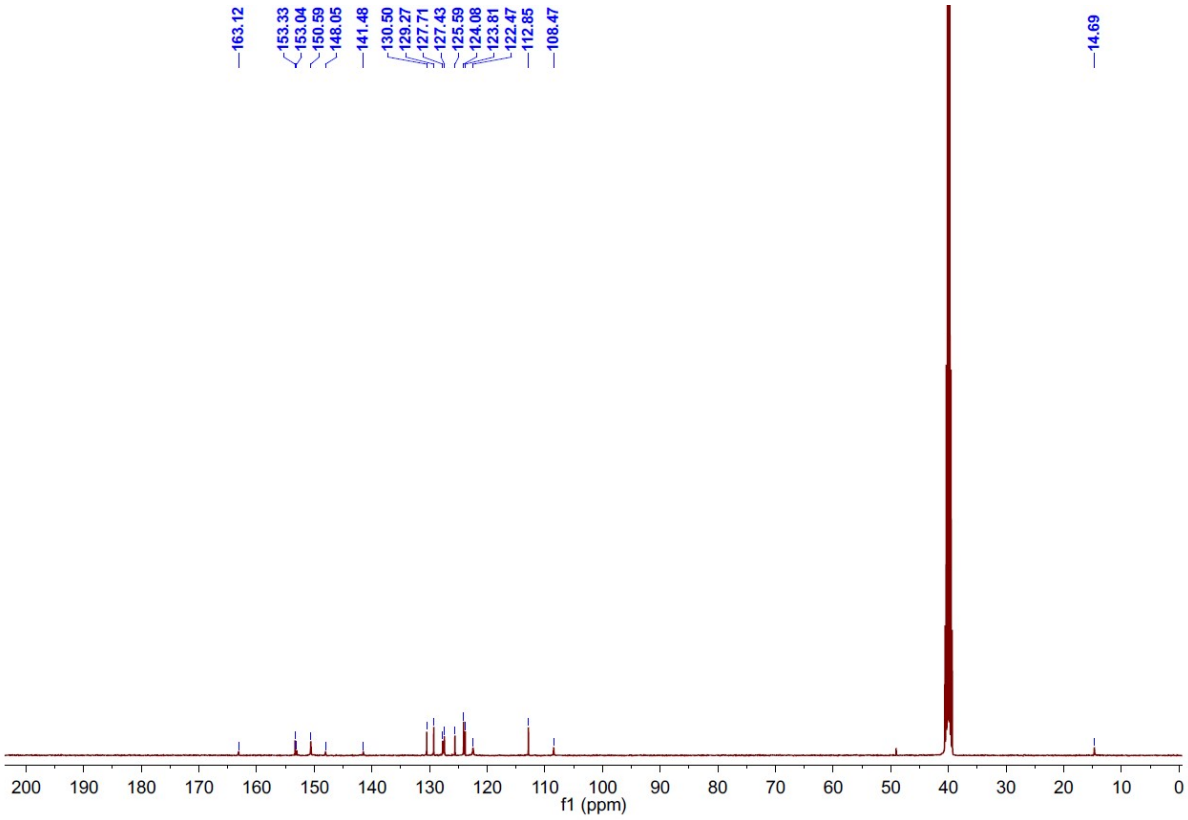

Fig. S25. ^{13}C NMR spectrum of L6 in d_6-DMSO.

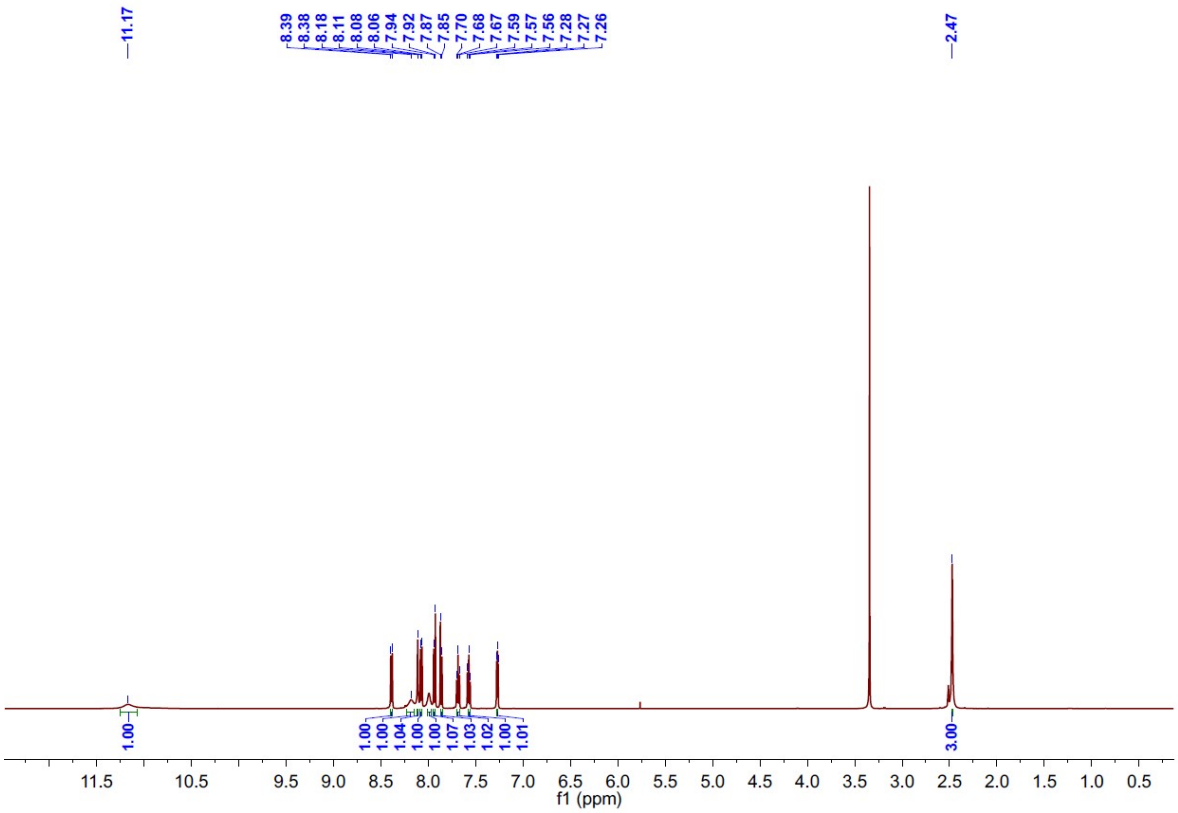

Fig. S26. ^{1}H NMR spectrum of L7 in d_6-DMSO.

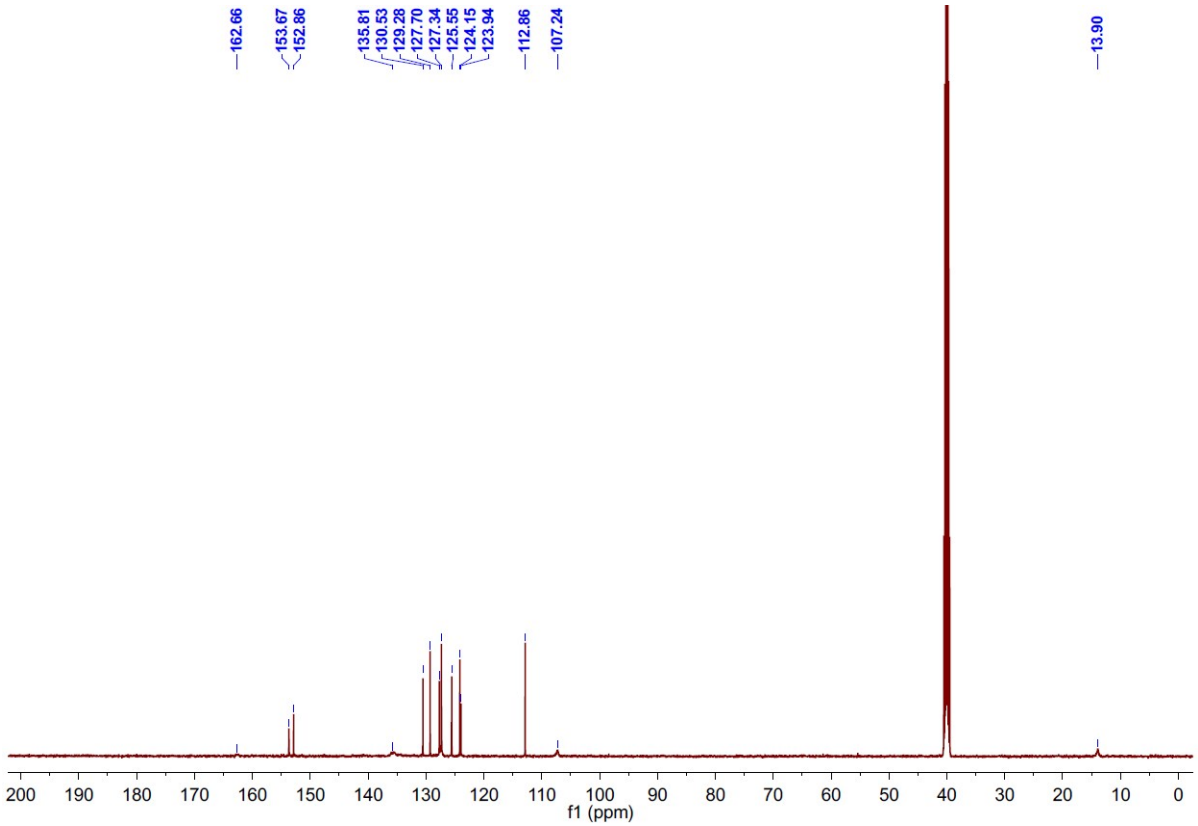

Fig. S27. ^{13}C NMR spectrum of L7 in d_6-DMSO.

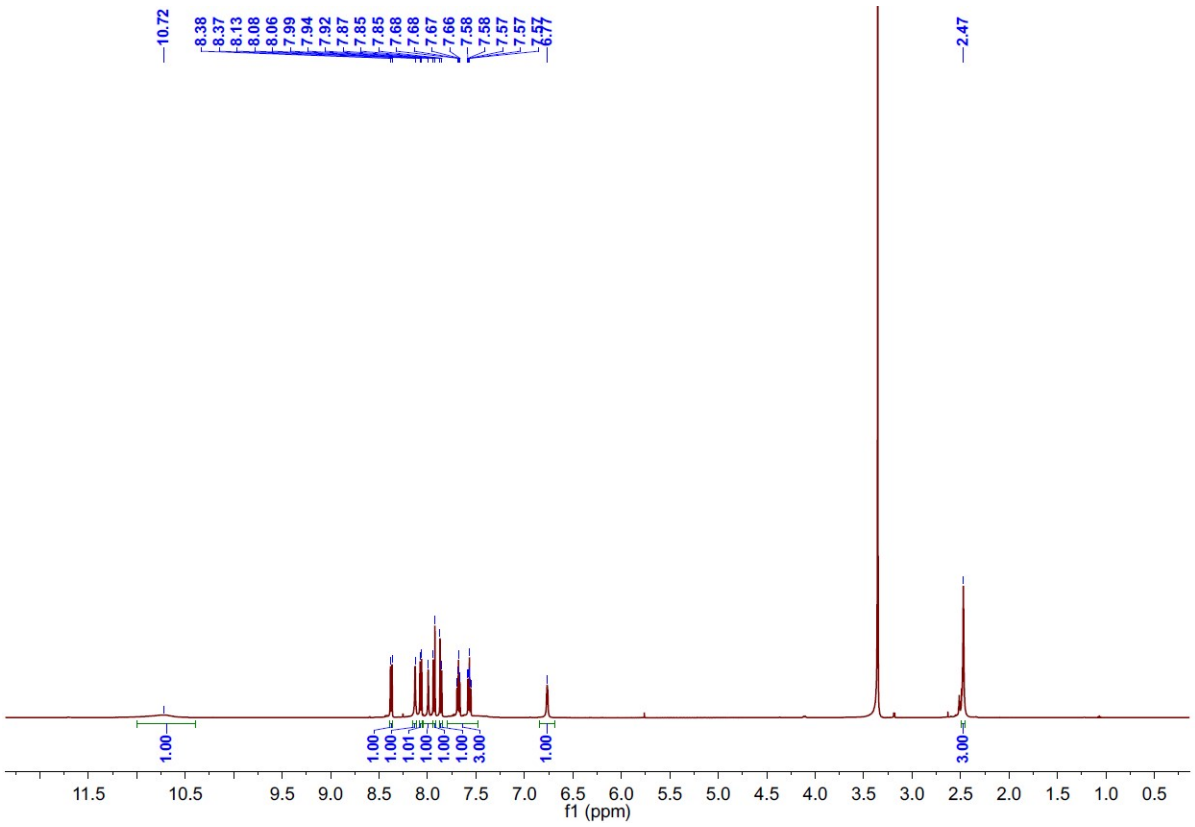

Fig. S28. ^{1}H NMR spectrum of L8 in d_6-DMSO.

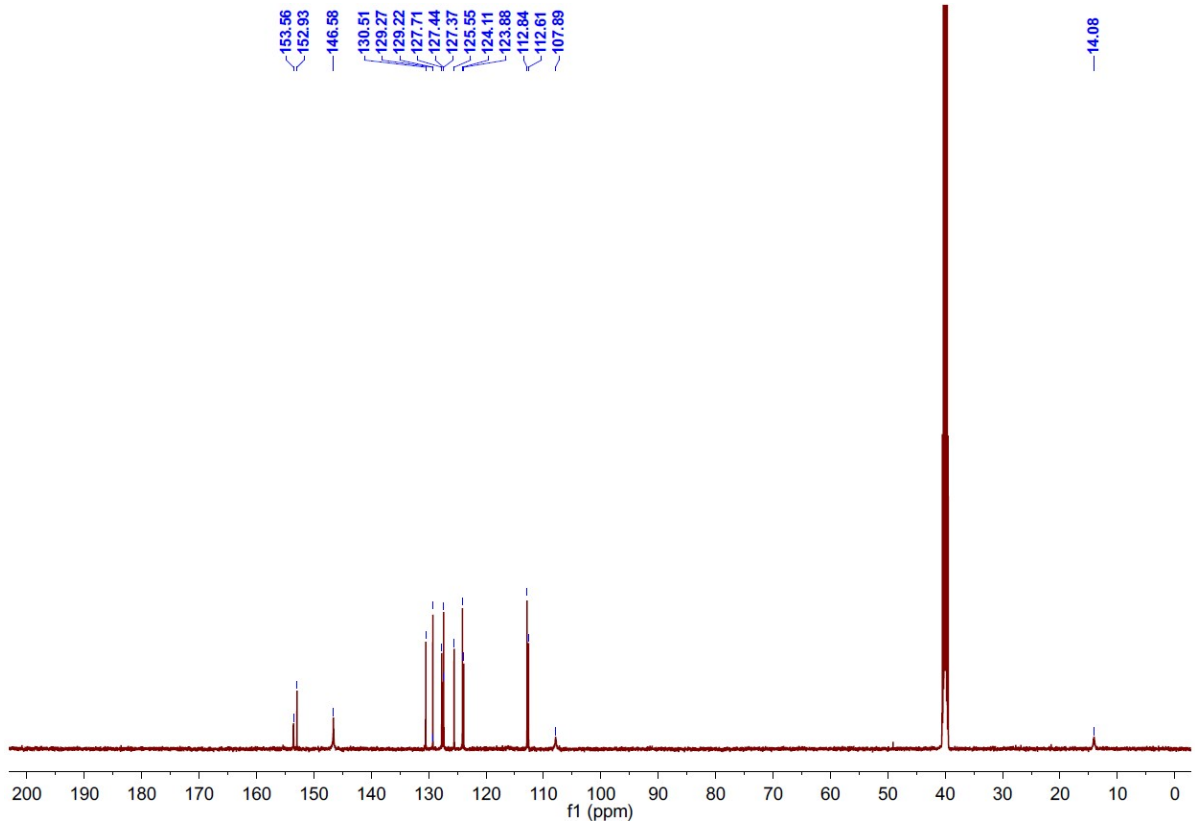

Fig. S29. ^{13}C NMR spectrum of L8 in d_6-DMSO.

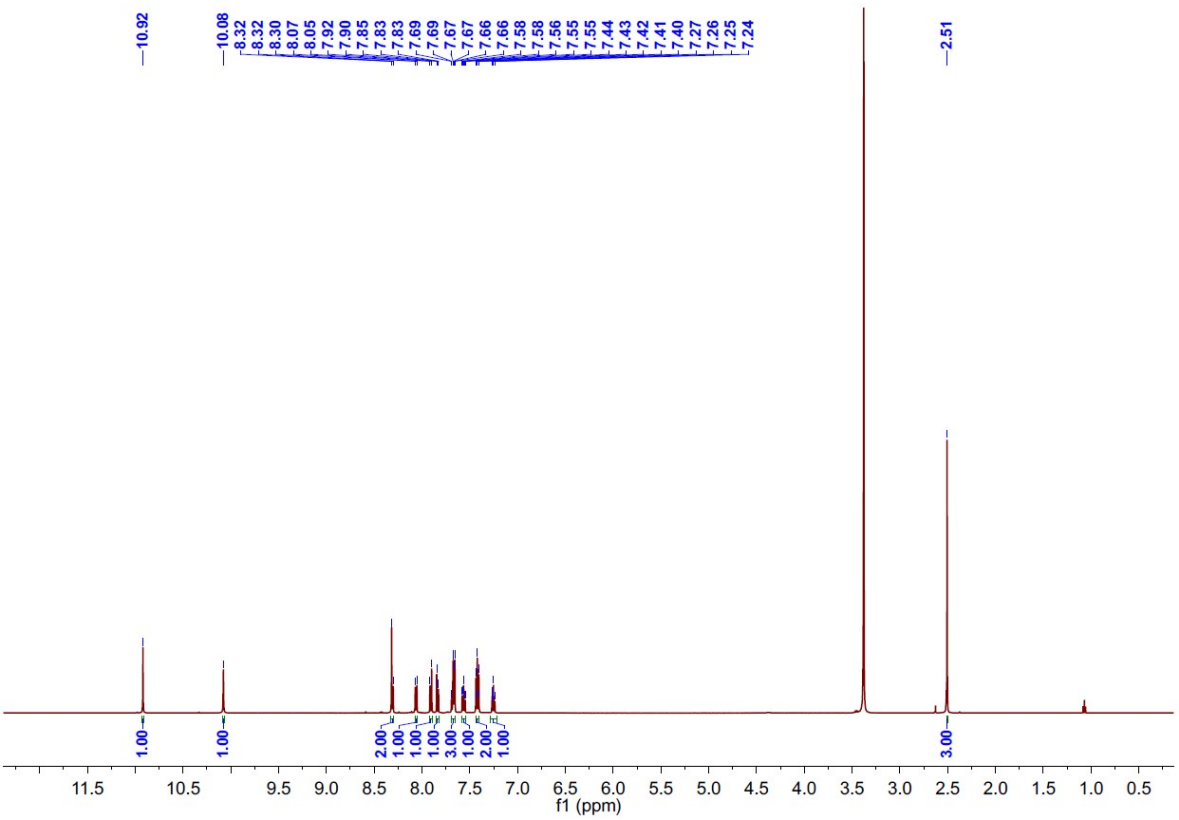

Fig. S30. ^{1}H NMR spectrum of L9 in d_6-DMSO.

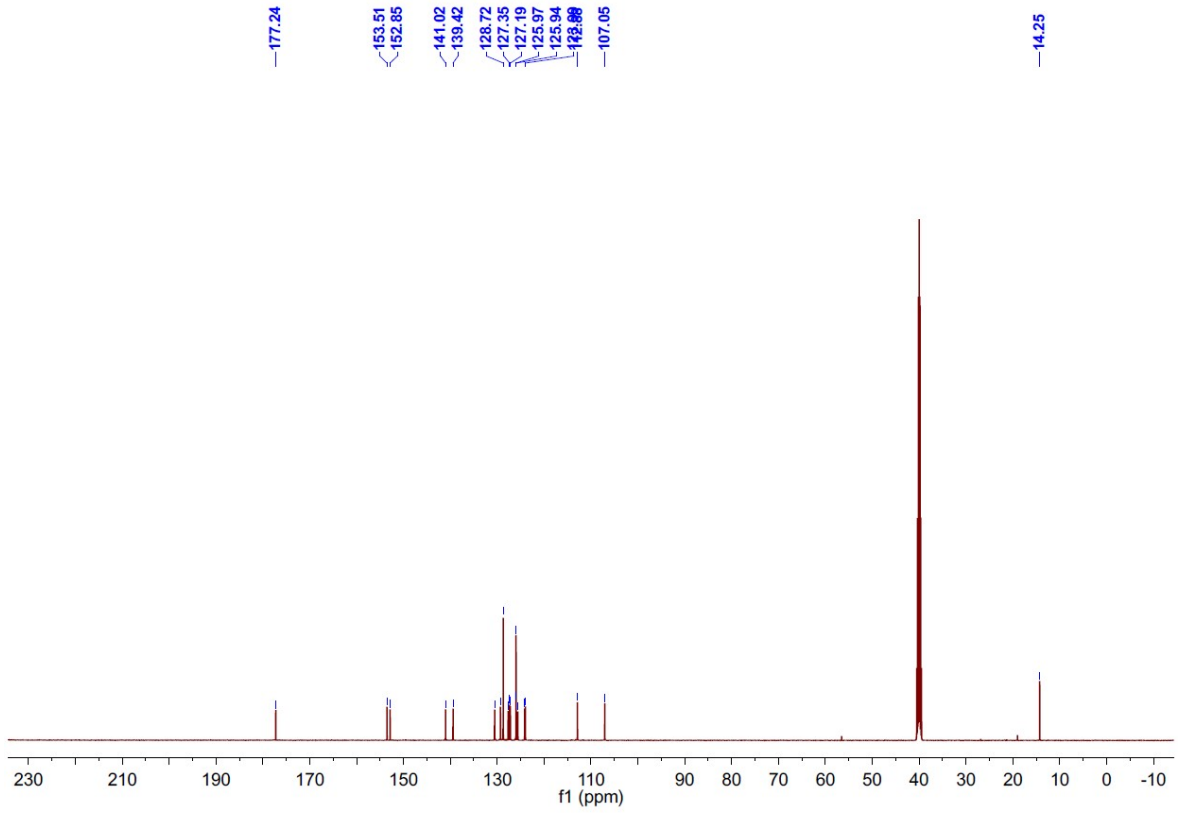

Fig. S31. ^{13}C NMR spectrum of L9 in d_6-DMSO.

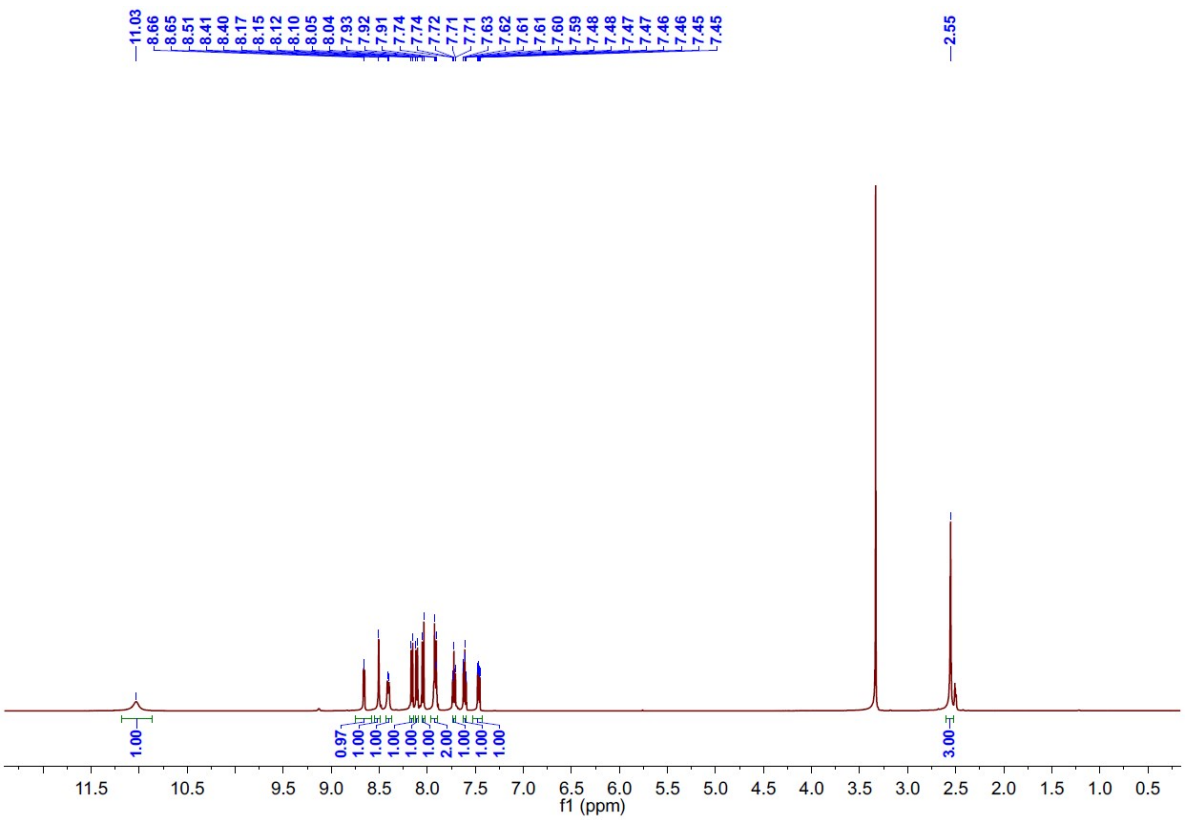

Fig. S32. ^{1}H NMR spectrum of L10 in d_6-DMSO.

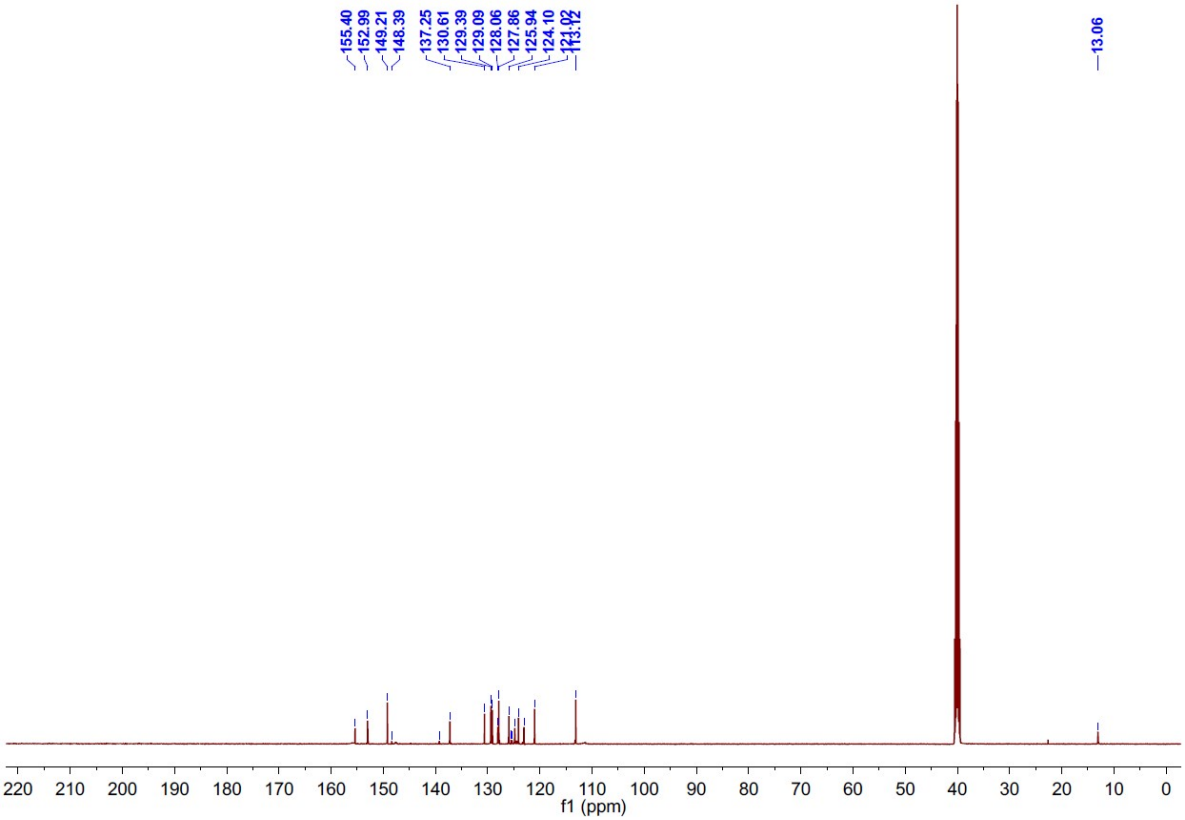

Fig. S33. ^{13}C NMR spectrum of L10 in d_6-DMSO.

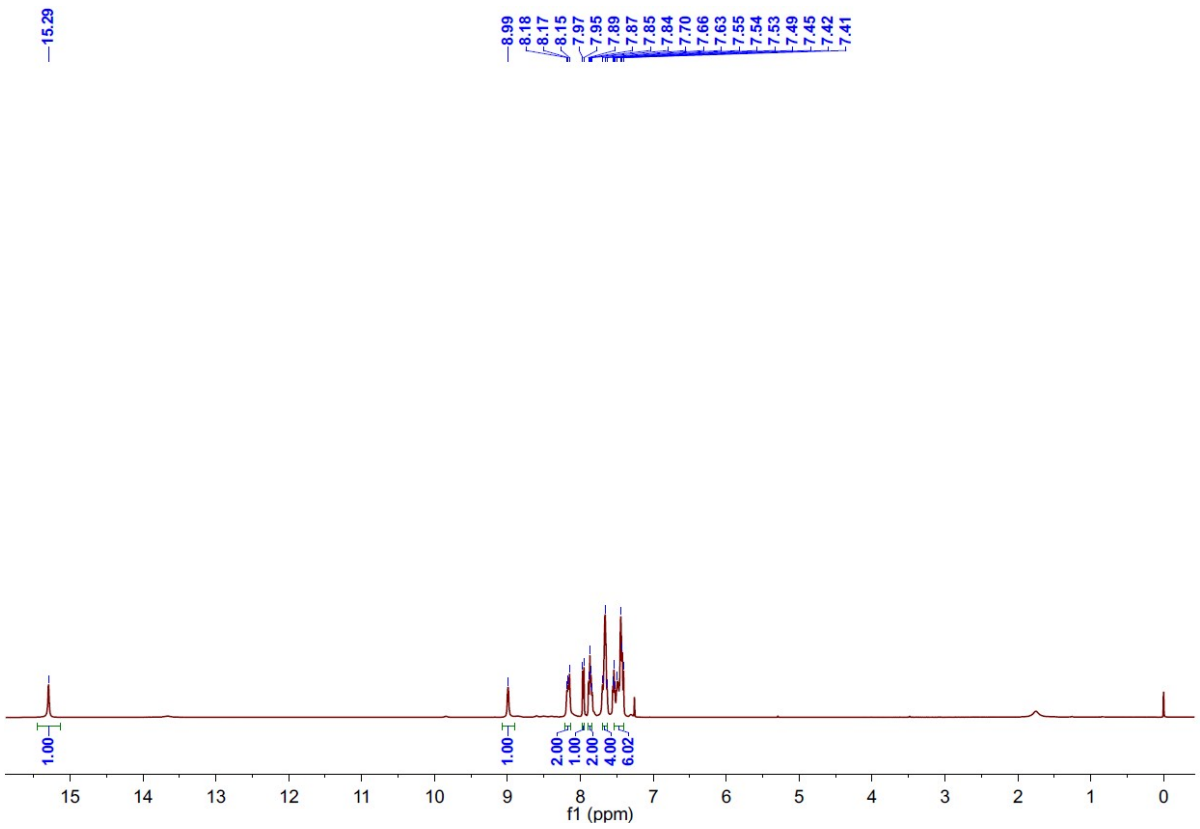

Fig. S34. ^{1}H NMR spectrum of L11 in $CDCl_3$.

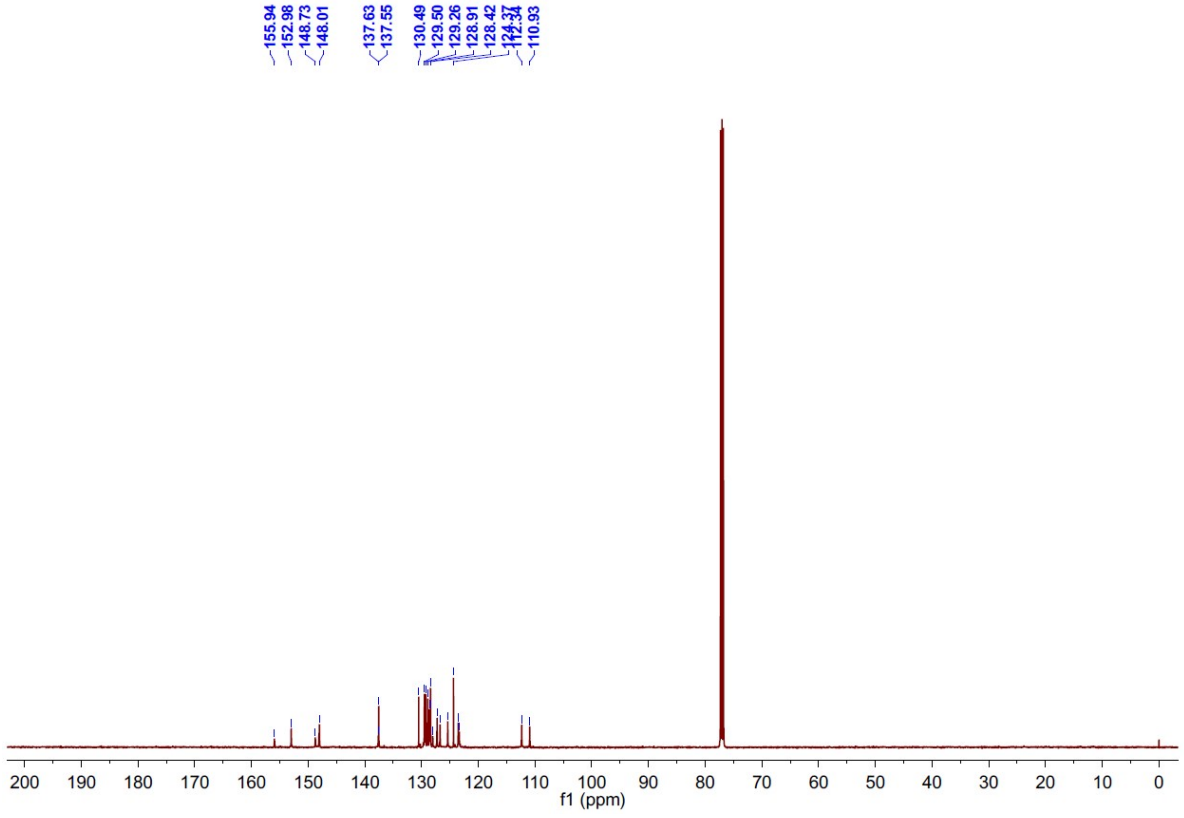

Fig. S35. ^{13}C NMR spectrum of L11 in $CDCl_3$.

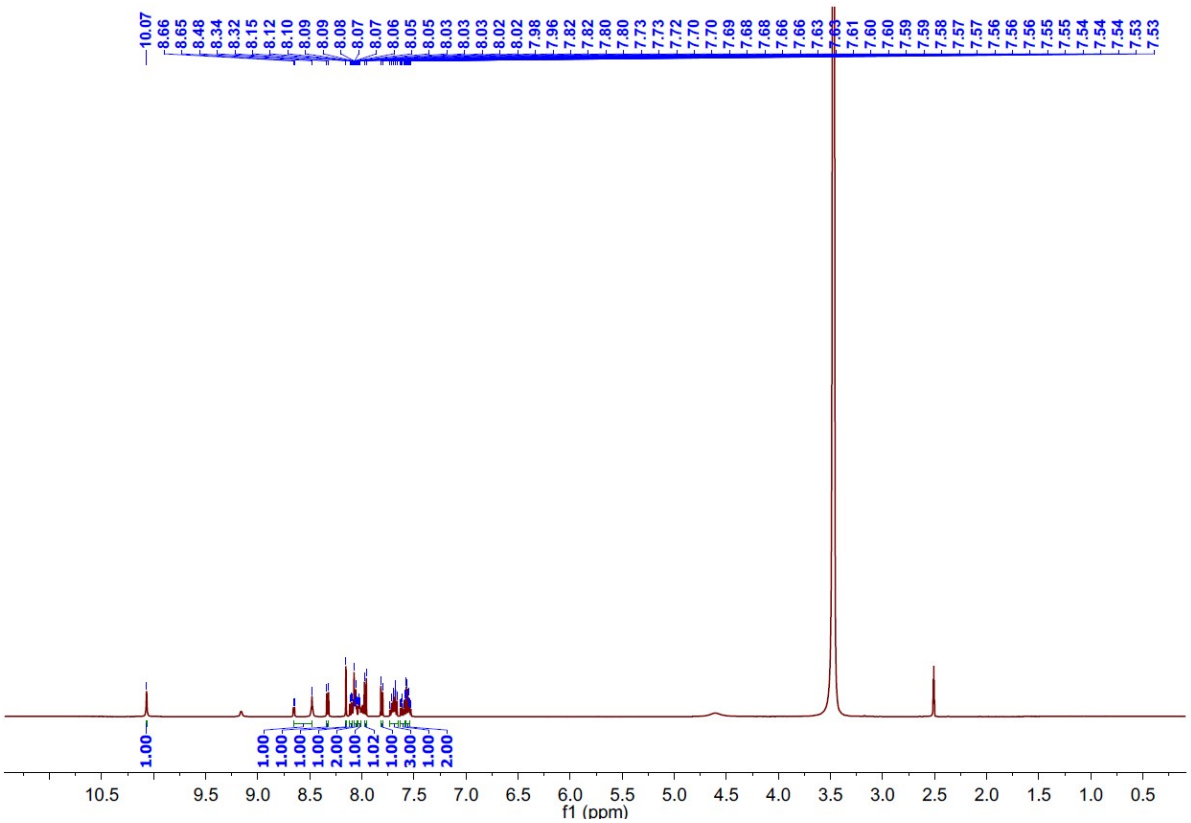

Fig. S36. ^{1}H NMR spectrum of L12 in d_6-DMSO.

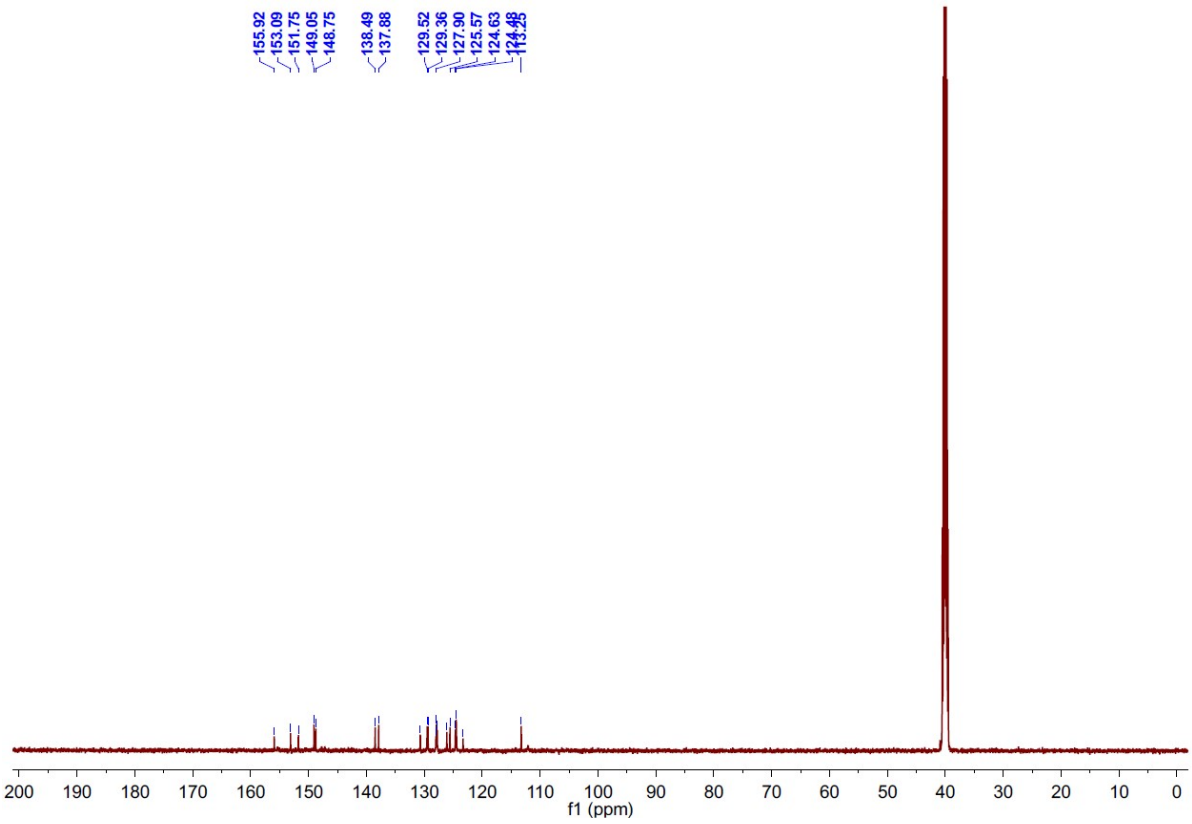

Fig. S37. ^{13}C NMR spectrum of L12 in d_6-DMSO.

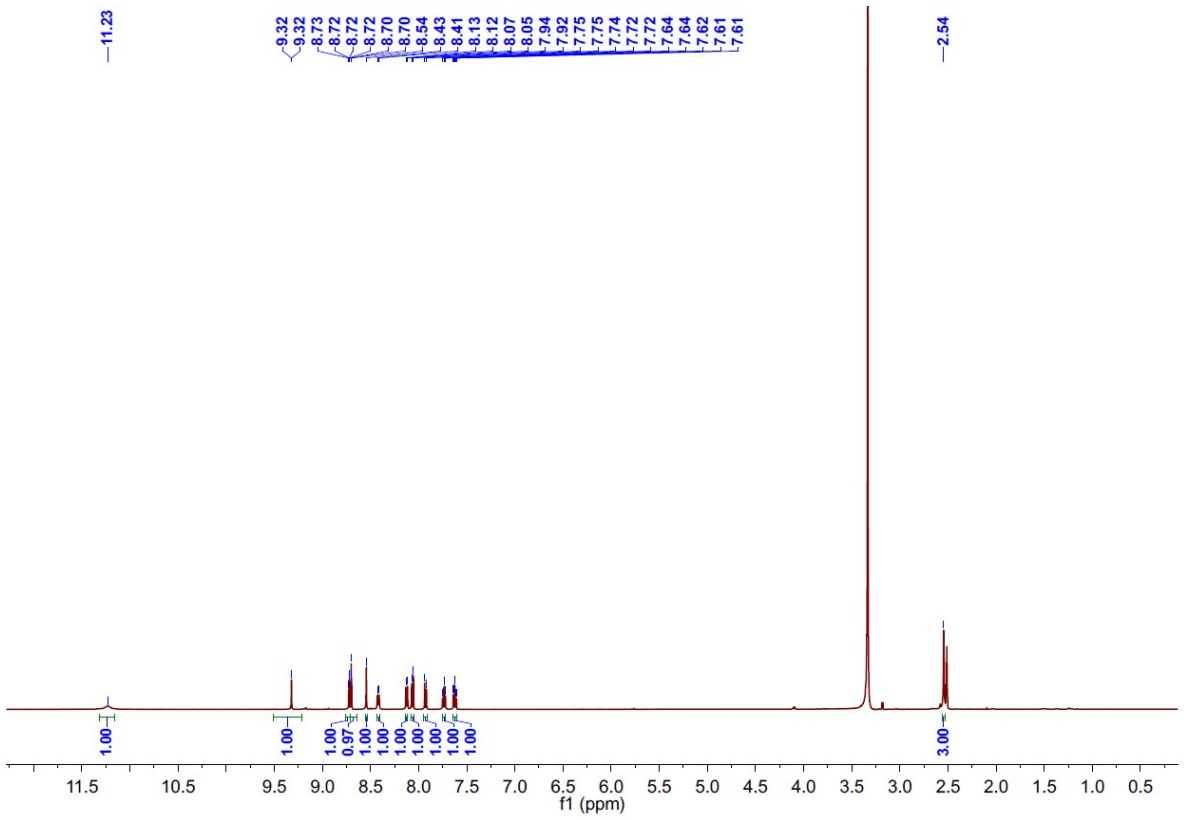

Fig. S38. ^{1}H NMR spectrum of L13 in d_6-DMSO.

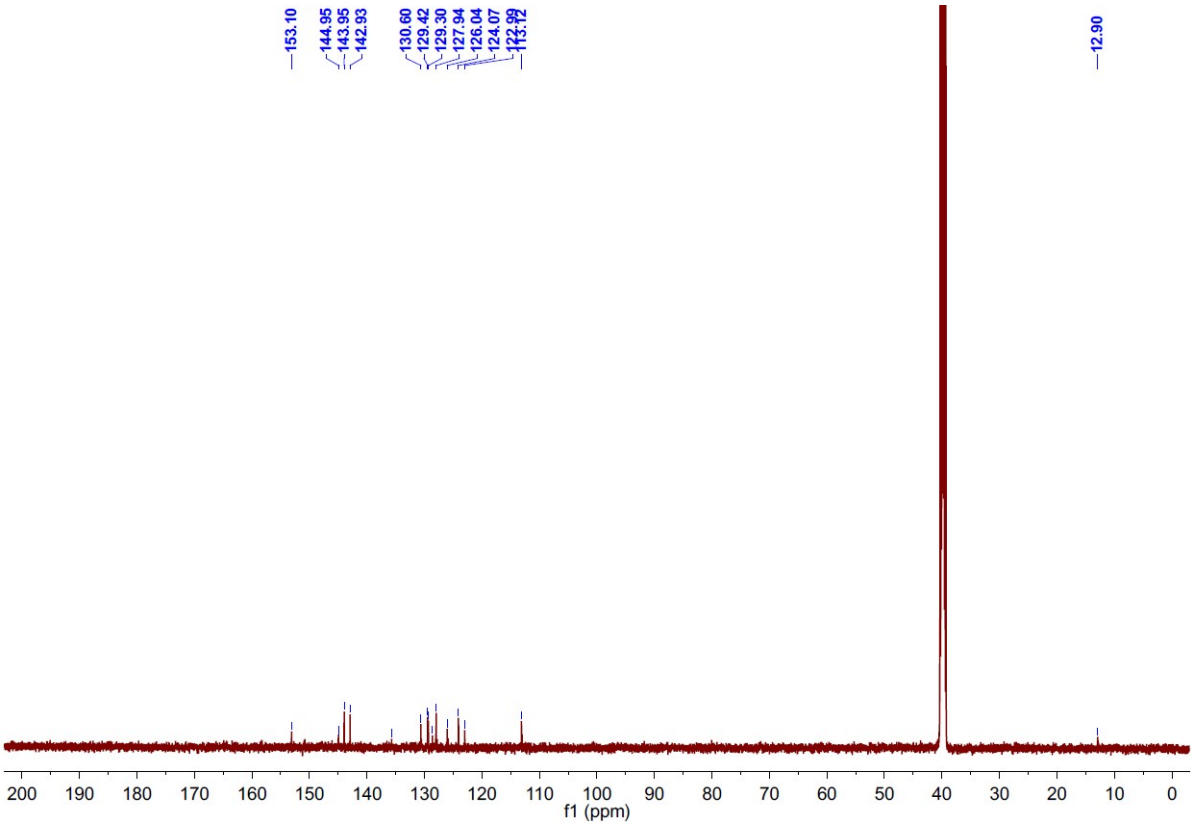

Fig. S39. ^{13}C NMR spectrum of L13 in d_6-DMSO.

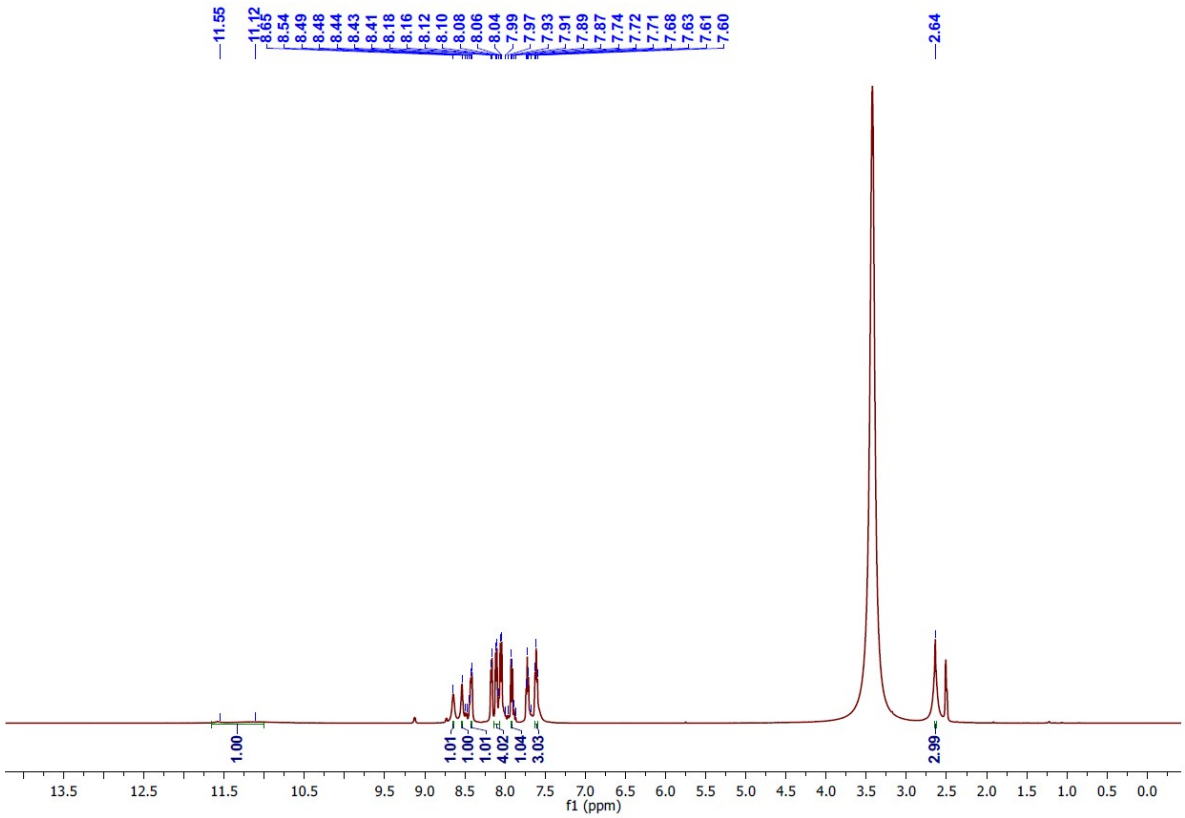

Fig. S40. ^{1}H NMR spectrum of [Zn(L10)Cl_2] in d_6-DMSO.

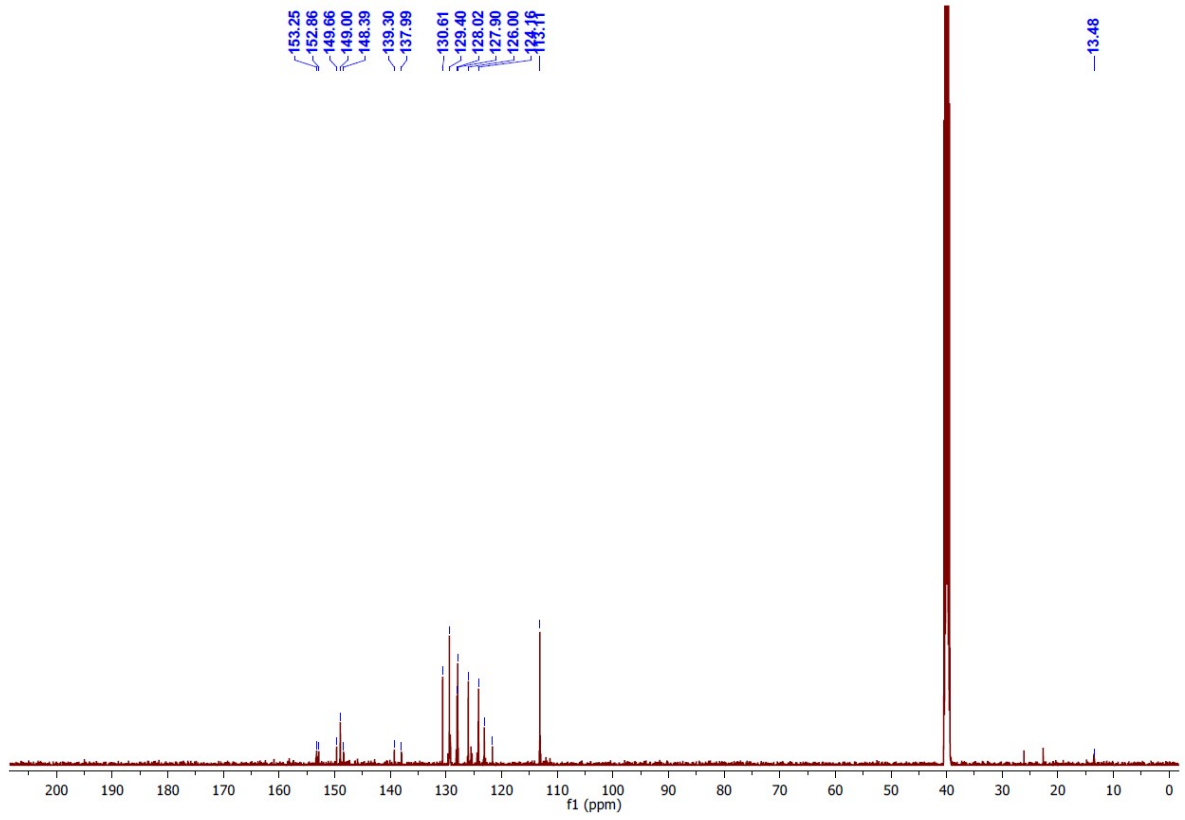

Fig. S41. ^{13}C NMR spectrum of [Zn(L10)Cl_2] in d_6-DMSO.

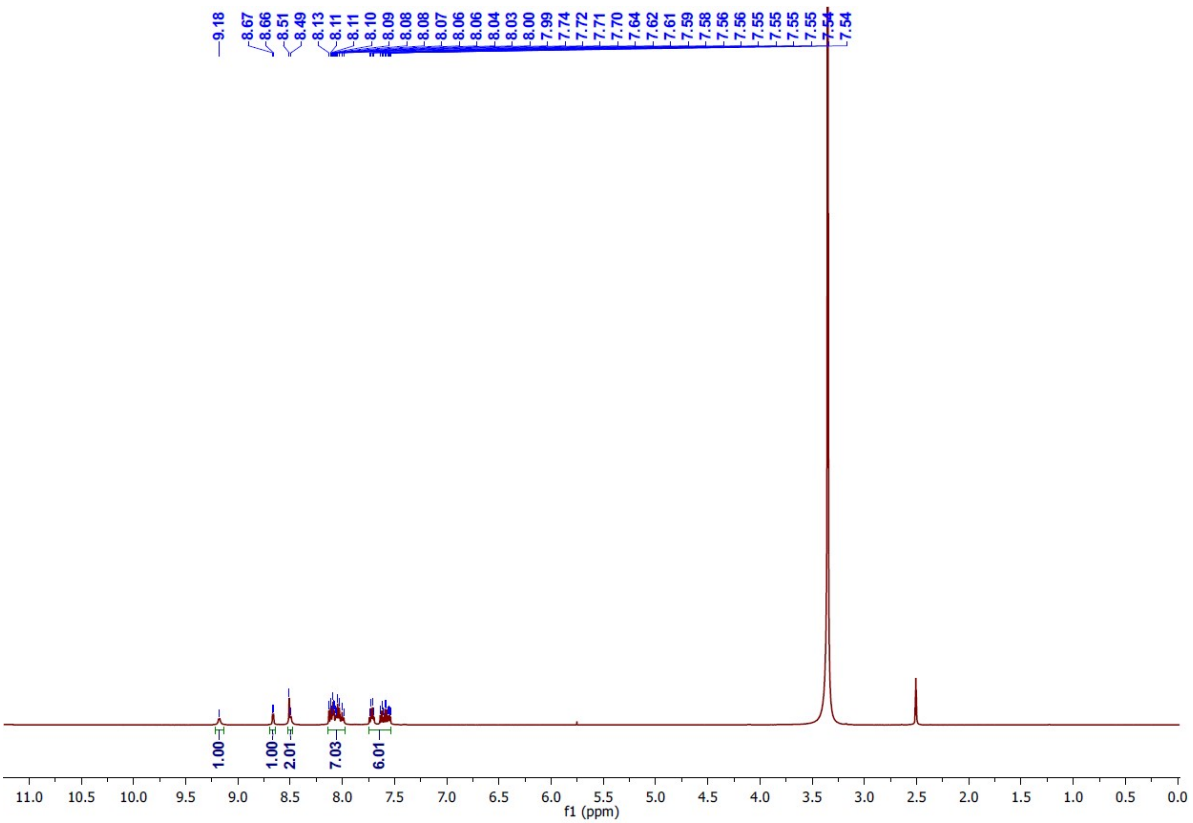

Fig. S42. ^{1}H NMR spectrum of [Zn(L11)Cl_2] in d_6-DMSO.

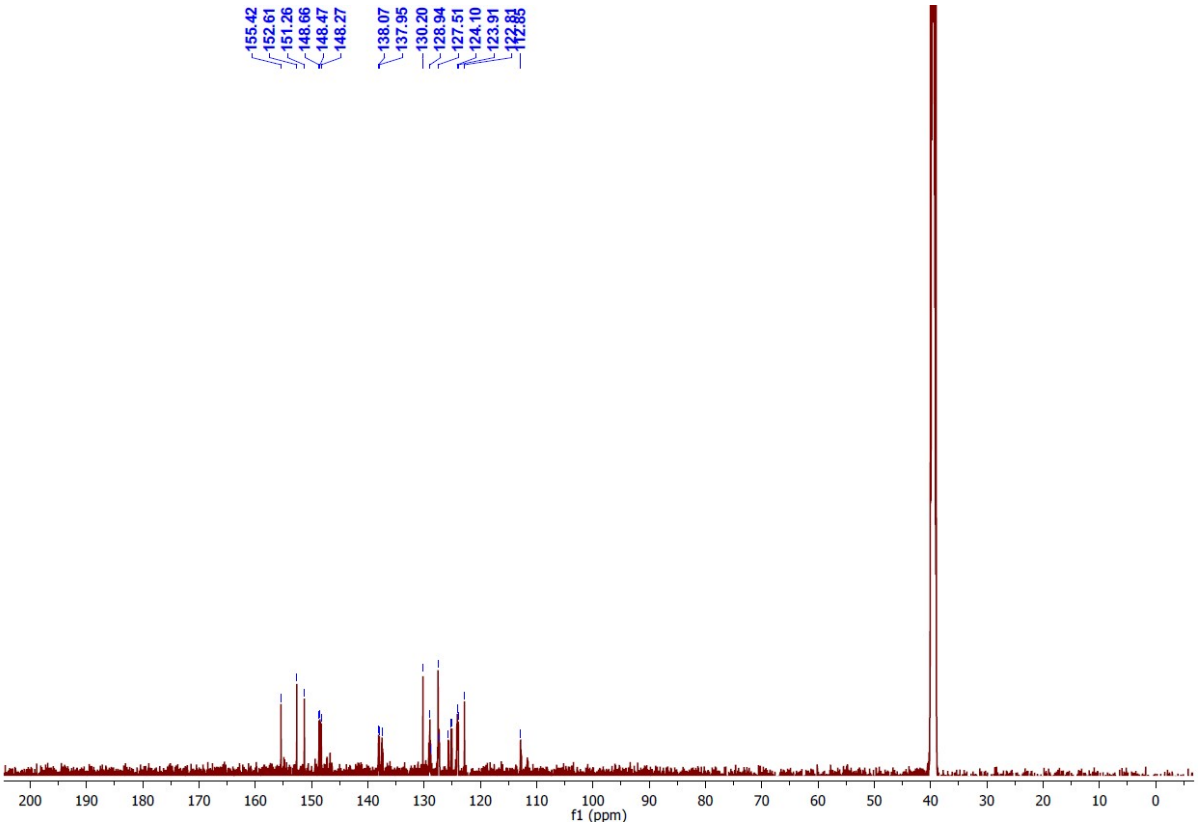

Fig. S43. ^{13}C NMR spectrum of [Zn(L11)Cl_2] in d_6-DMSO.

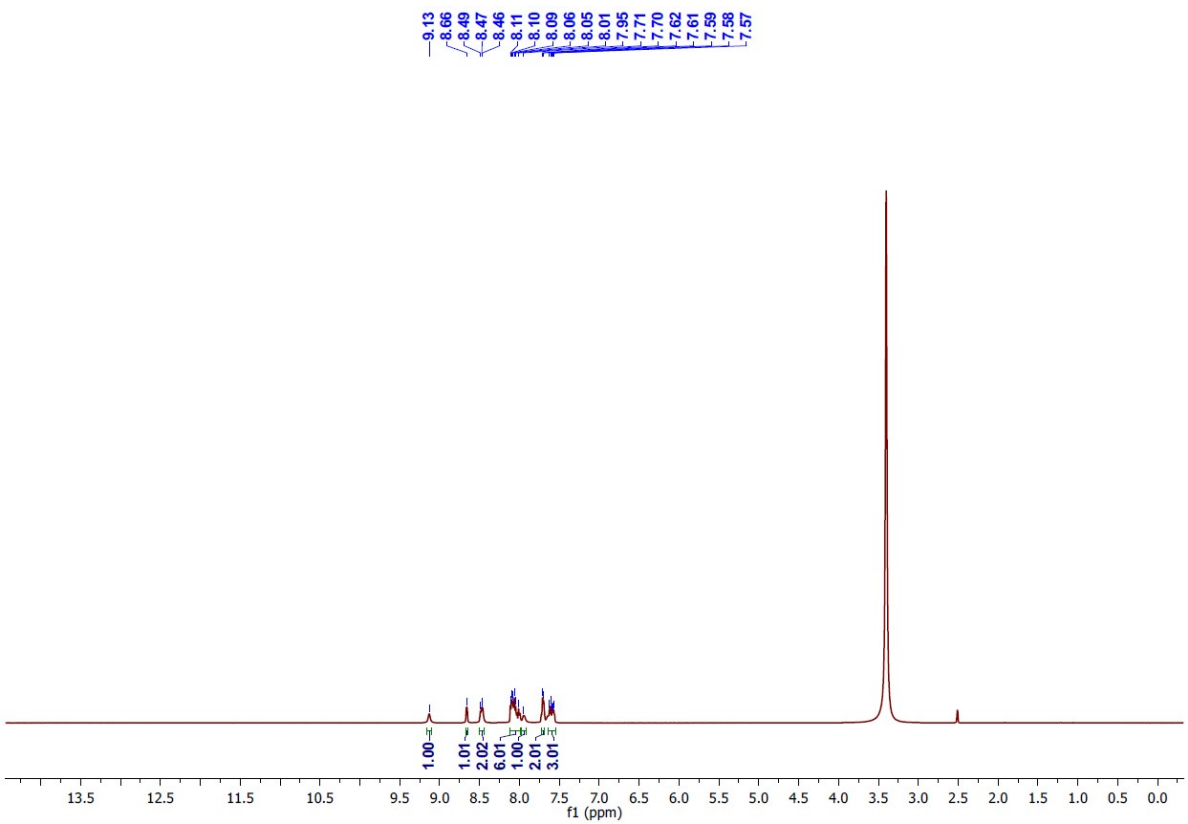

Fig. S44. ^{1}H NMR spectrum of [Zn(L12)Cl_2] in d_6-DMSO.

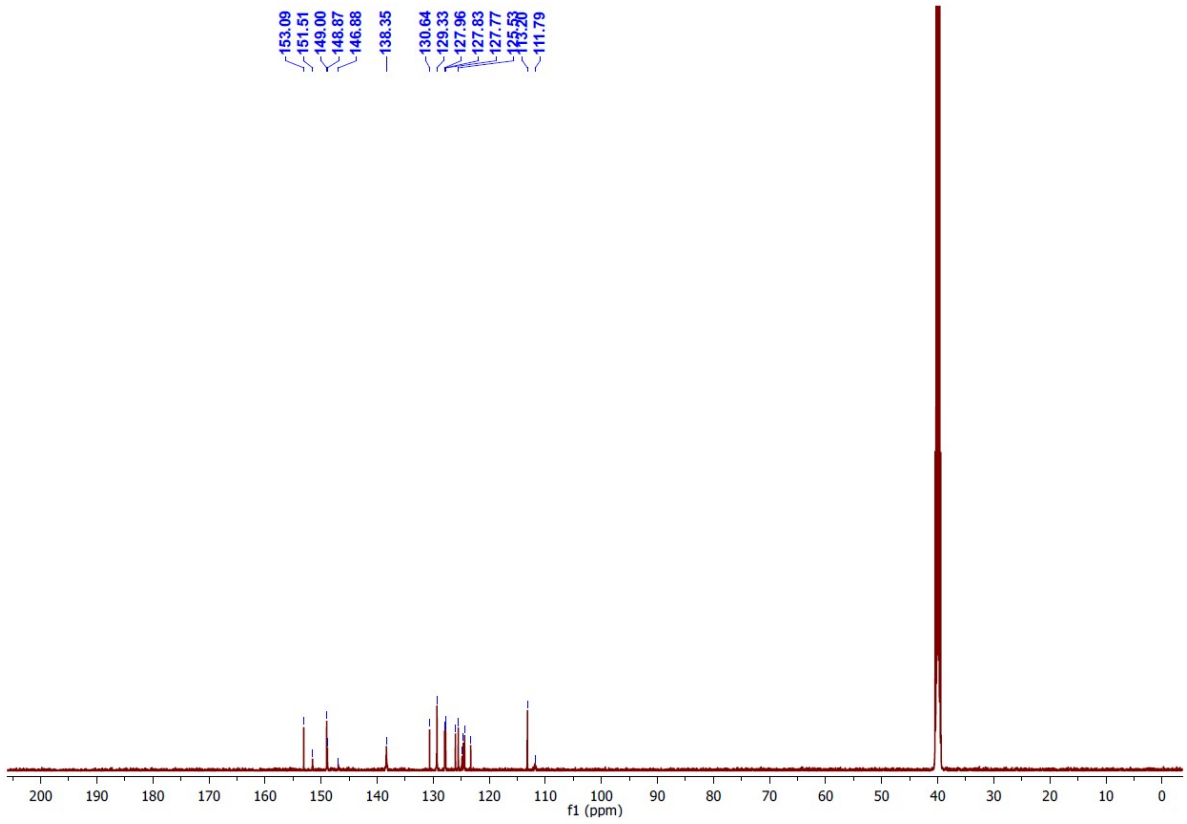

Fig. S45. ^{13}C NMR spectrum of [Zn(L12)Cl_2] in d_6-DMSO.

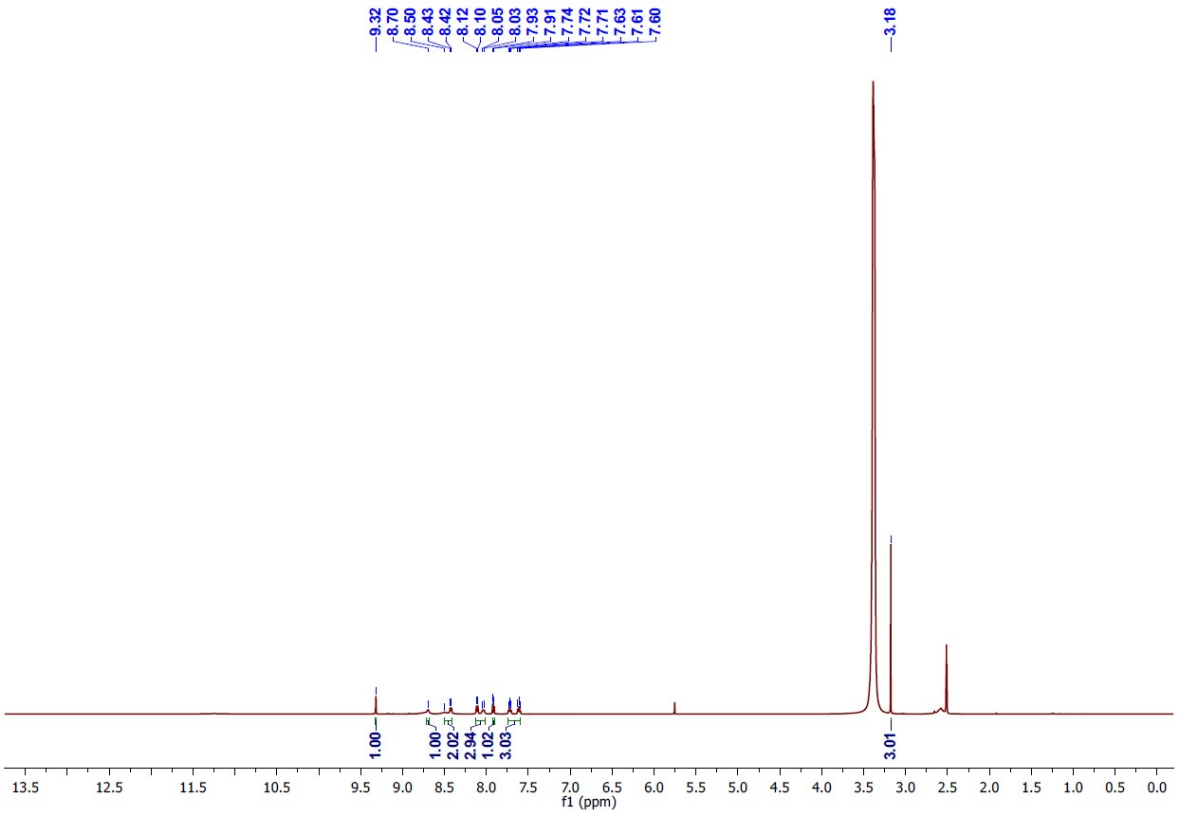

Fig. S46. ^{1}H NMR spectrum of [Zn(L13)Cl_2] in d_6-DMSO.

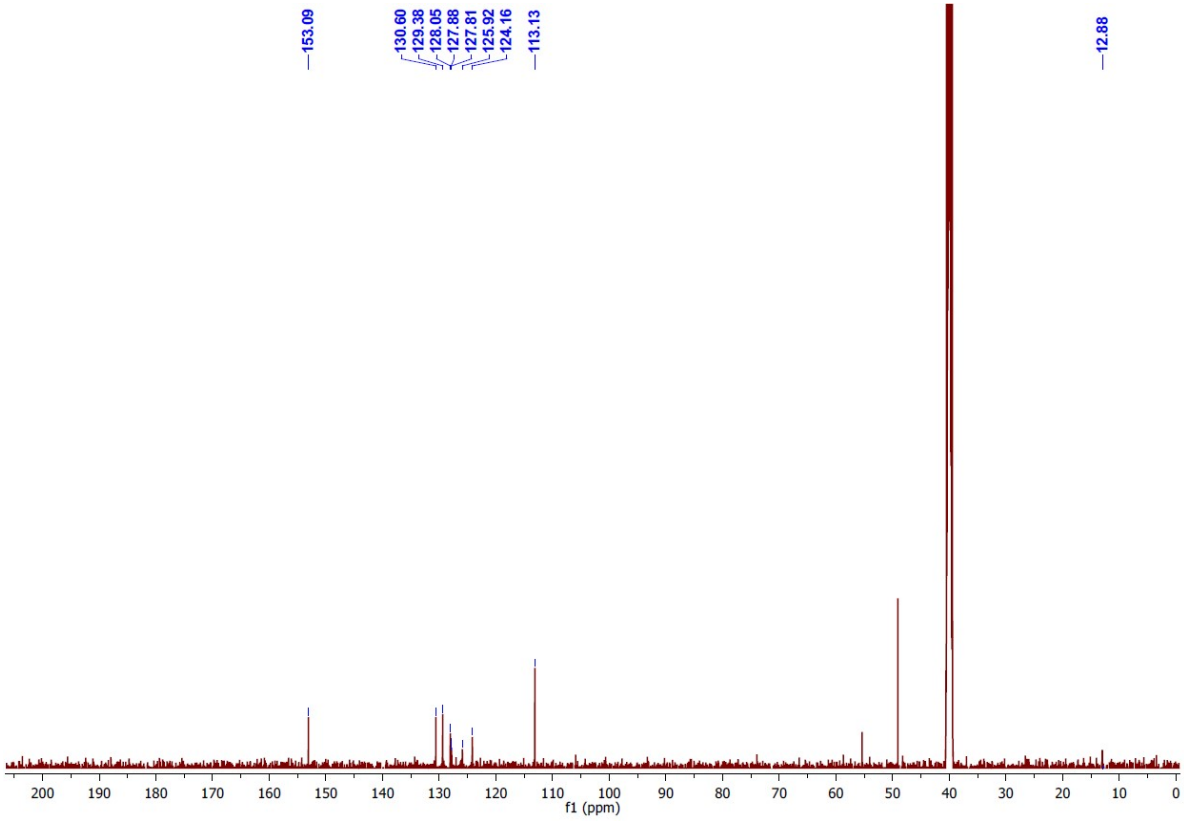

Fig. S47. ^{13}C NMR spectrum of [Zn(L13)Cl_2] in d_6-DMSO.

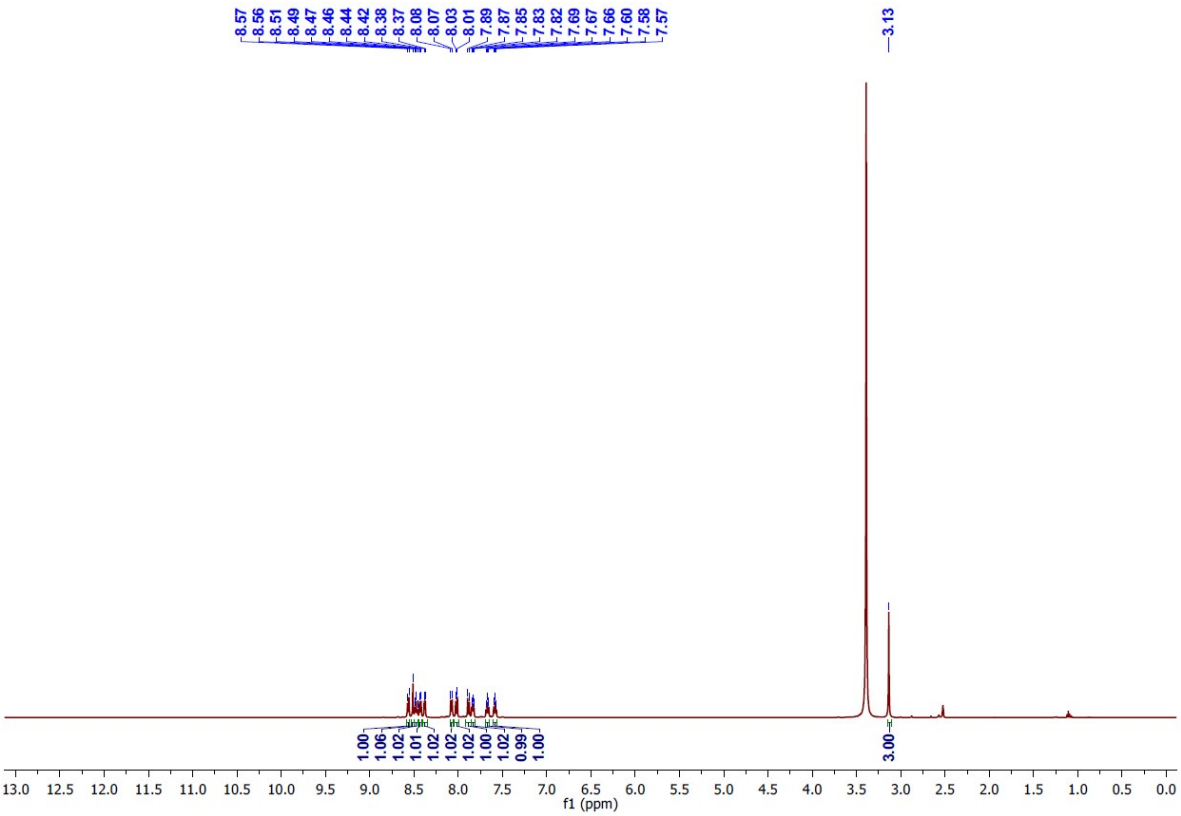

Fig. S48. ^{1}H NMR spectrum of $[Ga(L10)_2]^+$ in d_6-DMSO.

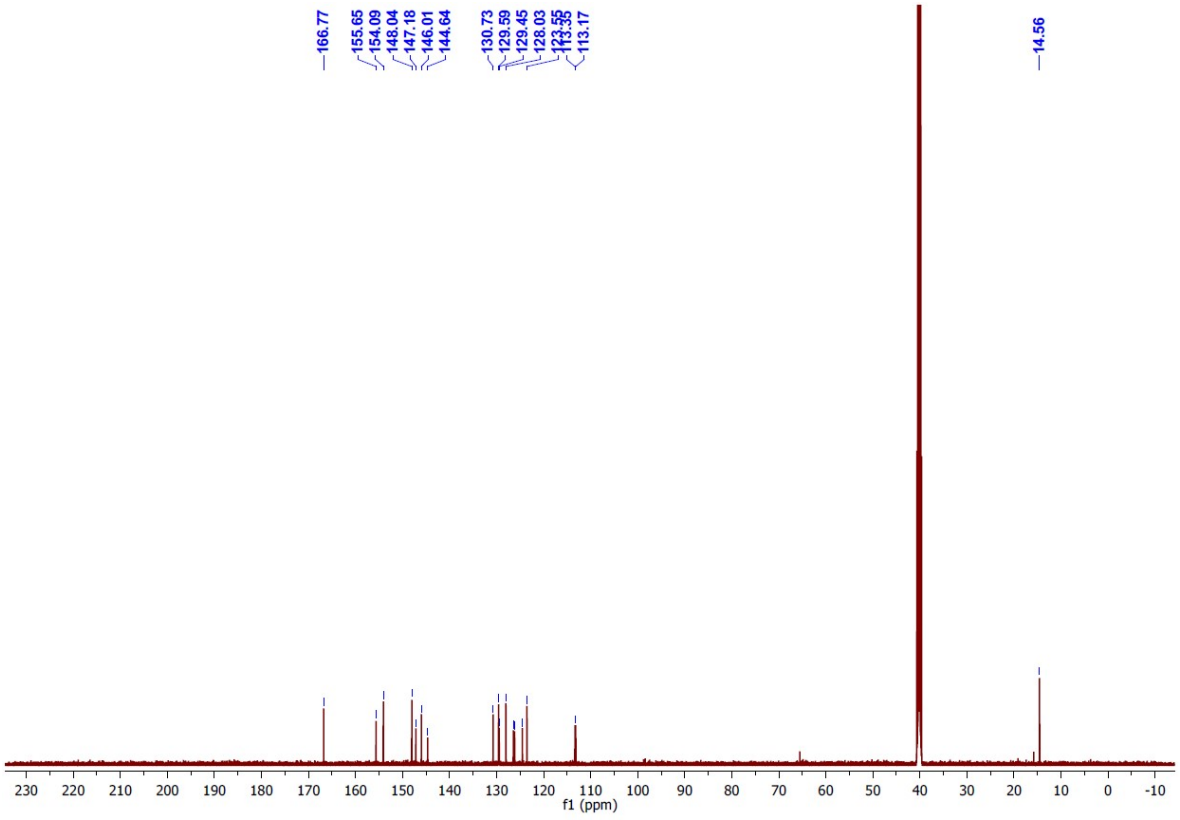

Fig. S49. ^{13}C NMR spectrum of $[Ga(L10)_2]^+$ in d_6-DMSO.

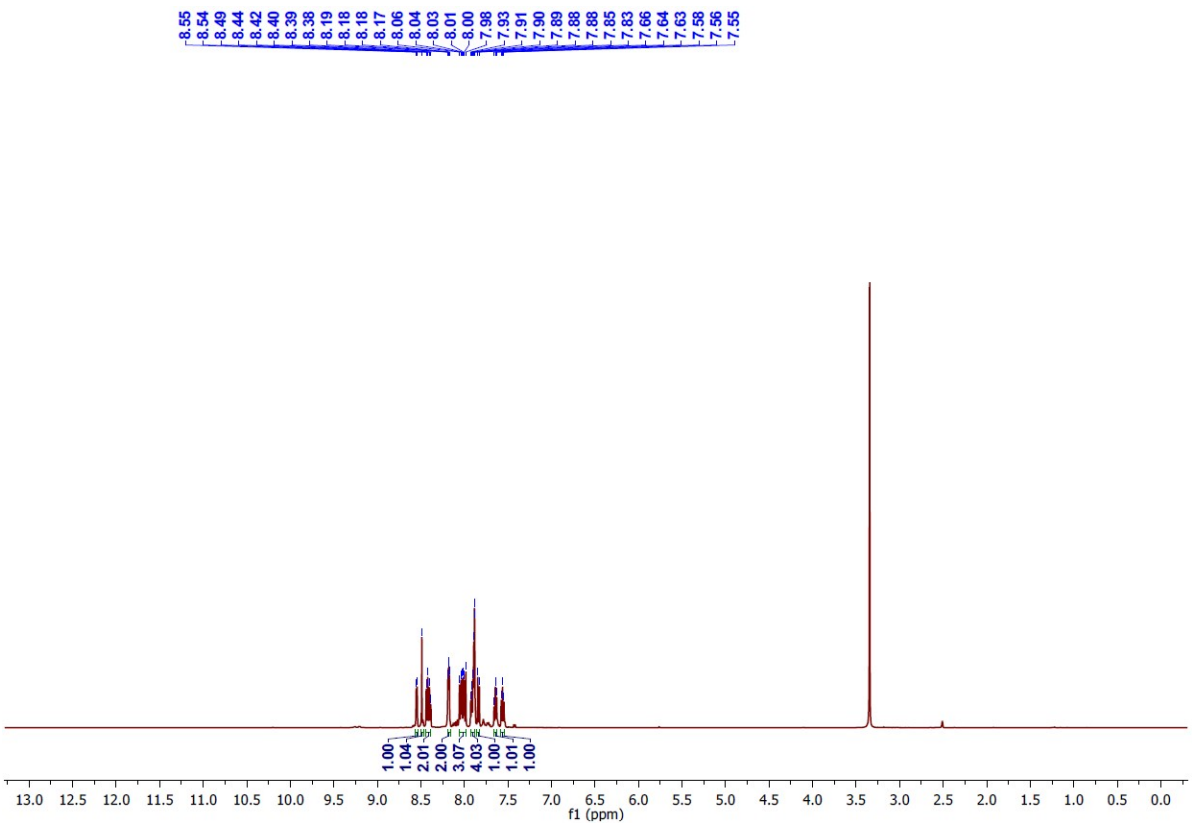

Fig. S50. ^{1}H NMR spectrum of $[Ga(L11)_2]^+$ in d_6-DMSO.

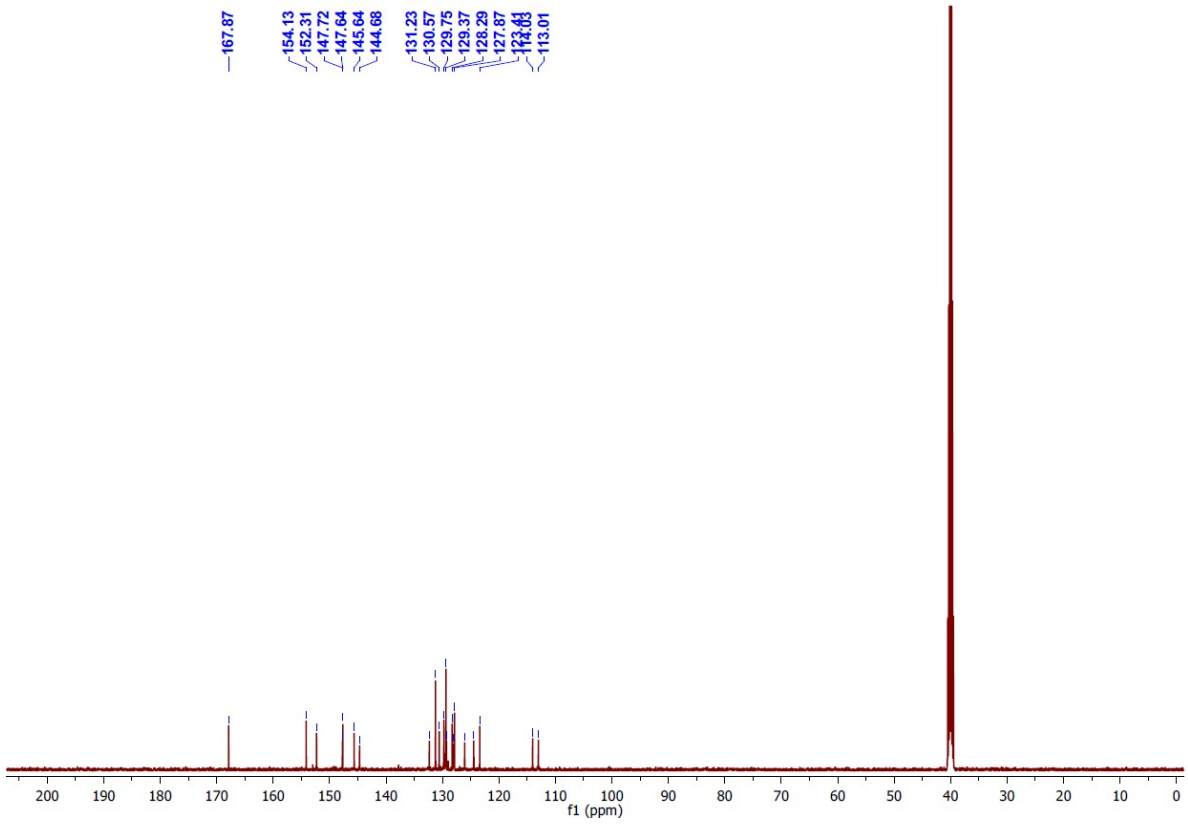

Fig. S51. ^{13}C NMR spectrum of $[Ga(L11)_2]^+$ in d_6-DMSO.

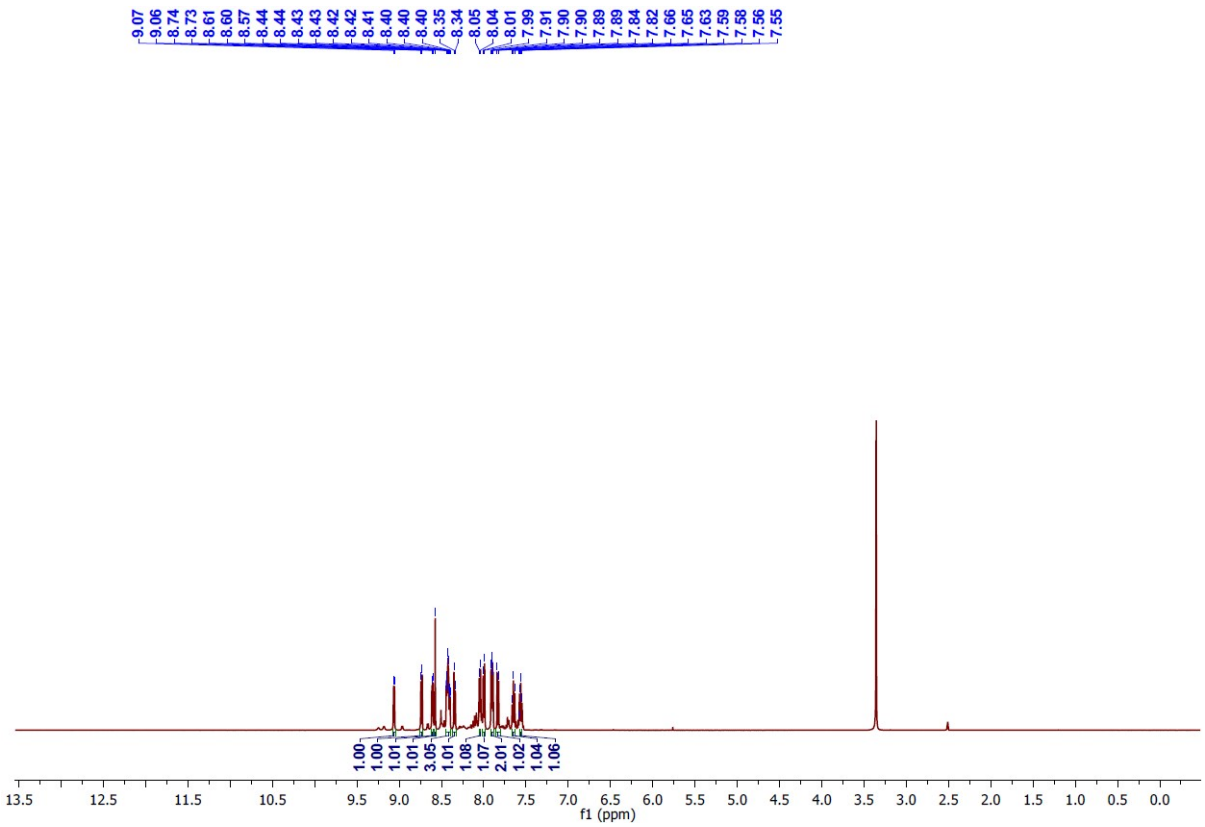

Fig. S52. ^{1}H NMR spectrum of $[Ga(L12)_2]^+$ in d_6-DMSO.

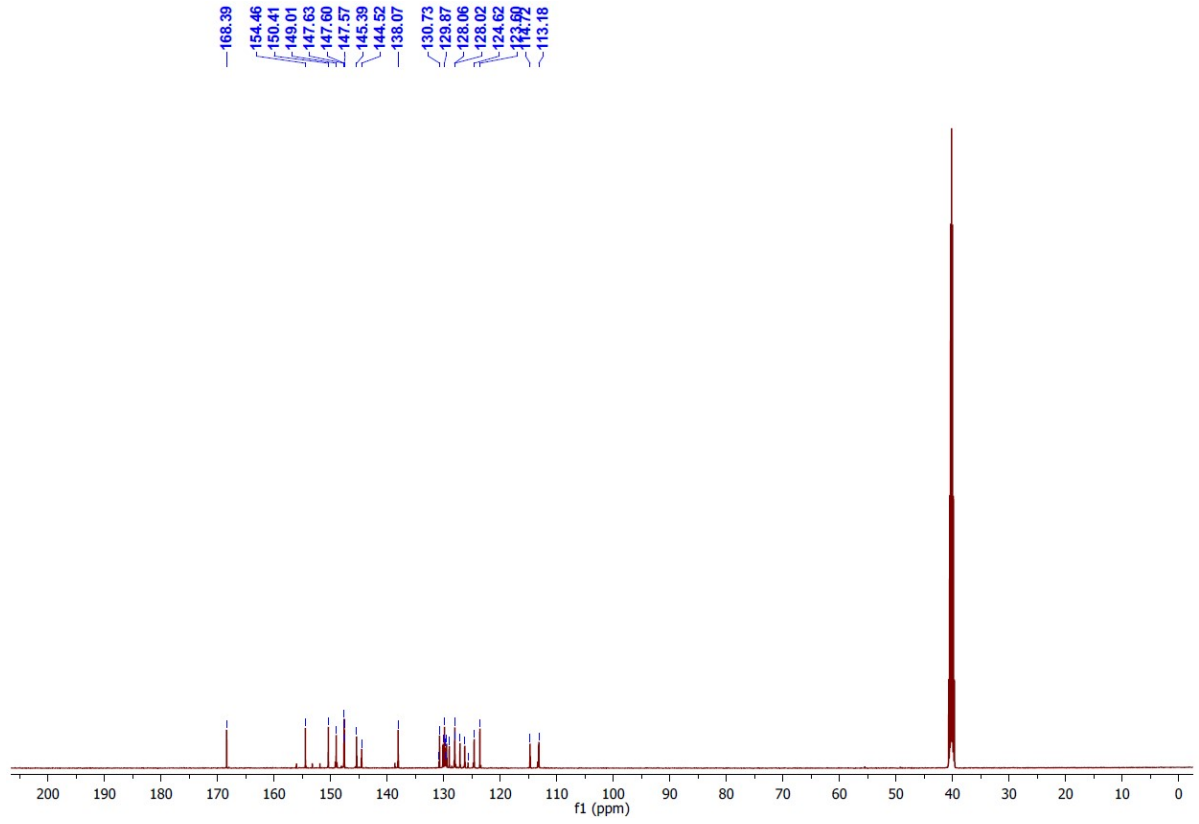

Fig. S53. ^{13}C NMR spectrum of $[Ga(L12)_2]^+$ in d_6-DMSO.

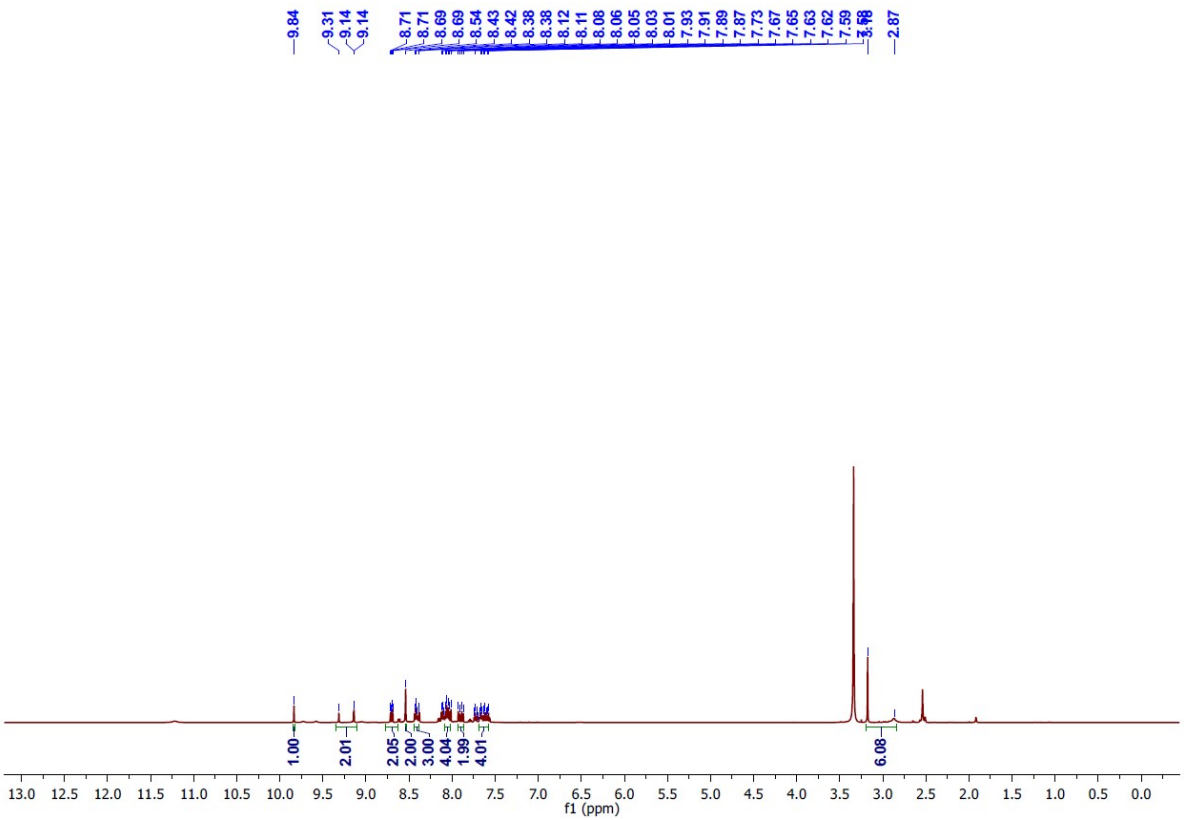

Fig. S54. ^{1}H NMR spectrum of $[Ga(L13)_2]^+$ in d_6-DMSO.

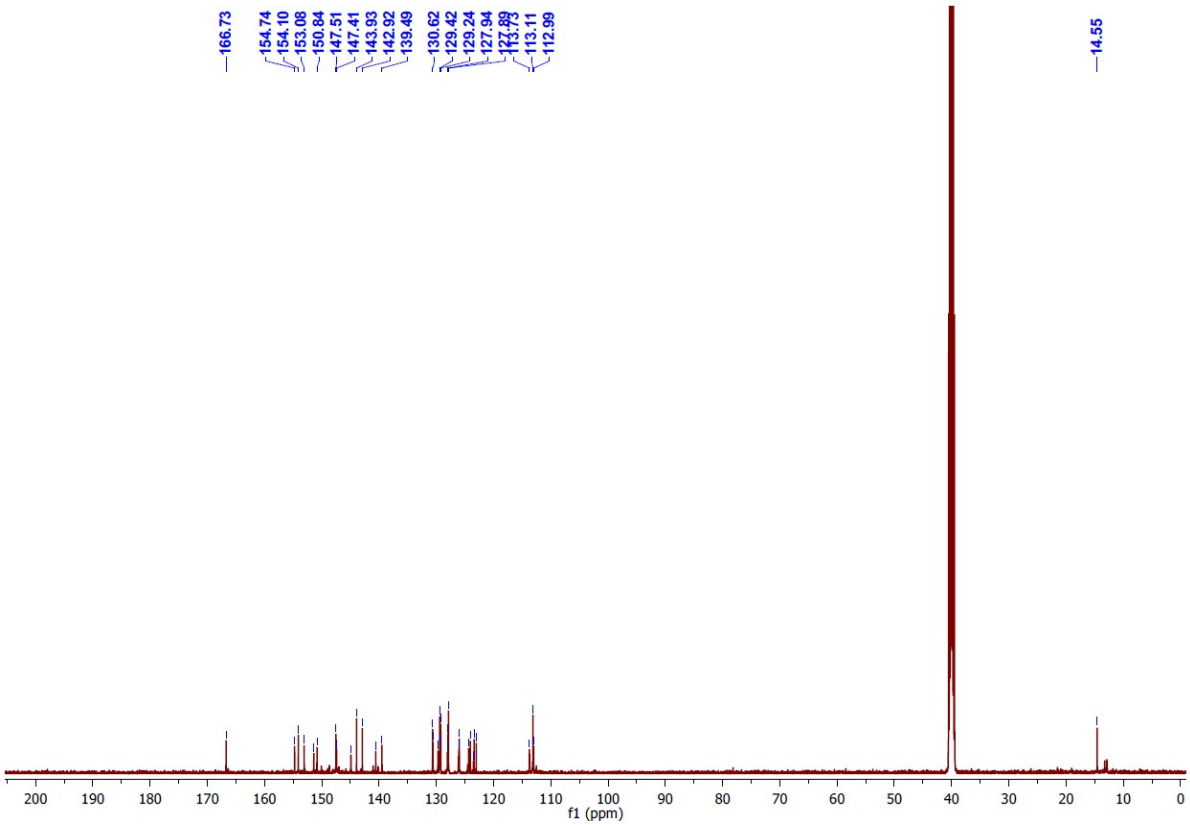

Fig. S55. ^{13}C NMR spectrum of $[Ga(L13)_2]^+$ in d_6-DMSO.

References:

1. G. M. Sheldrick, *Acta Crystallogr., Sect. A: Found. Crystallogr.*, 2008, **64**, 112-122.

2. G. M. Sheldrick, *Acta Crystallogr. C Struct. Chem.*, 2015, **71**, 3-8.

3. C. F. Macrae, I. J. Bruno, J. A. Chisholm, P. R. Edgington, P. McCabe, E. Pidcock, L. Rodriguez-Monge, R. Taylor, J. Streek and P. A. Wood, *J. Appl. Crystallogr.*, 2008, **41**, 466-470.

4. M. Dharmasivam, Busra, K., Wijesinghe, T., Gholam Azad, M., Gonzálvez, M.A., Hussaini, M., Chekmarev, J., Bernhardt, P.V., and Richardson, D.R, *J. Med. Chem.* , 2023, **66**, 1426–1453.

5. M. Kowalewska, H. Kwiecień, M. Śmist and A. Wrześniewska, *J. Chem.*, 2012, **2013**, 1-7.

6. S. Parekh, D. Bhavsar, M. Savant, S. Thakrar, A. Bavishi, M. Parmar, H. Vala, A. Radadiya, N. Pandya and J. Serly, *Eur. J. Med. Chem.*, 2011, **46**, 1942-1948.

7. M. Dharmasivam, B. Kaya, T. P. Wijesinghe, V. Richardson, J. R. Harmer, M. A. Gonzalvez, W. Lewis, M. G. Azad, P. V. Bernhardt and D. R. Richardson, *Chem. Sci.*, 2024, **15**, 974-990.

8. B. Kaya, Gholam Azad, M., Suleymanoglu, M., Harmer, J.R., Wijesinghe, T.P., Richardson, V., Zhao, X., Bernhardt, P.V., Dharmasivam, M., and Richardson, D.R., *J. Med. Chem.*, 2024, **67**, 12155–12183.

9. B. Kaya, M. Gholam Azad, M. Suleymanoglu, J. R. Harmer, T. P. Wijesinghe, V. Richardson, X. Zhao, P. V. Bernhardt, M. Dharmasivam and D. R. Richardson, *J. Med. Chem.*, 2024, **67**, 12155-12183.

10. T. P. Wijesinghe, B. Kaya, M. A. Gonzálvez, J. R. Harmer, M. Gholam Azad, P. V. Bernhardt, M. Dharmasivam and D. R. Richardson, *J. Med. Chem.*, 2023, **66**, 15453-15476.

11. D. Richardson, E. Tran and P. Ponka, *Blood*, 1995, **86**, 4295-4306.

12. D. Richardson and E. Baker, *Biochim. Biophys. Acta*, 1990, **1053**, 1-12.

13. D. B. Lovejoy, D. M. Sharp, N. Seebacher, P. Obeidy, T. Prichard, C. Stefani, M. T. Basha, P. C. Sharpe, P. J. Jansson and D. S. Kalinowski, *J. Med. Chem.*, 2012, **55**, 7230-7244.

14. C. Stefani, G. Punnia-Moorthy, D. B. Lovejoy, P. J. Jansson, D. S. Kalinowski, P. C. Sharpe, P. V. Bernhardt and D. R. Richardson, *J. Med. Chem.*, 2011, **54**, 6936-6948.

15. J. Yuan, D. B. Lovejoy and D. R. Richardson, *Blood*, 2004, **104**, 1450-1458.

16. F. Arjmand, F. Sayeed and M. Muddassir, *J. Photochem. Photobiol. B*, 2011, **103**, 166-179.

17. N. T. Le and D. R. Richardson, *Biochim. Biophys. Acta*, 2002, **1603**, 31-46.

18. D. Richardson, *Crit. Rev. Oncol. Hematol.*, 2002, **42**, 267-281.

19. J. C. Kwok and D. R. Richardson, *Crit. Rev. Oncol. Hematol.*, 2002, **42**, 65-78.

20. C. R. Chitambar, *Biochim. Biophys. Acta*, 2016, **1863**, 2044-2053.

21. C. R. Chitambar and W. E. Antholine, *Antioxid. Redox Signal.*, 2013, **18**, 956-972.

22. C. R. Chitambar, J. P. Wereley and S. Matsuyama, *Mol. Cancer Ther.*, 2006, **5**, 2834-2843.

23. N. P. Davies, Y. S. Rahmanto, C. R. Chitambar and D. R. Richardson, *J. Pharmacol. Exp. Ther.*, 2006, **317**, 153-162.

24. S.-r. Choi, M. A. Hassan, B. E. Britigan and P. Narayanasamy, *Curr. Issues Mol. Biol.*, 2024, **46**, 9149-9161.

25. Y. Guo, W. Li, H. Li and W. Xia, *ACS Infect. Dis.*, 2019, **5**, 1693-1697.

26. H. A. Benesi and J. H. Hildebrand, *J. Am. Chem. Soc.*, 1949, **71**, 2703-2707.